

**Conditional network measures using
multivariate partial coherence analysis for
spike train data with application to
multi-electrode array recordings.**

Siti Noormiza Binti Makhtar

PhD

**UNIVERSITY OF YORK
ELECTRONIC ENGINEERING**

February, 2017

Abstract

This thesis proposes a novel approach for functional connectivity studies of neuronal signal recordings based on statistical signal processing analysis in the frequency domain using Multivariate Partial Coherence (MVPC) combined with network theory measures. MVPC is applied to spike trains signals to make inferences about the underlying network structure. The presence of connections between single unit spike trains is estimated using both coherence and MVPC analysis. Scalability of MVPC analysis is investigated through application to simulated spike train data with up to 100 simultaneous spike trains generated from a network of excitatory and inhibitory cortical neurons. Stable MVPC estimates were obtained with up to 198 predictors in partial coherence estimates, using a combination of simulated cortical neuron data and additional Poisson spike train predictors. MVPC provides higher order partial coherence analysis for multi-channel spike trains signals, removing effects of common influences in pairwise connectivity estimates. Network measures applied to binary and weighted adjacency measures derived from coherence and partial coherence are compared to determine the differences in unconditional and conditional networks of spike train interactions. A combination of MVPC analysis along with network theory analysis provides a systematic approach for multi-channel spike train signals. The proposed method is applied to simulated and multi-electrode array (MEA) spike train data. The MEA data consists of 19 single unit channels recorded from a study of connectivity in a model of kainic acid (KA) induced epileptiform activity for mesial temporal lobe epilepsy (mTLE) in rat. The network theory analysis uses basic measures on both conditional and unconditional network, which highlights the differences in network structure and characteristics between the two representations. Complex analysis on conditional networks is useful in describing the properties of integration and segregation in the network.

Contents

Abstract	2
List of Figures	4
List of Tables	12
Acknowledgments	14
Author's declaration	15
1 Introduction	16
1.1 Motivation	18
1.2 Objectives	19
1.3 Thesis Outline	19
2 Literature Review	22
2.1 Brain levels of organization	23
2.2 Neurons	26
2.2.1 Local potentials	27
2.2.2 Action potentials	29
2.2.3 Synaptic signalling	31
2.2.4 Dendritic processing	34
2.3 Spiking neuron models	36
2.3.1 Hodgkin-Huxley model	37
2.3.2 Integrate-and-Fire neuron model	41
2.3.3 Izhikevich model	44
2.3.4 Cortical network model	45
2.4 Neuronal signals recording	46
2.4.1 Single unit recordings	47
2.4.2 MEA recordings	49
2.5 Spikes detection in MEA signals	50
2.6 Functional connectivity analysis.	51
2.7 Chapter summary	57
3 Spectral Analysis	59
3.1 Spectral estimation	60
3.2 Cross spectral estimation	61
3.3 Coherence analysis	62

3.4	Partial coherence analysis	64
3.5	Higher order partial coherence analysis	65
3.6	Multivariate partial coherence analysis	66
3.7	Chapter summary	71
4	Network Theory and Metrics	72
4.1	Network measures applied to neuronal interactions	73
4.1.1	Degree	76
4.1.2	Path length and network efficiency	77
4.1.3	Clustering coefficient	79
4.1.4	Modularity	80
4.2	Network motifs	81
4.3	Network small-worldness	83
4.4	Chapter summary	85
5	Spiking neuronal network model: Network measures analysis	86
5.1	Neuronal networks configuration	87
5.2	Scalability test for MVPC analysis	91
5.3	Conditional and unconditional network analysis	97
5.3.1	Node degree analysis on simulated network.	101
5.3.2	Path length analysis on simulated network.	103
5.4	Reproducibility of network motifs	111
5.5	Small world analysis: Binary and weighted network analysis . . .	116
5.6	Chapter summary	117
6	Application of network theory metrics to MEA epileptic seizure data	121
6.1	MEA data set-single unit spike train data from hippocampus . . .	122
6.2	Node degree	131
6.3	Path length	135
6.4	MEA: Clustering coefficient	140
6.5	MEA: Small-world network	142
6.6	MEA: Modularity	144
6.7	Chapter summary	146
7	Conclusions and Further Work	148
7.1	General Summary	148
7.2	Chapter Summaries and Conclusions	149
7.3	Future work	152
A		155
A.1	Neuronal parameters for cortical network model	156
A.2	Frequency of subgraphs in Network A	157
	References	158

List of Figures

2.1	Lateral surface of the cerebral hemisphere. Major regions of the brain: frontal, parietal, occipital and temporal lobes. Cerebellum is considered part of the motor system. (Figure from http://commons.wikimedia.org/)	23
2.2	Levels of organization in the central nervous system differentiated by spatial scales. (Figure from Trappenberg (2010))	24
2.3	The fifty two subregions based on cellular morphology and organization by Brodmann. (Gazzaniga et al., 1998)	26
2.4	Schematic view of a typical neuron. (Figure from http://commons.wikimedia.org/)	27
2.5	Ions moving across plasma through (a)The ion channel allows specific type of ions to flow across the channel, and (b)ion pumps maintain balance ions concentrations inside and outside the cell by forcing the ions to move against their concentration gradients when ion pumps break adenosine triphosphate, ATP into energy. (Figure from Elmslie (2001))	28
2.6	Schematic diagrams of the axon equivalent circuit. R_M , membrane resistance; R_I , intracellular resistance; C_M , membrane capacitance. (Figure from Kandel et al. (2000))	29
2.7	The trace shows depolarization and repolarization of the membrane potential. Depolarization phase occur when Na^+ ions enter the cell and decrease the internal ions negativity until the number of Na^+ ions entering the cell are more than the number of K^+ ions leaving the cell. Repolarization phase occur when the membrane permeability towards K^+ is increase and cause a flow of K^+ ions leaving the cell. Finally, inactivation of K^+ channels shifts the membrane potential to the initial resting state. (Figure from Freeman, 2005)	30
2.8	Synaptic signalling is initiated by electrical signalling followed by chemical event between neurons and finally producing excitatory postsynaptic potential (EPSP) or inhibitory postsynaptic potential (IPSP). (From Purves et al. (2008))	32
2.9	(A) Glutamat-induced EPSP generated when reversal potential, E_{rev} is more positive than the action potential threshold. (B) GABA-induced IPSP generated when E_{rev} is more negative than the action potential threshold. (Figure adapted from Purves et al. (2008))	33

2.10	High amplitude of EPSP generated at the synapse location will reduce after an attenuation results in lower amplitude of EPSPs at the soma. (Figure from Williams & Stuart (2002))	35
2.11	<i>Yellow</i> : Local nonlinear dendritic integration. <i>Green</i> : Longer dendritic pathway significantly attenuate EPSPs signal. <i>Brown</i> : Integration at the cell body followed by comparison against threshold level before firing an action potential. (Figure edited from London & Häusser (2005))	36
2.12	Representation of an equivalent electrical circuit for Hodgkin-Huxley model. This circuit includes a capacitor, two variable resistors to represent voltage-dependant conductances, a static resistor to represent small leakage current and a battery for each channel. (From Trappenberg (2010))	38
2.13	(A) The equilibrium functions (X_0 = probability for activation and inactivation events) and (B) time constants (in unit of msec) for variables n , m and h in HH model. (Membrane potential in unit of mV) (Figure from Trappenberg (2010))	40
2.14	Membrane potential of HH model shows a constant firing rate spike train initiated by constant external current with sufficient strength. (From Trappenberg (2010))	41
2.15	Integrate-and-fire neuron model integrates n input channels written as an α -function multiplied by a synaptic strength value w_j . An action potential will be fired when the total input potential reach a firing threshold. (Edited from Trappenberg (2010))	42
2.16	This figure illustrates a low-pass filter circuit at synapse location to filter presynaptic current $\delta(t-t_j^f)$ producing an input current pulse, $\alpha(t-t_j^f)$. The generated input current pulse will be attenuated to the soma. The IF model equivalent circuit in the soma consists of a resistor, R and a capacitor, C. The capacitor will be charged by the input current, $I(t)$. An output pulse, $\delta(t-t_i^f)$ is generated at time t_i^f when the voltage across capacitance increases and reach the threshold voltage, ϑ . (From Gerstner & Kistler (2002))	43
2.17	Output voltage of IF model with a threshold voltage, $\vartheta = 10\text{mV}$. (A) Constant current input with strength less than threshold voltage. (B) Constant input with strength greater than threshold voltage generating a spike train shown by dots in the upper figure. (From Trappenberg (2010))	44
2.18	An example of signals recorded using glass electrode showing rhythmic neuronal firing and non-rhythmic neuronal firing. (From Gandrathi et al. (2013)	48
2.19	An example of single unit activity of neuron recorded using microwire (black traces). Green circles show spikes event filtered using thresholding procedures. (Figure from David et al. (2010))	49

2.20	Intrinsic firing pattern of A) regular spiking neuron(top trace) in response to intracellular stimulation of prolonged depolarizing current (bottom trace) and B) fast spiking neuron (top trace) in response to the same stimulus current (bottom trace). (From Connors & Gutnick (1990))	51
2.21	Step by step of spike sorting methods; i) Signals filtering using band-pass filter. ii) Spikes detection using specified amplitude threshold. iii) Feature extraction to distinguish different features of the spikes. iv) Clustering to classify the signals into individual neuron spikes. (From Quiroga (2007))	52
2.22	Framework for estimation of pairwise neuronal interactions and connectivity analysis on MEA and simulated spike train signals. .	57
4.1	Binary and weighted network examples for A_b (left) in Eq. 4.1 and A_w (right) in Eq. 4.2. In the binary case the edge between two nodes is indicated by a line to indicate the presence of a connection from node i to node j . The strength of connection between two nodes can be represented by various thickness of the edge lines as shown in the weighted network (right).	75
4.2	A regular network (left) shows similar pattern of synchronized interactions across the entire network and a random network (right) shows random connections across a network with non-existence of specific pattern of interactions. Both regular and random networks consist of 20 nodes with an average of 4 connections per node. . .	76
4.3	Six possible sub-network patterns with undirected motifs ID: h_1 , h_2 , h_3 , h_4 , h_5 and h_6 from motif size, $M = 4$	82
4.4	This figure show (a) a regular network with high values of C and L , (b) a small world network with optimum connections with co-existence of segregation and integration properties represent high C and low L , and (c) a random network with low values of C and L . All of these networks consist of 20 nodes with an average degree of 4 connections per node.	84
5.1	2D planar sheet connectivity for simulation of excitatory (left) and inhibitory (right) neuron. Each character indicates the position of a neuron in Network A. 'O' is the presynaptic neuron, '+' are the postsynaptic neurons receiving excitatory inputs from 'O', '-' are the postsynaptic neurons receiving inhibitory inputs from 'O' and '•' are other neurons not receiving any input from 'O'. Designation of excitatory or inhibitory neuron for 2D connectivity in Network A is presented in figure 5.2.	89
5.2	Positions of excitatory and inhibitory neurons for simulation of Network A. Blue dots are the excitatory neurons and red dots are the inhibitory neurons. X and Y indicate the positions of neurons for pairwise connectivity analysis using different numbers of predictors in section 5.2.	89

5.3	Network B is a model of small-world network generated with rewiring probability of 0.05 (Watts & Strogatz, 1998). This network consists of 200 nodes that adopts similar connectivity pattern of excitation and inhibition.	90
5.4	Left column: histogram plot for the (a) output firing rates and (c) output COV for model A of 100 neurons. Right column: histogram plot for the (b) output firing rates and (d) output COV for model B of 200 neurons.	91
5.5	Figure shows different partial coherence values from MVPC analysis on 100 spike trains with different data lengths, 100 sec, 200 sec and 300 sec. Original coherence is included for comparison. Partial coherence should be less than or equal to ordinary coherence. Longer data lengths generate stable MVPC analysis.	92
5.6	Figure shows position of 10 predictor neurons located around neurons X and Y. Blue dots show the excitatory neurons and red dots show the inhibitory neurons.	93
5.7	Figure shows comparison between coherence and partial coherence values after gradually increasing the number of predictors from 1 to 10 neurons located around neurons X and Y as shown in Figure 5.6.	94
5.8	Figure (a) to (d) show neurons X and Y positioned in the middle of 2D network with the predictors highlighted in the green boxes. Blue dots show the excitatory neurons and red dots show the inhibitory neurons.	95
5.9	Figure shows comparison between coherence and partial coherence values after gradually increasing the number of predictors for pairwise interaction between neurons X and Y.	96
5.10	Figure shows comparison between coherence and partial coherence values after gradually increasing the number of predictors around neurons X and Y, with combination of additional 100 poisson spike trains.	98
5.11	Unconditional weighted network for simulated Network A with excitatory neurons (red) and inhibitory neurons (green). Links between nodes show weighted edges constructed from coherence analysis. Thicker edges show stronger connections.	99
5.12	Conditional weighted network for simulated Network A with excitatory neurons (red) and inhibitory neurons (green). Links between nodes show weighted edges constructed from multivariate partial coherence analysis. Thicker edges show stronger connections.	100

-
- 5.13 Top figure shows position of nodes using number 1 to 100 for simulated Network A. Blue and red circle distinguish between excitatory and inhibitory neurons, respectively. Middle figure shows color-coded graph of conditional node degree for Network A, and bottom figure shows the unconditional node degree for Network A. The values of degree for each nodes middle and bottom plots are arranged according to neurons positions as shown in top figure. Unconditional network shows high number of connections compared to the conditional network. Unconditional node degree range are higher between 6 to 80, compare to the conditional degree. Top figure clearly shows reduction in conditional node degree. Elimination of common effects reduces node degree in the range of 2 to 13 in conditional network as expected according to the simulated model of Network A. 102
- 5.14 Color-coded graphs of binary path length for unconditional network. Position of nodes is according to Figure 5.13(top). 106
- 5.15 Color-coded graphs of binary path length for conditional network. Position of nodes is according to Figure 5.13(top). 106
- 5.16 Color-coded graphs of weighted path length for unconditional network. Position of nodes is according to Figure 5.13(top). 107
- 5.17 Color-coded graphs of binary path length for conditional network. Position of nodes is according to Figure 5.13(top). 107
- 5.18 Binary and weighted path length distributions for unconditional and conditional connectivity of Network A. 108
- 5.19 Color-coded graphs of binary unconditional path length(top) and conditional path length(bottom) to show the shortest distance from neuron 1 to all other neurons in Network A according to the neurons position in Figure 5.13(top). Neuron 1 located at the top left of both graphs in dark blue color. Realistic distance can be seen in conditional path length, for example the highest path length is the distance to neuron 100 at the bottom right of the graph. 109
- 5.20 Color-coded graphs of weighted unconditional path length(top) and conditional path length(bottom) to show the weighted shortest distance from neuron 1 to all other neurons in Network A according to the neurons position in Figure 5.13(top). Weighted conditional path length in this graph is consistent with binary conditional path length in Figure 5.19 with gradual increment in the distance from Neuron 1 to all other neurons according to the location of the neuron. Weighted path length is also affected by the strength of interactions between neurons contributed by the neuronal excitatory and inhibitory activities. 110
- 5.21 The expected pattern for subgraph connecting 6 excitatory neurons with maximum number of edges according to Figure 5.1(left). . . 114
- 5.22 Conditional weighted network for simulated Network B. Links between nodes show weighted edges constructed from MVPC analysis. Thicker edges show stronger connections between nodes. . . . 118

5.23	Unconditional network for simulated Network B. This network does not exhibit SWN properties as expected for Network B. . . .	119
6.1	Simultaneous recordings of multiple hippocampal neuronal activity. This trace illustrates a sample representation of spontaneous hippocampal unit firing observed over a 600 sec. The colours of the raster represent the firing rate of the neurons ranging from black (slow), red (medium) and yellow (high).	123
6.2	Shape and size of the principle neurons in the Dentate Gyrus, CA1 and CA3. Number indicate the dendritic length of the cells. Figure from Shepherd (1990)	124
6.3	A: Schematic representation of the hippocampal recording sites. B: Histological verification of hippocampal recording sites with electrode placement was confirmed by the visible blue dye mark. . .	125
6.4	Time-line experimental protocols for kainic acid administration. Saline was injected intravenously after 10 min baseline recording followed by local injection of KA after 20 min saline injection. Effect of KA was recorded until 210 minute.	126
6.5	Unconditional weighted network for bilateral hippocampal single unit dataset at four different stages: a) baseline, b) saline injection, c) KA injection and d) effect of KA. Different nodes color show different subregions of the hippocampus; orange - CA3 Left, blue - CA1 Left, green - CA3 Right, pink - CA1 Right. Links between nodes show weighted edges constructed from coherence analysis. Thicker edges show stronger connections.	129
6.6	Conditional weighted network for bilateral hippocampal single unit dataset at four different stages: a) baseline, b) saline injection, c) KA injection and d) effect of KA. Different nodes color show different subregions of the hippocampus; orange - CA3 Left, blue - CA1 Left, green - CA3 Right, pink - CA1 Right. Links between nodes show weighted edges constructed from multivariate partial coherence analysis. Thicker edges show stronger connections. . . .	130
6.7	Top figure shows color-coded graph of node degree for conditional network, and bottom figure shows the node degree for unconditional network for 19 channels of spike train signals that are split into approximately 5 min time-blocks. The degree is depicted using similar color scale for both conditional and unconditional network. Node degree for unconditional network shows high number of connections compared to the conditional network. Elimination of common effects reduces node degree and most of the node degree in conditional network are less than 5 across all time-blocks except for node 13 with a maximum degree of 9. This node is considered as the possible network hub as seen in figure 6.6 where node 13 from left CA3 is a possible connector node for all subregions. This functional role for node 13 is hidden in unconditional network. . .	132

-
- 6.8 Node degree distribution in four stages; baseline, saline injection, KA injection and effect of KA, as described in Table 6.1. Top figure shows histogram for conditional network, and bottom figure shows histogram for unconditional network 134
- 6.9 Color-coded graphs of the shortest path length of conditional network for each pairwise connections at four different stages of the experiment. Each channel is presented as an individual node on X- and Y-axis. This depicted using color scale as shown on the right of the graph. 136
- 6.10 Boxplot graphs of (a) weighted path length distributions for unconditional network, (b) binary path length distributions for unconditional network, (c) weighted path length distributions for conditional network and (d) binary path length distributions for conditional network, for each 5 min time-block. X-axis of the graph presents the time-blocks up to 120 minutes. Black dotted line in each graph represents the characteristic path length. 137
- 6.11 Boxplot graphs of (a) characteristic path length distributions and (b) characteristic weighted path length distributions for overall 120 mins. X-axis of the graph presents the type of network. 138
- 6.12 Boxplot graphs of weighted and binary path length distributions for overall 120 mins. X-axis of the graph presents the type of network. The mean for both unconditional and conditional binary path length is 2. 139
- 6.13 Boxplot graphs of (a) binary clustering coefficient distributions for conditional network, (b) binary clustering coefficient distributions for unconditional network (c) weighted clustering coefficient distributions for conditional network, and (d) weighted clustering coefficient distributions for unconditional network, for each 5 min time-block. X-axis of the graph presents the time-blocks up to 120 minutes. 141
- 6.14 Graphs of normalized measure for clustering coefficient, C^w/C_{rand}^w (black line), normalized measure of shortest path length, L^w/L_{rand}^w (red line) and SWN index (blue line) for weighted conditional network. Each measure was calculated for each 5 min time-block up to 120 minutes. Black dotted line was plotted to show the limit of 1, where a network is said to be a small-world network if $S^w \gg 1$. This graph seems to indicate that the network topology is disrupted after KA injection but gain it optimal communication 15 minutes after KA injection. 143

- 6.15 Top: Color-coded modularity measure for 19 MEA nodes separated into 4 subregions as described in Table 6.2. The color-coded graph displays community detections on conditional network using 6 different colors to show the existence of different modules ranging between 4 to 6 modules for each 5 min time-block across the experiment. Each module is assigned a different color. X-axis of the graph presents the time-blocks up to 120 minutes. Bottom: Average of weighted modularity measure across experimental stages shows increasing number of weighted modularity after the injection.145

List of Tables

2.1	Specific functions correspond to each cortical region. (Gazzaniga et al., 1998)	25
5.1	Connectivity configurations for Network A and Network B.	88
5.2	High frequency occurrence subgraph for conditional network.	112
5.3	High frequency occurrence subgraph for unconditional network.	113
5.4	High frequency occurrence subgraph for sparse unconditional network with similar number of edges to conditional network.	115
5.5	Network analysis for binary and weighted conditional network with 600 seconds length of spike trains data for simulated Network B.	117
6.1	Experimental stages for connectivity analysis across time.	127
6.2	Four different regions of hippocampus with the corresponding nodes identification number and color of nodes in Figure 6.5 and 6.6.	127
A.1	Neuronal parameters for cortical neuron model of Network A and Network B (Halliday, 2005).	156
A.2	Frequency of subgraphs with motif size 3, 4 and 5 for conditional and unconditional Network A.	157

Acknowledgments

In the name of Allah, most Gracious, most Compassionate. The One who continually showers all of creation with blessings and prosperity without any disparity. The One who is most kind, loving and merciful. All praise be to Allah, with your blessings and mercy I managed to complete this thesis.

I would like to show my sincere gratitude to Dr David Halliday for his supervision, guidance, encouragement and supports throughout the years of research until the submission of this thesis. His enthusiasm and critical view on research has made a deep impression on me and I have learned so much from him. I am very grateful to my collaborator, Dr Mohd Harizal Senik, from Universiti Sains Malaysia (previously in the University of Nottingham) for kindly sharing his data.

A special thanks to the person who without him I would not have finished this thesis, the one who supported me as much as he could, my husband, Raja Khairulzaman Raja Hamid. My children Idris, Aisyah, Anis, Yusof, Husna and Khayra. Your laughs and smiles gave me the strength to pursue this study to the end.

I would like to express my sincere gratitude to my mother, Siti Khadijah Ismail for her continuous love and Dua.

Thank you to all Malaysian York family, particularly those that have made my time in the UK more pleasant.

Finally, I would like to acknowledge the Universiti Pertahanan Nasional Malaysia and the Ministry of Higher Education Malaysia for providing me with the financial supports to pursue this study.

Author's declaration

I, Siti Noormiza Makhtar, declare that this thesis titled, 'Conditional network measures using multivariate partial coherence analysis for spike train data with application to multi-electrode array recordings' is a presentation of original work and I am the sole author. This work has not previously been presented for an award at this, or any other, University. All sources are acknowledged as References.

List of Publications

- Makhtar, S. N., Halliday, D. M., Senik, M. H., & Mason, R. *Multivariate partial coherence analysis for identification of neuronal connectivity from multiple electrode array recordings*. In IEEE Conference on Biomedical Engineering and Sciences, pages 7782, 2014.
- Makhtar, S. N., Halliday, D. M., Senik, M. H., & Mason, R. *Conditional neuronal connectivity from multiple electrode array recordings using multivariate partial coherence analysis*. In British Neuroscience Association Abstracts, Volume 23: page 531, Festival of Neuroscience, Edinburgh, 2015.

Chapter 1

Introduction

Brain neuronal interaction has received much attention in the neuroscience field due to its functional connectivity properties, which offer better understanding of the brain cognitive and behavioural functions. Neuronal interaction in the brain happens through electrical signalling and chemical interaction within and between neurons. Interaction between billions of brain cells through electrical and chemical synapses create a massive neural network. Functional connection among the neurons produce complex network of information inside the brain. Different analysis and modelling methods are being developed by researchers to study the brain functional interactions. Studying the neuronal pattern of interactions may help us to understand the underlying processes of functional connectivity in the brain.

The process of sending, receiving and processing information in the brain involves two scales of complex networks, macro level and micro level. Macro level is the network for interaction between different part of the brain which classified into several regions according to its functionality. Micro level is the network of interaction between neurons that can be within the same region as well as across the different brain regions. Functionality of the brain while performing a task rely on the integration of information. Movement is an important activity that is coordinated by the nervous system and can include walking, flying or swimming depending on the species.

Currently there are various methods to record neurons electrical activity in the brain such as Electroencephalography (EEG), functional Magnetic Resonance Imaging (fMRI), Magnetoencephalography (MEG) and Multiple Electrode Array (MEA)(Fiecas et al., 2010; Salvador et al., 2005; Kostecki et al., 2011; Wu et al., 2007). Usage of these recording methods depends on what type of information is needed and each method has technological advantages which complement each other. Invasive experiments are very difficult and rare in humans. Studies of neuronal connectivity of the human brain normally focus on the macro level network using physiological signals recorded by EEG, MEG and fMRI. Animal like rat, cat and monkey have been used as a subject for brain research on micro level. MEA is widely been used to record neuronal signals in studies of neuronal connectivity at the micro level of the brain network. Network analysis on both level of brain network are equally important to understand the working process of the whole brain system.

Spike train signal represent the electrical activity of a neuron through continuous emission of action potentials. Simultaneous recording of electrical activity from a large number of interactive neurons provide important information about the system of interconnected neurons. Functional interaction between neurons can be estimated by statistical signal processing. One way to describe linear interactions between neuronal signals is using estimated auto- and cross-spectrum measurements undertaken in frequency domain (Rosenberg et al., 1998). Pairwise spike train analysis usually focus on pair of spike trains interaction without consideration of all possible influences from other spike trains that simultaneously recorded. These pairwise connectivity estimates can lead to inaccuracies and classified as unconditional interaction in this thesis. Pairwise spike train interaction with consideration of common influences from other spike trains is then classified as conditional interaction.

In order to analyse the neuronal connectivity, we need to comprehend the theory of networks. This subject is widely been used in neuroscience to explore

various type of network information like network metrics, network structures and network models. Application of these network methods on connectivity estimates derives from the statistical signal processing provide valuable insight on neurons functional network.

1.1 Motivation

With the emergence of Multiple Electrode Array (MEA) technology for recording high volumes of neuronal signals, appropriate statistical and computational methods of multivariate analysis become crucial. The construction of neuronal connectivity mapping from simultaneously recorded spike train signals has attracted numerous studies, based on different approach of signal and network analysis. Each one of the technique has their advantages and disadvantages in order to discover useful information from the physiological signals. The aim of this thesis is to use efficient method to demonstrate accurate interactions between large number of neurons and infer useful information from the neuronal connectivity using network theory. Previous studies of multivariate analysis in the frequency domain successfully described the possibilities to analyse brain connectivity from 90 channels of the human brain using fMRI signal (Salvador et al., 2005). Implementation of multivariate analysis in the frequency domain can help in identification of connected neurons using a representation of the signal as a point process for single unit spike trains. Moreover, frequency domain analysis is good for oscillations whereby signals localize in frequency.

Analysis of neuronal signals in the frequency domain will infer the pairwise association between neurons based on coherence for unconditional connectivity and partial coherence for conditional connectivity. The spike train signals are assumed to be stationary, stochastic and orderly. The multivariate partial coherence (MVPC) analysis will investigate conditional connectivity between associated neurons adapting the inverse covariance matrix technique (Dahlhaus, 2000). A computationally efficient approach to compute higher order partial coherence

using ordinary second order spectra will be adapted for simulated and MEA spike train data. Quantification of neuronal interactions is then established using network analysis.

1.2 Objectives

The objective of this study is to develop efficient techniques for analysing large number of spike trains and provide useful insights on the understanding of neuronal interactions. The proposed method will be implemented on simulated spike train data from cortical network model based on a conductance formulation to show the stability and scalability of MVPC analysis. Analysis on real data will be implemented on simultaneously recorded signals from four different hippocampal subregions in isoflurane-anaesthetized Lister-hooded rats before, during and after local unilateral kainic acid (KA)-induced epileptiform activity (Senik et al., 2013). MVPC analysis on MEA spike train data is expected to show the differences between conditional network and unconditional network properties. Different stages of the MEA recording is expected to show different outcome in network analysis due to the effect of KA on neuronal interactions. Connectivity mapping will help to visualize the functional interactions of each neuron within the same subregion as well as the functional interactions between neurons from different subregions.

1.3 Thesis Outline

This section provides an overview of the structure and contents of the thesis. The thesis contains eight chapters.

Chapter 1 is an introduction with overview of the project including motivation and objectives.

Chapter 2 describes the background information about brain organization and

neurons as the basic signalling unit. It includes the electrical and chemical properties of neuronal communication and examples of spiking neuron model. This continues with a description about different techniques for recording neuronal signal and preprocessing technique for the detection of spike trains from recorded neuronal signals.

Chapter 3 begins with the statistical and computational part of this work. It includes the mathematical tools and statistical measures for analysis of the spike trains. The focus is on coherence and partial coherence analysis to define the unconditional and conditional interactions, respectively. It continues with computational of multivariate partial coherence (MVPC) analysis as a stable and efficient technique to obtain conditional interaction from multiple spike trains. Finally, this chapter describes the functional connectivity strength of the neuronal network based on the measure of conditional and unconditional interactions.

Chapter 4 consists of several network metrics that are used for the functional connectivity analysis. This network analysis method consists of basic measure of degree, path length and clustering coefficient. It continues with more complex measure of modularity and motifs. Network measures are defined using mathematical descriptions and equations for binary and weighted networks. Network topology of small-worldness is also described in this chapter.

Chapter 5 presents the results from functional connectivity analysis on simulated signals of cortical neuron network model based on a conductance formulation. The simulated signals were used to test the scalability of MVPC for analysis of a large number of spike train signals. Network analysis is then conducted using network measures previously discussed in Chapter 4. Conditional network quantified based on MVPC analysis is then compared with unconditional network quantified by coherence analysis. This comparison highlight the importance of removal of common influence in multivariate connectivity analysis, so more accurate functional neuronal network from multiple spike trains can be constructed.

Chapter 6 presents the results from functional connectivity analysis on MEA signals using a combination of MVPC and network metrics. It begins with network analysis using basic measure of node degree, path length and clustering coefficient to compare the conditional and unconditional networks using binary and weighted connectivity strength. The comparisons highlight the importance of MVPC analysis in discovering network characteristics from simultaneously recorded neuronal signals. It continues with complex measures like small-worldness and modularity conditional network to highlight the network integration and segregation properties. All of these measures are analysed across time to look for any network disruption at different stages of the experiment.

Chapter 7 provides general summary and conclusions about the proposed techniques and their applications in the discovery of neuronal network properties. It also describes possible future directions on the issue of multivariate connectivity analysis.

Chapter 2

Literature Review

Neural science focuses on the principles of how the brain perceives, learns, processes information and stores memories. Brain carries out complex activities by integrating different types of mental processes. For example, an easy task of cycling a bike can be done when brain integrates several localized regions specialized for vision and motor control. Visual information on direction as well as movement of hands, arm, feet and leg need to be processed simultaneously in order to generate appropriate body movements to control the speed and direction of the bike. Communication between regions while performing functional mental processes is known as brain functional interactions. Brain region is a specialized areas of the brain consists of large group of neurons responsible for processing specific types of information. Studies at the cellular level of the brain can help to understand the basic concept of localized neuronal activity in certain brain regions. These concepts are useful to aid in demystifying the question of the relationship between localized regions with the specific functionalities by identification of the internal mechanisms.

Neurons as the basic elements of the brain play an important role to convey information within and between neurons through neuronal signalling and synaptic transmission. Functional connection among the neurons within the same brain region or from different brain regions produce complex network of information. For example, information of images with different shapes and colors can stimu-

late and activate different group of neurons. Due to the neuron ability to select a specific pathway during transmission of information (Kandel et al., 2000), there are possibilities to construct the connectivity mapping of neurons by measuring the electrical activities of the neurons on different mental processes. Communication behaviour between neurons can be monitored using electrical recording techniques that are able to capture signals from single-unit and multi-unit neuronal activities.

This chapter provides background information about organization of the brains and neurons as the basic signalling unit that includes the electrical and chemical properties for neuronal communication. The review of spiking neuron models is presented to show the development of computational models for spiking neuron signal, specifically on selection of parameters that take into account the characteristics of neuronal signalling and synaptic transmission.

2.1 Brain levels of organization

The brain is constructed from several cortical regions with their own specific function (see Figure 2.1). Information is transmitted between and within re-

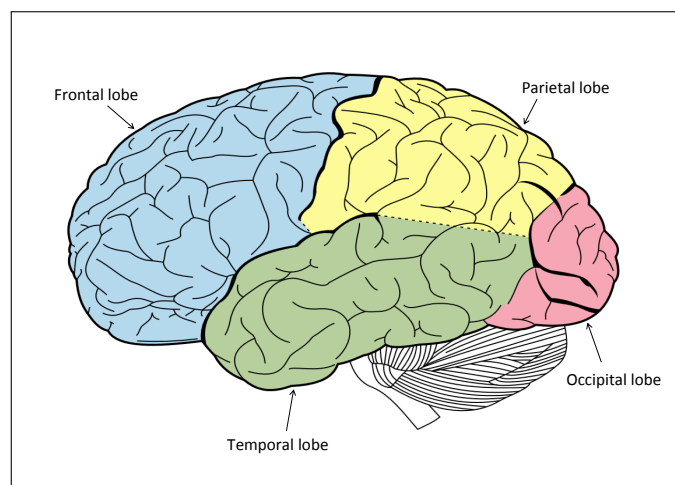


Figure 2.1: Lateral surface of the cerebral hemisphere. Major regions of the brain: frontal, parietal, occipital and temporal lobes. Cerebellum is considered part of the motor system. (Figure from <http://commons.wikimedia.org/>)

gions through neuronal communications. The information is then processed by continuous integration among cortical regions. The challenges to map brain functionalities need comprehensive understanding of the complex biological systems in the brain. Thoughtful studies of anatomical and physiological concept is necessary for the initial stage of modelling and analysis of the functional connectivity.

Organization of brain levels illustrates a complex system of the brain as a combination of several different structures (see Figure 2.2). Separation on differ-

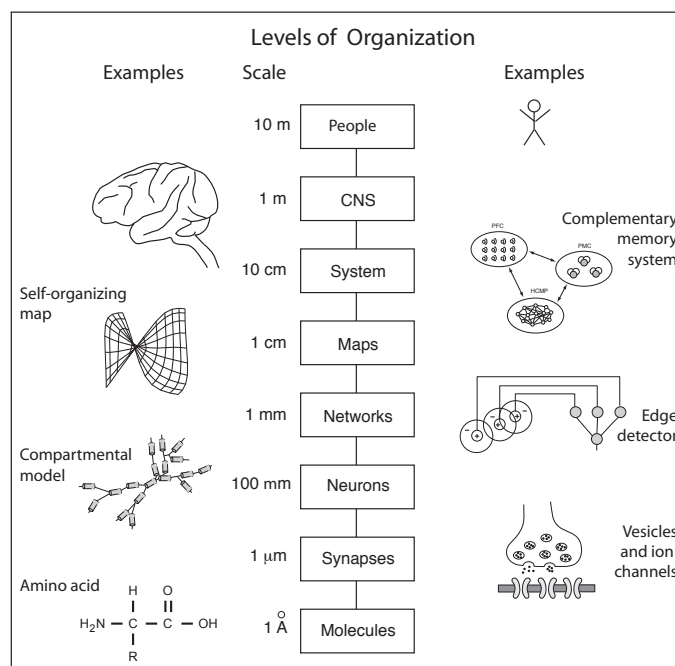


Figure 2.2: Levels of organization in the central nervous system differentiated by spatial scales. (Figure from Trappenberg (2010))

ent levels comprehend the detail structure of complex information networks from the smallest scale at the level of synapse towards the largest scale at the level of a whole brain as a complex system. Specific physiological theories of selected brain level can be the essential basis and reasonable consideration for devising an algorithm of communication in neuron networks. Implementation of computational estimation for functional networks depends on detail understanding of brain levels because each level will contribute to the information transfer in a different ways (Tononi et al., 1998).

To begin with the highest level of brain organisation, it might be useful to introduce the anatomical structure of the brain. Brain which is known as the most important part in central nervous system is divided into two hemispheres by longitudinal fissure that runs from the frontal lobe to the occipital lobe. The left and right hemispheres are integrated by inter-hemisphere communications through a bundle of neural fibres called corpus collasum (Gazzaniga et al., 1998). At the system level, each cortical region corresponds to main functions of central nervous system (See Table 2.1).

Table 2.1: Specific functions correspond to each cortical region. (Gazzaniga et al., 1998)

Region	Function
Frontal lobe	Motor controller for planning and control of movement.
Parietal lobe	Centre of sensory systems.
Temporal lobe	Control of audition, learning and memory.
Occipital lobe	Vision activities.

Functionally, four major regions of the brain are finely divided into fifty two subregions according to cellular morphology and organization and known as Brodmann's area (see Figure 2.3). For example functional neurons specialized in visual processing located in occipital lobe are further classified into area 17, 18 and 19 in order to illustrate detail neuronal pathways in the region. (Gazzaniga et al., 1998)

Despite different subregions with particular functionalities, brain essentially works as a global and dynamic complex system by integration of incoming information with present information in memory. In order to understand the processes underlying functional interactions of the central nervous system, it is useful to have in mind the essential aspects of neuronal information-processing and signalling elements. Organisation of actions within and between each subregion occur with the transmission of electrical signals and biochemical reactions among several neuronal assemblies. Recognition of neuronal assembly depends on the structure of neurons and their processes while receiving, transmitting and passing on information. Different functional capabilities of cortical areas are related

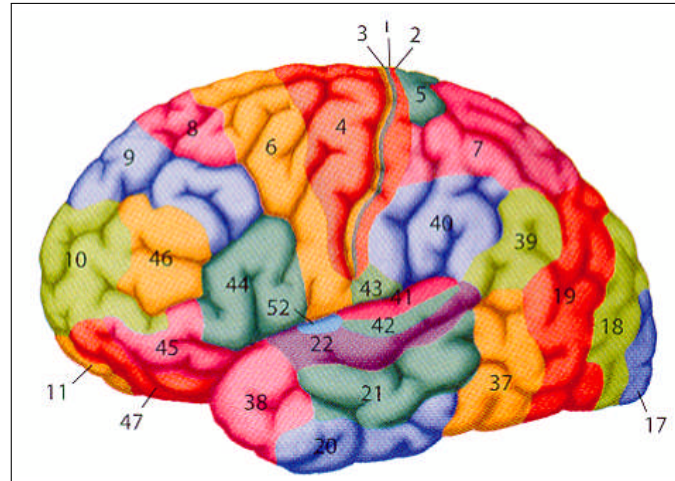


Figure 2.3: The fifty two subregions based on cellular morphology and organization by Brodmann. (Gazzaniga et al., 1998)

to different subregions anatomical structure (Sporns et al., 2000). Localization of electrical signals within cortical regions yield different circuitry pattern for each functional activities (Buzsáki et al., 2004, 2012). Integration between subregions generate various connectivity patterns among neuronal assembly during functional activities (Cabeza & Nyberg, 1997, 2000). Further characterisation of neuronal assembly network needs deeper understanding of neurons as the basic signalling units of the brain.

2.2 Neurons

The diversity of connections inside brain link approximately 10 billion nerve cells using a few stereotype electrical signals (Nicholls et al., 1992). At this level of brain organization, it is important to understand the essential aspects of the electrical signalling and chemical interaction within and between neurons. Despite the great variance of neurons morphology, typically neuron consists of dendrites, cell body, axon and axon terminal with specialized function for each part (see Figure 2.4). Dendrites receive inputs and forward the signals towards the cell body where the inputs will be integrated as an information in a form of electrical signals. The signals propagate along the axon towards axon terminals through

shared intracellular volume called the cytoplasm.

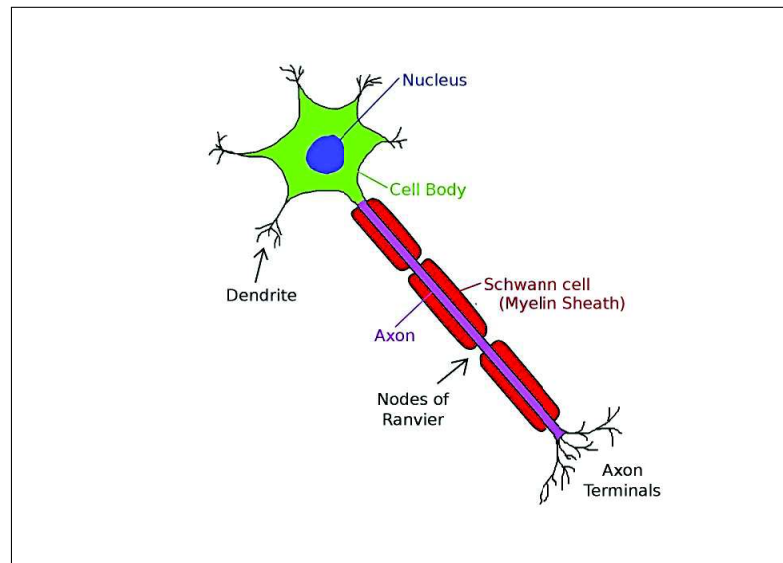


Figure 2.4: Schematic view of a typical neuron. (Figure from <http://commons.wikimedia.org/>)

2.2.1 Local potentials

Central nervous system transmits information by interplay of two types of electrical signals called localized potential and action potential. Localized potentials are produced physically by sensory stimulation and neurotransmitters activation (see Section 2.2.3). Transmission of information within neuron occurs through passive propagation of these potentials. Increase distance from the source gives exponential decrement of the localized potentials which may be caused by the membrane resistance and capacitance. Ions flow in axoplasm, the intracellular fluids of axon can be described as a current flow in a poorly insulated cable (Aidley, 1989).

Generation of electrical signals results from the movement of ionic currents such as sodium(Na^+), potassium(K^+), calcium(Ca^{2+}) and chloride(Cl^-) across the cell membrane. Movement of ions are regulated by the selective permeability of the membrane that allows diffusion of selected ions through the ion pumps and

ion channels (see Figure 2.5). The distribution of different types of ion channels and ion pumps across the cell membrane determine the resulting membrane capacitance. Most of the ion channels are highly selective permitting specific type of ions to flow across the channels. Similar properties for ion pumps which highly selective to ions in order to restore balance in the ion concentrations inside and outside the cell (Dayan & Abbott, 2005).

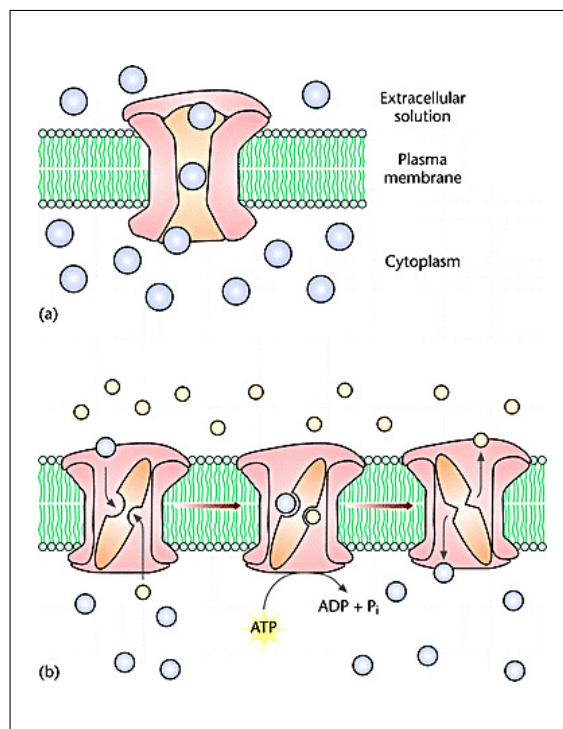


Figure 2.5: Ions moving across plasma through (a)The ion channel allows specific type of ions to flow across the channel, and (b)ion pumps maintain balance ions concentrations inside and outside the cell by forcing the ions to move against their concentration gradients when ion pumps break adenosine triphosphate, ATP into energy. (Figure from Elmslie (2001))

Ionic conductions across neuronal membranes can be represented as voltage and current changes in an equivalent electrical circuit. Considering resistive, capacitive and conductive measures of neuronal membrane, the equivalent circuit model essentially presents the transmission cable properties of neurons (see Figure 2.6) (Ruben, 2001). Propagation of electrical potentials along axon subject to the membrane resistance, R_M and intracellular resistance, R_I . R_M is the transverse resistance of the membrane represents the ion channels. The distance of propagations are subjected to relative differences between R_M and R_I . Mem-

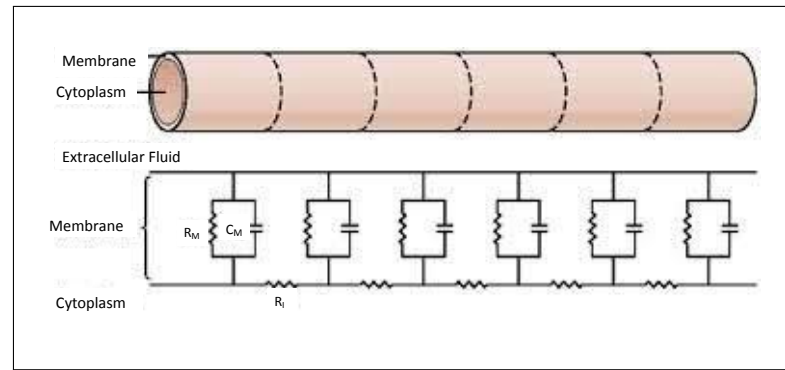


Figure 2.6: Schematic diagrams of the axon equivalent circuit. R_M , membrane resistance; R_I , intracellular resistance; C_M , membrane capacitance. (Figure from Kandel et al. (2000))

brane capacitance, C_M represents the capacitive properties of neurons membrane with its capabilities in separating ionic charges between extracellular fluids and cytoplasm.

2.2.2 Action potentials

Movement of ions inward and outward of the neurons is controlled by different internal and external membrane concentrations. This leads to the establishment of electrical potential difference caused by high concentration of potassium (K^+) inside of the membrane and high concentration of Sodium (Na^+) outside of the membrane. Equilibrium point is reached if the flow of ions inside and outside of the ions are in balance.

At equilibrium, the cell will have a steady resting condition with excess of negative charges in the intracellular solution compared to extracellular solution (Dayan & Abbott, 2005). The negative potential inside the cell membrane known as resting membrane potential, V_m typically about -65 mV. The magnitudes of these potentials possibly range between -40mV and -100mV depending on the distribution of electrically charged ions on either side of the membrane and the selective permeability properties of the membrane (Hodgkin & Huxley, 1952). Reduction of membrane resting potential towards 0mV is called depolarization; and increase negativity of membrane potential is called repolarization.

Action Potential is automatically excited when membrane potential reaches the threshold level (see Figure 2.7). Generation of action potential is controlled by moving ions across voltage-gated Na^+ channel and voltage-gated K^+ channel (Ruben, 2001). Rapid membrane depolarization increase the probability of voltage-gated Na^+ channel being open. After the gate is open Na^+ ions enter the cell and influence neighbouring Na^+ channels to be activated as well. This increase the membrane permeability towards Na^+ ions and cause increased amount of Na^+ currents entering the cell which eventually decreased internal ions negativity. Depolarization continues until the number of Na^+ ions entering the cell are more than the number of K^+ ions leaving the cell. In less than one millisecond, action potential will be generated when depolarization shifts membrane potential from resting state towards threshold level and overshoot the 0mV level (Ruben, 2001).

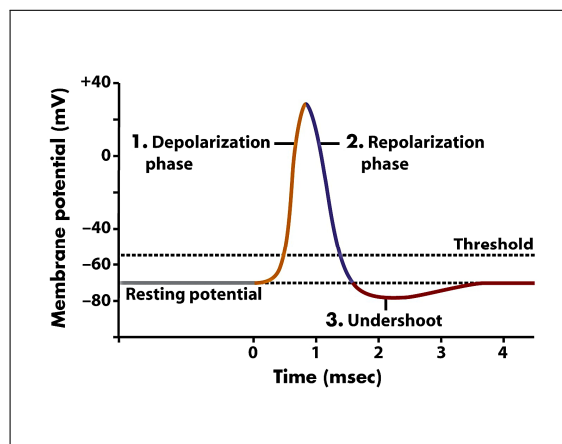


Figure 2.7: The trace shows depolarization and repolarization of the membrane potential. Depolarization phase occur when Na^+ ions enter the cell and decrease the internal ions negativity until the number of Na^+ ions entering the cell are more than the number of K^+ ions leaving the cell. Repolarization phase occur when the membrane permeability towards K^+ is increase and cause a flow of K^+ ions leaving the cell. Finally, inactivation of K^+ channels shifts the membrane potential to the initial resting state. (Figure from Freeman, 2005)

Repolarization phase occur when voltage-gated K^+ channels are activated simultaneously with inactivation of Na^+ channel. During this phase, the intracellular potential is decreasing towards resting potential due to increased membrane permeability towards K^+ . Flow of K^+ ions shifts the membrane potential to the

initial resting state. This phase will continue and shifts the membrane potential to undershoot level due to increasing number of K^+ ions. Inactivation of K^+ channels eventually shifts the membrane potential to the initial resting state (Ruben, 2001). Refractory period is a short duration where the action potential needs to complete the initial process before initiation of the next action potential. A spike train of action potentials may be produced by prolonged depolarization.

All-or-nothing property of action potential results in automatic response of membrane potential not related to the initial stimulus (local potential) duration and amplitude (Nicholls et al., 1992). Undistorted and rapid propagation of action potentials along myelinated axon, can be described as information conveyed as an electrical conduction within a good insulated cable that is strengthened by regenerative action from the nodes of Ranvier. Voltage-gated ion channels mediate the active signalling process of action potential along the axon without reducing the magnitude of action potential over the distance. Information received by dendrites are integrated in cell body and transmitted to axon terminal through the propagation of action potentials. Action potentials arriving at axon terminal then initiate the chemical synapse to convey the information towards another neuron.

2.2.3 Synaptic signalling

Synaptic signalling is a neuronal communication mechanism that occurs at the molecular level of the brain. Synaptic signalling initiated after arrival of action potential in presynaptic axon terminal followed by opening of voltage gated Ca^{2+} channels. An influx of Ca^{2+} ions into the terminal area triggers vesicles containing neurotransmitters to bind with receptors located at presynaptic membrane (see Figure 2.8). The chemical reactions called exocytosis will release neurotransmitters that carry the information from presynaptic neuron into the synaptic cleft. There are two main types of neurotransmitters; excitatory neurotransmitter (amino acid glutamate) & inhibitory neurotransmitter (γ -amino-butyric-acid,

GABA). Both types of neurotransmitters will bind with receptors at postsynaptic neurons and form an ions channels (Nicholls et al., 1992; Purves et al., 2008).

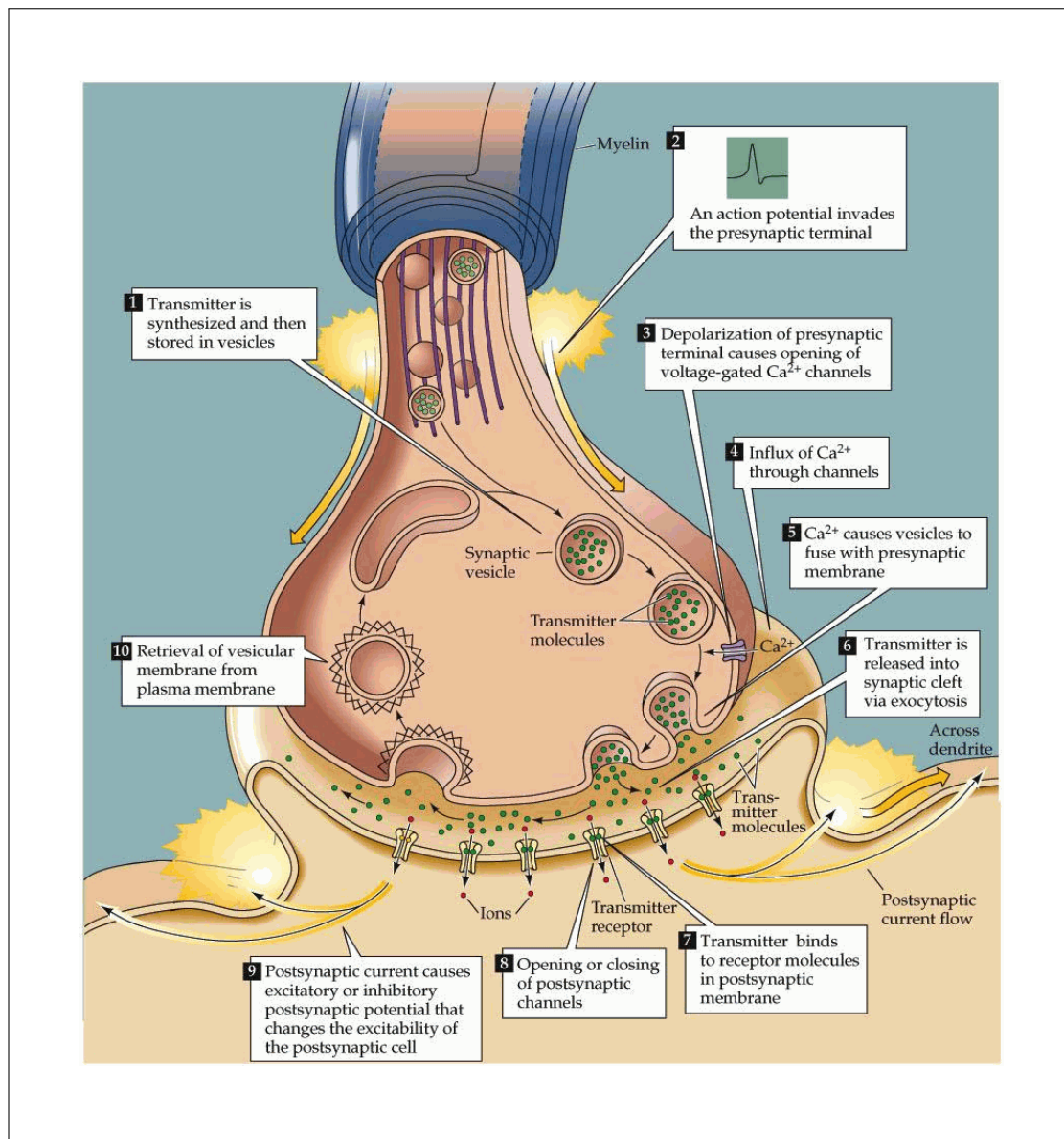


Figure 2.8: Synaptic signalling is initiated by electrical signalling followed by chemical event between neurons and finally producing excitatory postsynaptic potential (EPSP) or inhibitory postsynaptic potential (IPSP). (From Purves et al. (2008))

Chemical binding between neurotransmitters and receptors will cause an opening or closing of the ion channels leading to ionic flow through the membrane thereby produce a conductance change in postsynaptic membrane. Changes in the membrane conductance generate post synaptic current (PSC) which eventu-

ally produces postsynaptic potential (PSP). PSPs determine the probability of action potentials firing in the postsynaptic neurons whereby PSPs that increase the probabilities for action potential firing is known as excitatory postsynaptic potential (EPSP) and PSPs that reduce the probabilities of action potential firing is known as inhibitory postsynaptic potential (IPSP). Reversal potential is the membrane potential when the net of ionic flows through an ion channel is equal to zero. Generation of EPSPs and IPSPs depends on comparison of reversal potential against action potential threshold (see Figure 2.9). EPSP is generated when reversal potential is more positive than action potential threshold and IPSP is generated when reversal potential is more negative than action potential threshold (Purves et al., 2008).

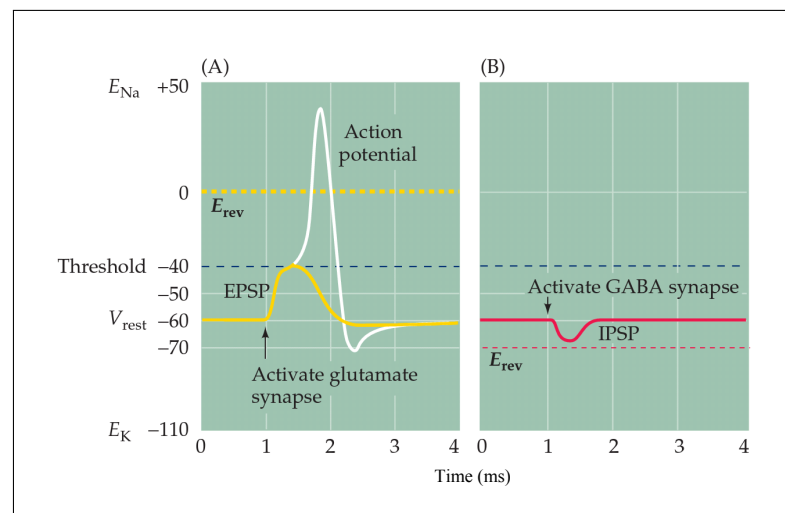


Figure 2.9: (A) Glutamat-induced EPSP generated when reversal potential, E_{rev} is more positive than the action potential threshold. (B) GABA-induced IPSP generated when E_{rev} is more negative than the action potential threshold. (Figure adapted from Purves et al. (2008))

Significant properties of synaptic interaction between neurons can be represented as a basis of the connectivity patterns between neurons. Two examples of neuronal connectivity patterns are synaptic divergence and synaptic convergence. Synaptic divergence is a combination of outputs from single axon terminal towards multiple postsynaptic dendrites. Synaptic convergence is a combination of inputs from multiple axon terminals onto a single postsynaptic neuron (Shepherd, 1990). For example, a single motor neuron may integrate up to 10,000

combination of inhibitory and excitatory signals (Kandel et al., 2000). Temporal and spatial distribution in convergence and divergence synapse will give an impact on generation of action potentials at postsynaptic neurons (Williams & Stuart, 2002).

2.2.4 Dendritic processing

Postsynaptic neurons receive excitatory and inhibitory inputs from hundreds of presynaptic neurons through various type of neurotransmitters during chemical synapse (Nicholls et al., 1992). Active dendritic processing generally consists of three main processes; integration, comparison and decision making (London & Häusser, 2005). The electrical information from thousands of synapses which converged into a postsynaptic neuron will be integrated by summation of EPSPs and IPSPs. The summed potentials result in depolarization or repolarization of the cell membrane. Sufficient depolarization will change the membrane potential towards the threshold level and eventually trigger the action potential at cell body (Hodgkin & Huxley, 1952). In short, firing of one spike of action potential is a result from integration of EPSPs and IPSPs that reach the threshold level. However, neuronal firing patterns affected by temporal and spatial factor of passive dendritic processing (Euler & Denk, 2001).

Integration of EPSPs and IPSPs is subject to temporal delay in the transmission of electrical potentials caused by the relative distance between synapse location and the cell body. Furthermore, amplitude of PSPs along the dendrites affected by location of voltage-dependent ion channels at the dendritic membrane due to possible leakage of ions along the dendrites during transmission which reduce the amplitude of PSPs arriving at the cell body (see Figure 2.10) (Gabbiani & Midtgaard, 2001; Williams & Stuart, 2002). Dendritic processing mechanisms depends on interrelation between dendritic functional properties and morphological structures. Spatial organization of ion channels and neurotransmitter receptors in different type of neurons form different mechanism of dendritic

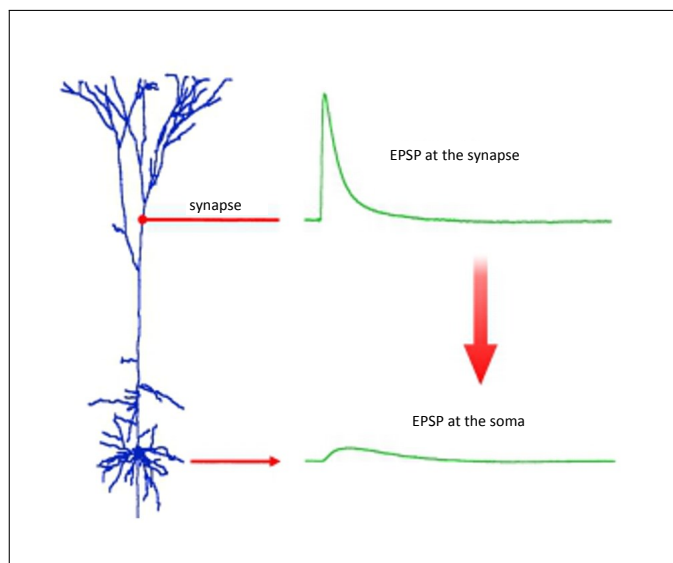


Figure 2.10: High amplitude of EPSP generated at the synapse location will reduce after an attenuation results in lower amplitude of EPSPs at the soma. (Figure from Williams & Stuart (2002))

processing (see Figure 2.11). For example, adjacent location of several synapses may cause local dendrite nonlinear integration of simultaneous inhibitory and excitatory potentials and separation between synaptic location will result in parallel linear integration of EPSPs in the cell body. Position of IPSPs along the EPSPs pathways toward the cell body will also reduce the probability of action potential firing (London & Häusser, 2005).

Dendrites as a sophisticated computational machine process information from synaptic input by combination of various dendritic mechanisms. Complex dendritic mechanisms however can be modelled to study on single dendrite of single identified neuron (London & Häusser, 2005). Focusing on particular dendrite can help to describe the specific properties of its functional synaptic processing mechanisms. Computational description is necessary to classify the dendritic processing into several processes such as signal filtering, convolution and pattern recognition (London & Häusser, 2005). Representation of convergence of synaptic input by the integration between numerous stimulation sites can be used along with axonal processing mechanisms to determine the firing patterns of the neurons for comprehensive illustration of functional effect of single neuron. Established

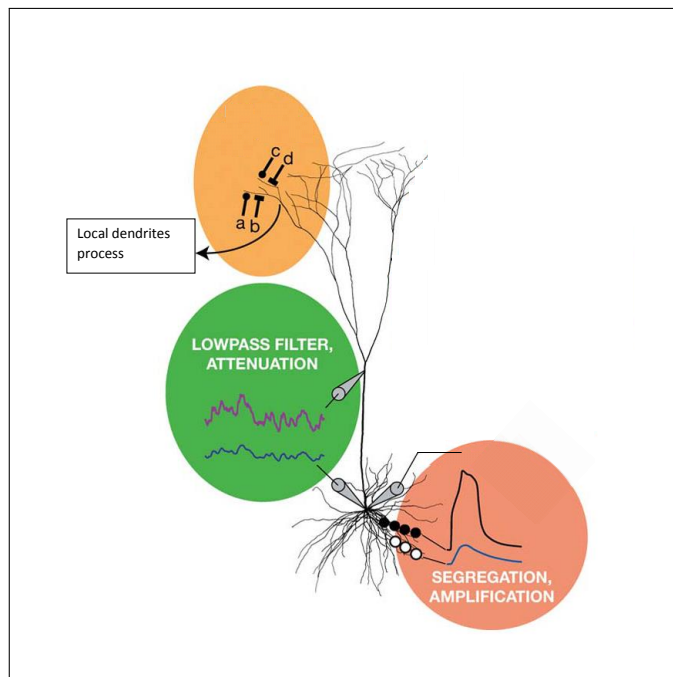


Figure 2.11: *Yellow* : Local nonlinear dendritic integration. *Green* : Longer dendritic pathway significantly attenuate EPSPs signal. *Brown* : Integration at the cell body followed by comparison against threshold level before firing an action potential. (Figure edited from London & Häusser (2005))

functional synaptic map may be associated to functional contributions of the neuron on the networks it belongs to (Euler & Denk, 2001).

2.3 Spiking neuron models

Different types of neuron model have been constructed based on different findings in biophysical, anatomical and physiological properties (Dayan & Abbott, 2005). The development of appropriate model considering several main characteristics of neuronal signalling and synaptic transmission is crucial so that essential communication principles between neurons can be represented. The behaviour of brain interactions can be mapped out by taking into account the functional contribution of neurons in transmitting the information within and between neurons.

Computational and mathematical modelling have long been used to study the complex electrical and chemical interaction of the neurons that lead to the

generation of action potentials. As discussed in the previous section, variable measures of resistance, capacitance and conductance of neuronal membrane exist with respect to the physiological properties of the neuron. Description of such properties by electrical circuits and mathematical models is useful to study the information transmission mechanisms within and between neurons. Three types of neurons modelling approaches briefly described in this section; 1) Hodgkin-Huxley model to describe the functional properties of voltage-dependent membrane conductances in firing an action potential by approximating the ion-channel dynamics (Trappenberg, 2010); 2) Integrate-and-fire model to describe functional properties of transmitter-dependent synaptic conductances by approximating the dynamic responses after the integration of presynaptic input (Dayan & Abbott, 2005); 3) Izhikevich model to describe the dynamical properties of various type of neurons; and 4) cortical neural network model for simulation of neuronal network.

2.3.1 Hodgkin-Huxley model

The firing of action potential is initiated by depolarization of membrane potential above the threshold level. Hodgkin-Huxley (HH) model is approximating the mechanism to fire an action potential by taking into account the dynamic properties of moving ions through the voltage-gated ion-channel (Trappenberg, 2010). HH model presents the action potential generation mechanisms by the probability that the channel is active for ion conducting state. The membrane conductance in this model is approximated by the movement of ions across the cell membrane through three different channels. Figure 2.12 shows HH model as an equivalent electric circuit. The total movement of ions, I_m results from the net movement of a sodium current I_{Na} , a potassium current I_K , and a small leakage current I_L from non-gated ion channels,

$$I_m = I_{Na} + I_K + I_L. \quad (2.1)$$

The membrane electrical potentials can be measured by the relation between the ionic currents, I_{ion} with the electrical conductance, \bar{g}_{ion} which controls by the

number of ion channels and the membrane permeability. Such relation is given by the Ohm's law,

$$I_{\text{ion}} = \bar{g}_{\text{ion}}(V - E_{\text{ion}}) \quad (2.2)$$

which corresponds to each ionic component of I_{Na} , I_{K} and I_{L} . E_{ion} is the equilibrium potential for each channels when no ionic current moving across membrane due to the same concentration inside and outside the cell.

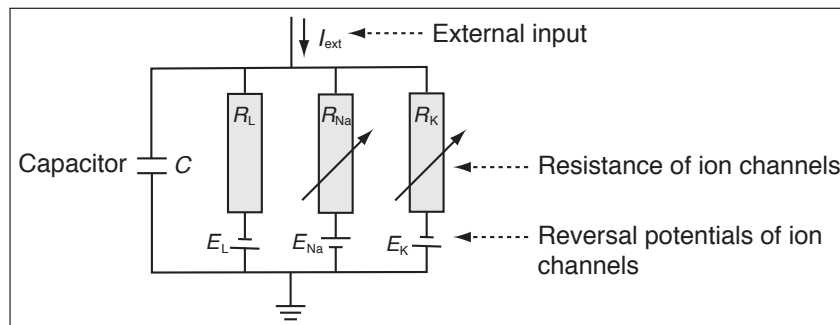


Figure 2.12: Representation of an equivalent electrical circuit for Hodgkin-Huxley model. This circuit includes a capacitor, two variable resistors to represent voltage-dependant conductances, a static resistor to represent small leakage current and a battery for each channel. (From Trappenberg (2010))

Following to the membrane conductions which are controlled by a set of ion channels, the dynamic properties of the membrane can be determined by the probabilities of activation and inactivations of the ion channels (K^+ and Na^+). The probabilities for the voltage dependence ionic channels to open the gate and allow the flow of ions can be described by three dynamic variables; 1) n indicates the activation of the potassium channels, 2) m indicates the activation of sodium channels and 3) h indicates the inactivation of the sodium channels. The dimensionless variables n , m and h were assumed to vary with time and have a functional dependence on the voltage. The probabilities for ionic flows through potassium channels controlled by four identical events of n , whereby the probabilities for ionic flows through sodium channels controlled by three identical events of m and one event of h . Such probabilities lead to the estimation of the

sodium and potassium conductance,

$$\bar{g}_{\text{Na}}(V, t) = g_{\text{Na}}m^3h \quad (2.3)$$

$$\bar{g}_{\text{K}}(V, t) = g_{\text{K}}n^4. \quad (2.4)$$

These variables were selected by Hodgkin and Huxley to fit with the experimental data and can be expressed by the following formula

$$\frac{dn}{dt} = -\frac{1}{\tau_n(V)} [n - n_0(V)] \quad (2.5)$$

$$\frac{dm}{dt} = -\frac{1}{\tau_m(V)} [m - m_0(V)] \quad (2.6)$$

$$\frac{dh}{dt} = -\frac{1}{\tau_h(V)} [h - h_0(V)]. \quad (2.7)$$

Figure 2.13(A) describe the equilibrium potentials (in mV) for each variables in a function of V with resting potential is equal to 0 mV. The flip trend of $h_0(V)$ plot relative to $m_0(V)$ distinguish the event of inactivation and activation of sodium channels. Activation of sodium and potassium channels depicted by the same trend plotted by $m_0(V)$ and $n_0(V)$, respectively (Dayan & Abbott, 2005). At resting potential of 0 mV, the probability for sodium channel to be activated is less than 0.1 which is significantly low compared to the event of channels inactivation with probability 0.6. In contrast, the probability for potassium channel to be activated is equal to 0.35. This probability values means that the sodium conductance is much smaller than the potassium conductance at equilibrium potential of 0 mV.

The time constant τ_n is the duration for variable, n to approach the equilibrium value of n_0 within a fixed voltage value, V (Gerstner & Kistler, 2002). The same condition applied for other variables of m and h . Figure 2.13(B) shows the time constant (in msec) that controls the rate of change for the three variables. At resting potential of 0 mV, τ_h is the highest (0.85 msec) followed by τ_n (0.55msec) and τ_m with the lowest time constant (0.1 msec). This shows that the sodium channels activated rapidly compared to the potassium channels in

response to external stimulation leading to an increase flow of sodium into cell. Sufficient depolarization of the cell membrane will trigger the action potential.

The static conductance from leakage channel remain as constant,

$$\bar{g}_L = g_L. \quad (2.8)$$

From equation 2.3, 2.4 and 2.8, summation of the three ionic currents can be expressed as (Trappenberg, 2010)

$$\sum_{\text{ion}} I_{\text{ion}} = g_K n^4 (V - E_K) + g_{\text{Na}} m^3 h (V - E_{\text{Na}}) + g_L (V - E_L). \quad (2.9)$$

HH model equivalent circuit consists of two variable resistors to present voltage dependent ion channels, a constant resistor to represent leakage current, a battery to set the reversal potentials of each ion channel and a parallel capacitor, C to present electric charges stored by the neurons. The changes of the mem-

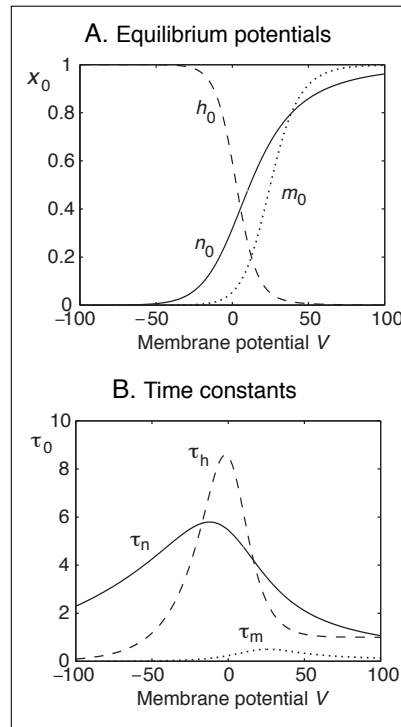


Figure 2.13: (A) The equilibrium functions (X_0 = probability for activation and inactivation events) and (B) time constants (in unit of msec) for variables n , m and h in HH model. (Membrane potential in unit of mV) (Figure from Trappenberg (2010))

brane potential with time according to the behaviour of HH model circuit can be expressed in a first order differential equation,

$$C \frac{dV}{dt} = - \sum_{\text{ion}} I_{\text{ion}} + I(t). \quad (2.10)$$

External input, $I(t)$ represents an external current which may come from presynaptic potentials. Inserting equation 2.9 into equation 2.10 and rewriting equation 2.5 to equation 2.7 yields the standard differential equations of HH model, (Trappenberg, 2010)

$$C \frac{dV}{dt} = -g_K n^4 (V - E_K) - g_{Na} m^3 h (V - E_{Na}) - g_L (V - E_L) + I(t) \quad (2.11)$$

$$\tau_n(V) \frac{dn}{dt} = -[n - n_0(V)] \quad (2.12)$$

$$\tau_m(V) \frac{dm}{dt} = -[m - m_0(V)] \quad (2.13)$$

$$\tau_h(V) \frac{dh}{dt} = -[h - h_0(V)]. \quad (2.14)$$

Figure 2.14 illustrates an example of HH neuron model producing a constant firing rate spike train in response to a constant external current.

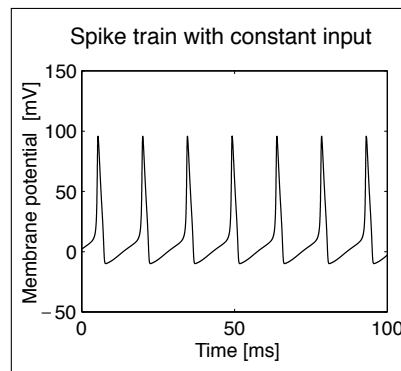


Figure 2.14: Membrane potential of HH model shows a constant firing rate spike train initiated by constant external current with sufficient strength. (From Trappenberg (2010))

2.3.2 Integrate-and-Fire neuron model

Integrate-and-fire (IF) neuronal model integrates multiple non-interacting presynaptic inputs written as an a -function with individual synaptic strength value, w_j

(See Figure 2.15). α -function is the time course for the postsynaptic current which maybe caused by the chemical interaction of neurotransmitter from presynaptic toward postsynaptic membrane (Trappenberg, 2010). The total input current to

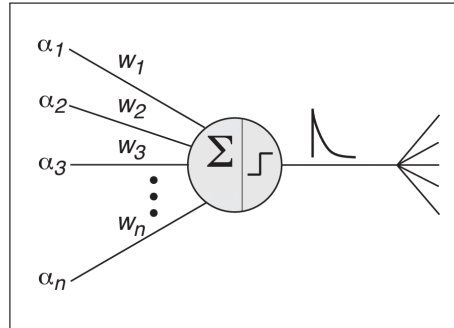


Figure 2.15: Integrate-and-fire neuron model integrates n input channels written as an α -function multiplied by a synaptic strength value w_j . An action potential will be fired when the total input potential reach a firing threshold. (Edited from Trappenberg (2010))

the postsynaptic neurons expressed by the summation of individual presynaptic events,

$$I(t) = \sum_j \sum_{t_j^f} w_j \alpha(t - t_j^f), \quad (2.15)$$

where t is the postsynaptic firing time and t_j^f denotes the presynaptic firing time for each synapses, j (Trappenberg, 2010).

Figure 2.16 shows the equivalent electrical circuit for IF neuron model located in the soma. The circuit consists of parallel components of a resistor and a capacitor. The input current, $I(t)$ will split into a resistive current, I_R and a capacitor charging current, I_C

$$I(t) = I_R + I_C. \quad (2.16)$$

Referring to membrane potential, $v(t)$ equation 2.16 and can be expressed as

$$I(t) = \frac{v(t)}{R} + C \frac{dv}{dt}. \quad (2.17)$$

Multiplying equation 2.17 with R and replace RC with a time constant, τ_m yield

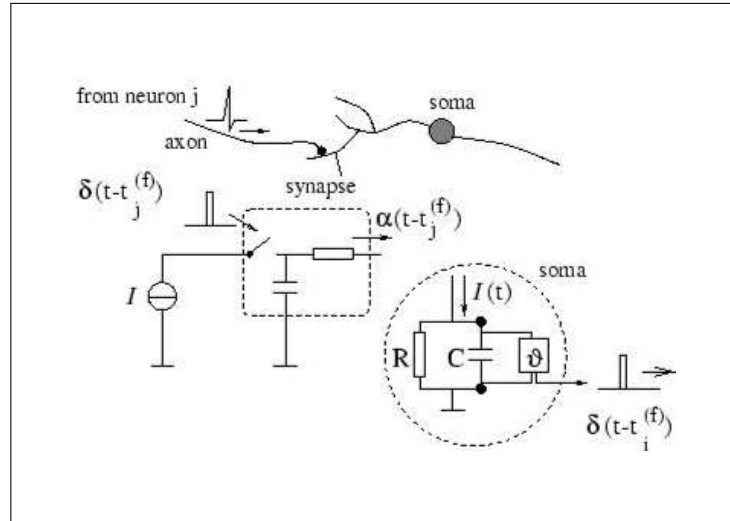


Figure 2.16: This figure illustrates a low-pass filter circuit at synapse location to filter presynaptic current $\delta(t-t_j^{(f)})$ producing an input current pulse, $\alpha(t-t_j^{(f)})$. The generated input current pulse will be attenuated to the soma. The IF model equivalent circuit in the soma consists of a resistor, R and a capacitor, C . The capacitor will be charged by the input current, $I(t)$. An output pulse, $\delta(t-t_i^{(f)})$ is generated at time $t_i^{(f)}$ when the voltage across capacitance increases and reach the threshold voltage, ϑ . (From Gerstner & Kistler (2002))

the standard equation for IF model,

$$\tau_m \frac{dv}{dt} = -v(t) + RI(t). \quad (2.18)$$

An action potential will be generated at firing time, t^f when potential value across the capacitor reaches the threshold voltage, ϑ

$$v(t^f) = \vartheta. \quad (2.19)$$

With a small delay after the spike generation, the control mechanism will change the membrane state from depolarization into repolarization which will change the membrane potential back to the initial resting potential, v_{res}

$$\lim_{\delta \rightarrow 0} v(t^f + \delta) = v_{res}. \quad (2.20)$$

Figure 2.17 illustrates an example of IF neuron model producing a spike trains depending on the value of the threshold voltage. A constant interspike interval generated by a stimulation from constant current input with amplitude higher

than the threshold level. External input less than threshold level will not produce a spike.

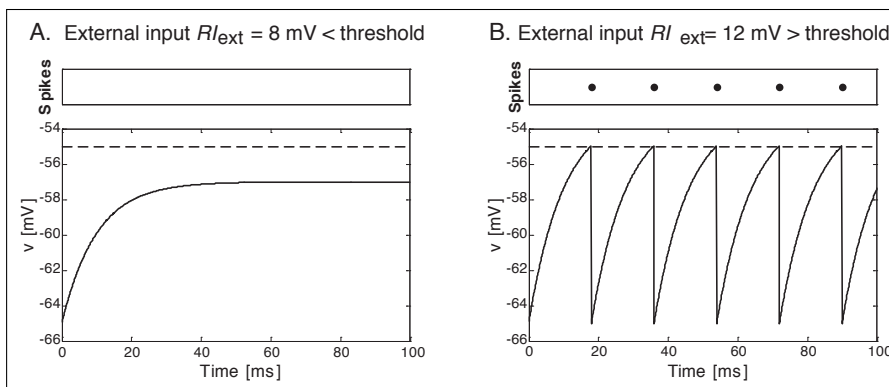


Figure 2.17: Output voltage of IF model with a threshold voltage, $\vartheta = 10\text{mV}$. (A) Constant current input with strength less than threshold voltage. (B) Constant input with strength greater than threshold voltage generating a spike train shown by dots in the upper figure. (From Trappenberg (2010))

2.3.3 Izhikevich model

Izhikevich model is non-linear leaky-integrate-and-fire neurons model. This is a dynamical model that looks at the bifurcation properties of excitable neurons, which refers to a near to transitional state of a neuron from resting to sustained spiking activity (Izhikevich, 2007). Biophysically accurate HodgkinHuxley-type neuronal models can be reduced to a two-dimensional system of nonlinear differential equations using the bifurcation methodologies of the form (Izhikevich, 2003)

$$\begin{aligned} v' &= I + 0.04v^2 + 5v + 140 - u \\ u' &= a(bv - u) \end{aligned} \quad (2.21)$$

with the auxiliary after-spike resetting

$$\text{if } v \geq 30 \text{ mV, then } \begin{cases} v \leftarrow c \\ u \leftarrow u + d. \end{cases} \quad (2.22)$$

The development of this model is based on the characteristics of two dimension-

less variables; (1) membrane potential, v and (2) membrane recovery potential, u for the activation of K^+ ionic currents and inactivation of Na^+ ionic currents, and u provides negative feedback to v . Equation 2.21 defines the membrane potential varies in time as a function of its past value and the inputs it receives. The part $0.04 v^2 + 5v + 140$ was obtained by fitting the spike initiation dynamics for the unit measurement of v in mV and the time scale in $mSec$. I is the synaptic current or injected dc-currents as the total input current. This model is also based on four dimensionless parameters; (1) a (rate of u), (2) b (sensitivity of u), (3) c (after-spike reset of v) and (4) d (after-spike reset of u). The variables u and v are reset to a baseline value according to equation 2.22 after the spike reaches its apex ($+30 mV$), and wait for the next incoming stimuli to drive it above threshold for the next spiking activity (Izhikevich, 2003).

Various choices of the parameters in Izhikevich model result in simulation of various type of spiking neurons. This is suitable for the development of a model of interconnected neurons according to the principles of known brain anatomy for further exploration of neuronal connectivity. This spiking neuron model had been used in this project to test the suitability of the proposed MVPC method in analysing a mixture of spiking and bursting neurons signals (Makhtar et al., 2014).

2.3.4 Cortical network model

Simulated spike train data in this thesis were obtained from a network of cortical neurons based on a synaptic conductance formulation (Troyer & Miller, 1997). The spiking neuronal network model used here is a variant of leaky-integrate-and-fire neurons model that include conductance based synaptic inputs. The conductance-based integrate-and-fire model for regular spiking neurons with a partial reset mechanism is given by the intracellular membrane potential of (Halliday, 2005)

$$C_m \frac{dV_m}{dt} = -I_{leak}(V_m) - \sum_{j=1}^n I_{syn}^j(V_m, t). \quad (2.23)$$

In the above equation, C_m is the cell capacitance and V_m is the membrane potential at time t .

$I_{leak}(V_m)$ represents the passive cell leakage current and $I_{syn}^j(V_m, t)$ the current due to the j th presynaptic spike. n is the total number of presynaptic inputs. The cell leakage current in this model is defined by the cell input resistance, R_m and the cell resting potential, V_r as

$$I_{leak}(V_m) = \frac{V_m - V_r}{R_m}. \quad (2.24)$$

The values of these passive membrane parameters were set according to Troyer & Miller (1997).

The cell will fire an output spike when V_m is greater than a fixed firing threshold, V_{thresh} . Then V_m is immediately reset to a fixed rest value, V_{reset} . V_{thresh} and V_{reset} are the two fixed parameters that specify the partial reset mechanism of the cell. Time-dependent conductance change, $g_{syn}(t)$ and the equilibrium potential for the ionic current, V_{syn} are the two parameters used in estimation of $I_{syn}(V_m, t)$. The synaptic current due to a single presynaptic spike at time $t = 0$ is calculated as

$$I_{syn}(V_m, t) = g_{syn}(t)(V_m - V_{syn}). \quad (2.25)$$

$g_{syn}(t)$ is associated with the opening of ionic channels following neurotransmitter release, which represents the conductance at the time of the synaptic event. Each presynaptic input triggers one term in the $\sum_{j=1}^n I_{syn}^j(V_m, t)$ of equation 2.23 over the time course of the synaptic event.

2.4 Neuronal signals recording

Electrical activities can be recorded from intracellular or extracellular fluid of the cell using different type of electrodes. Communication behaviour between and within neurons can be monitored using several recording techniques. This

section presents several recording techniques previously being used to capture signals from single-unit and multi-unit neurons electrical activities.

2.4.1 Single unit recordings

Electrical activities of a single neuron can be recorded using glass or metal wire electrode. Intracellular activities of a neuron is commonly recorded using liquid electrolyte filled glass electrode while extracellular activities commonly recorded from exposed patch of fine wire (Nicholls et al., 1992). These techniques allow researchers to investigate the mechanism of electrical current and voltage generation within single neurons. Extracellular and intracellular neuronal recording had proven to be useful in elucidate neuronal behaviour using various signal processing methods. Some of the methods have been developed to investigate correlated activities in single neurons from different region of the brain (Gandrathi et al., 2013). The following subsections are discussing about different research method and analysis previously being used in recording single unit activity of neurons.

Glass electrode

An in vivo single unit recording was done by a group of researchers from The University of Melbourne to study the effect of anti-epileptic drugs on neuronal network behaviour (Gandrathi et al., 2013). Investigation on the effect of drug was done in a genetic rat model of absence epilepsy using Borosilicate glass capillaries filled with neurobiotin electrolyte. The glass electrodes with tip diameter of $\approx 1 \mu\text{m}$ and resistance of 15-30 $\text{M}\Omega$ being used to record two single unit firing patterns in reticular thalamic neurons. Spikes signals recorded from glass electrodes was maintained between 1 and 4 mV to remove low signal-to-noise ratio (SNR) from low signals of $< 1 \text{ mV}$ and the possibilities of cell injury with higher spikes amplitude of $> 4 \text{ mV}$.

Signals recorded from paired glass electrodes was amplified, conditioned and arranged into 15-min time intervals; baseline, following saline injection and fol-

lowing drug injection. Several parameters were defined from the neuronal firing patterns to classify the firing properties, followed by correlation analyses. The implementation of autocorrelation analysis was done by searching the rhythm in each of the neuron to define the periodicity of spikes train signals. Figure 2.18 shows an example of rhythmic and non-rhythmic neuronal firing recorded by Gandrathi et al. (2013). Then, cross-correlation of the spike train were analysed using synchronisation index method to infer simultaneous firing activity of the two neurons in responses to the epileptic drugs (Gandrathi et al., 2013).

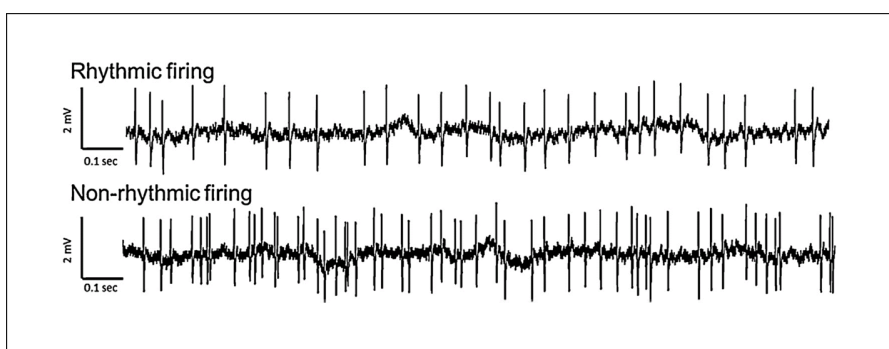


Figure 2.18: An example of signals recorded using glass electrode showing rhythmic neuronal firing and non-rhythmic neuronal firing. (From Gandrathi et al. (2013))

Fine wire electrode

Another technique commonly used for in vivo single unit recording is using single micro-wire electrodes. A method was previously developed by a group of researchers to decouple spikes and local field potential (LFP) signals recorded by microelectrodes using linear filtering techniques (David et al., 2010). They used tungsten microelectrodes with resistance of 1-50 M Ω to record the extracellular activity of neurons located in primary auditory cortex of ferrets. The effect of audio stimulations on auditory tuning was recorded, filtered and digitized. Spikes and LFP signals was extracted using low-pass filter with frequency band of 1-1000 Hz and high pass filter with frequency band of 3000-6000 Hz. Digitization was done with a 3125 Hz and 25000 Hz sampling rate on low and high frequency band signals, respectively.

They identify the single unit spiking activities by thresholding procedures extracting spike signals with rapid voltage amplitude change during a single time step of 0.04 ms (See figure 2.19). LFP signals were then filtered by removing the signal components that is directly correlated to the spikes signals. The methods was validated on simulated signals with higher number of recording sites generated according to the activities recorded in the actual experiments. Simulated waveforms of spikes and LFP was added to the signals prior to the validation analysis (David et al., 2010).

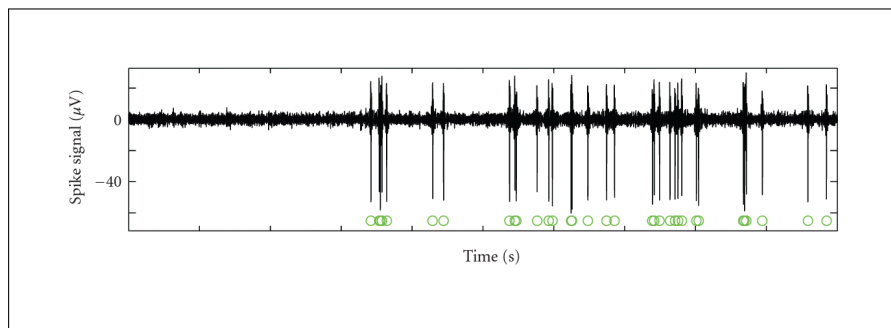


Figure 2.19: An example of single unit activity of neuron recorded using microwire (black traces). Green circles show spikes event filtered using thresholding procedures. (Figure from David et al. (2010))

2.4.2 MEA recordings

Multi Electrode Array (MEA) is one of the current technologies used to record simultaneous extracellular activities from multiple number of neurons. There are several types of MEA being used and this thesis generally refer to micro-wire electrode array. MEA signals normally measure potential fields generated by a few neurons located in vicinity of the electrodes. MEA simultaneously records two types of signals; 1) action potential or spikes train signals from the single neurons and 2) local field potential (LFP) signals from multiple number of neurons.

LFP is a low frequency signal compared to spike signals. LFP comprises of signals from extracellular activity of neurons located in vicinity of the recording electrode. The signals possibly contributed by synaptic potentials, action

potentials, flow of ionic flux through gated membrane channels and membrane oscillations (Buzsáki et al., 2012). Ambiguous composition of LFP yield difficult interpretation of the signals. A study on the connectivity of neurons within the same or different populations need reliable signal processing methods depending on the types of signals; spike train signals, LFP signals or combination of spike train and LFP signals.

Raw data from MEA recording normally will go through several stages of signal processing in order to produce good quality of clean signals. Extraction of spikes and LFP signals from MEA recording can be done using different band pass filter. Different frequency band filter normally selected to distinguish different frequency component of the signals; 1) a very fast firing action potential approximately within every 1 msec which produce a signal up to a few kHz and 2) a slow signals of LFP with lower frequency component up to hundreds Hz. Artefact and noise contamination in signals recorded from multiple site of neurons need to be filtered out before implementing the next stage of signals features detection.

2.5 Spikes detection in MEA signals

Characteristics for the sequence of spike pulses can be quantified in temporal patterns. For example, figure 2.20 shows two different pattern of spikes; 1) fast spiking neuron and 2) regular spiking neuron, classified by Connors & Gutnick (1990) in response to an intracellular stimulation from suprathreshold prolonged injected current. Classification of specialized spike train patterns would be useful in interpreting how neurons represent, transmit and integrate information.

Recent advances in spike sorting algorithm offer new possibilities to classify neuronal spikes in order to produce a high quality spike trains signals. Figure 2.21 illustrates an example of spike sorting methods available for analysis of multi-unit neuronal recordings previously developed by Quiroga et al. (2004).

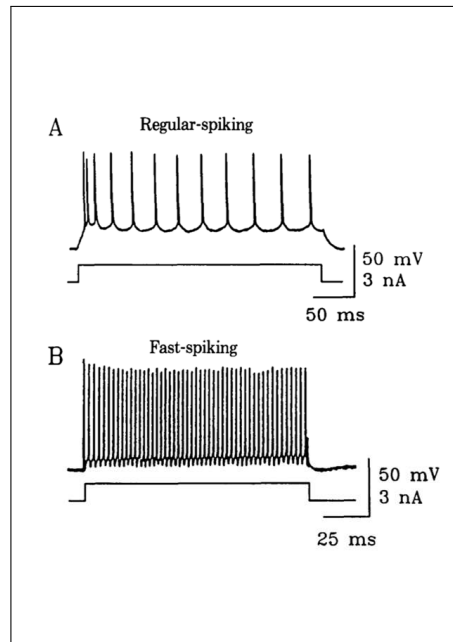


Figure 2.20: Intrinsic firing pattern of A) regular spiking neuron (top trace) in response to intracellular stimulation of prolonged depolarizing current (bottom trace) and B) fast spiking neuron (top trace) in response to the same stimulus current (bottom trace). (From Connors & Gutnick (1990))

This method was developed and compared to conventional spike sorting algorithm using simulated datasets with in-vivo recording environments. Simulated multi-unit neuronal signals will be filtered prior to the unsupervised signal processing which comprise of three stages; spike detection, feature extraction and clustering. Extraction of good quality spike train signals is crucial to produce better estimations of connectivities between neurons.

2.6 Functional connectivity analysis.

The availability of massive amount of neuronal signals are attracting widespread interest in connectivity analysis which are classified into anatomical, functional and effective network analysis (Rubinov & Sporns, 2010). Anatomical network consists of links between different brain regions. Effective connectivity analysis is based on the idea of probability of causal effects between neuronal signals. Functional interactions are normally estimated in the form of the spectral coherence in the frequency domain or correlation in the time domain. The connectivity

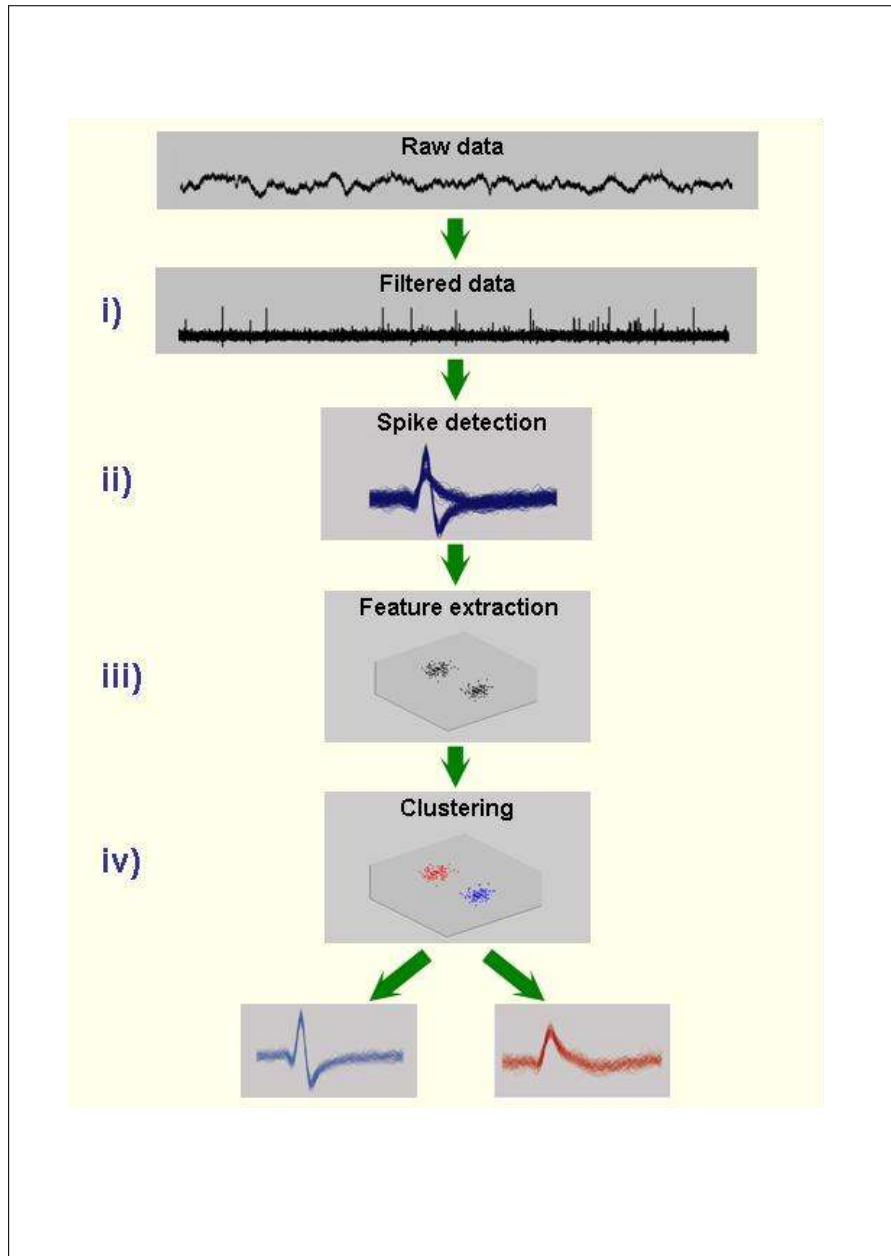


Figure 2.21: Step by step of spike sorting methods; i) Signals filtering using band-pass filter. ii) Spikes detection using specified amplitude threshold. iii) Feature extraction to distinguish different features of the spikes. iv) Clustering to classify the signals into individual neuron spikes. (From Quiroga (2007))

strength between all neurons in these networks usually represented by a connectivity matrix for further network analysis.

Granger causalities is one of the popular method being used in effective connectivity analysis. The prediction of a signal is based on the information of its own past values together with past values from other signals which may have causal influence on the predicted signal. This methods is clearly rely on the flow of time to predict the connectivity (Le Van Quyen & Bragin, 2007). Previous study on connectivities analysis based on Granger causality was done by Freiwald et al. (1999) using linear multivariate regression analysis. The relationship between the MEA signals is predicted based on history of the preceding event. The analysis was applied on LFP signals recorded from posterior part of the inferotemporal cortex of macaque monkey to find the neuronal connectivities in response to visual stimulation.

A similar autoregressive model based analyses also applied by Cadotte et al. (2010) to analyse neuronal connectivities between LFP signals recorded from 4 distinct region of rat brain. Electrical stimulation seizures induced in the right posterior ventral hippocampus to initiate a chronic temporal lobe epilepsy. The effect of stimulation was observed on both sides of the brain by the directional relationship from CA1 area to the dentate gyrus. Six temporal transitions of the directional relationship is quantified using parametric Granger causality analysis.

Studies on brain functional connectivities showed several analyses techniques being used on different type of signals (Fiecas et al., 2010; Fiecas & Ombao, 2011; Salvador et al., 2005; Kostecki et al., 2011). Functional neuronal connectivities were investigated by using MEA signals due to its capability to record simultaneous spikes activity from multiple number of neurons. MEA signals recorded from experimental procedures normally being analysed using various methods depending on the goal of the studies. This section discusses about different methods used to infer functional neuronal connections from simultaneously recorded MEA signals.

Correlation analysis is a technique widely used to measure functional connectivity among neurons. This technique was applied by Devilbiss & Waterhouse (2002) to study the interaction among neurons in somatosensory systems with an influence of systemically administered drugs. The extracellular electrical activities was simultaneously recorded using implanted bundles of MEA from ventroposterior medial and posteriomedial thalamus in awake and free moving rat. Recorded signal was analysed to investigate the neuronal responses towards electrical and mechanical stimulation in whisker's area. Signal analysis began by online spike sorting algorithm followed by offline waveform validation procedures. Decomposed individual neurons signals was validated according to these waveform characteristics; peak voltage amplitude, waveform slope, scatter plot of the waveform principle component and auto-correlogram of the spikes signals. Functional connectivity between a pair of neuronal signals was then described using cross-correlation histogram analysis.

Laubach et al. (1999) studied the functional activities in ensembles of neurons according to the correlation of the reaction times. Signals in rat motor cortex recorded during behavioural experiments. The analysis was done by comparing several correlation analysis techniques based on principle component analysis (PCA) and independent component analysis (ICA) methods in the notion that these techniques represent the connectivity among neuronal assemblies by detection of correlated firing bin on each trial. The results was statistically tested to compare the efficiencies among the selected techniques. ICA techniques showed the suitability for higher order correlation analysis and PCA was found suitable for broader distribution of correlation.

A different approach of applying correlation analysis to infer functional relationship explained by Wu et al. (2007) as multivariate analysis of variance (MANOVA). This technique is subject to equal covariance matrices among variables, however is not suitable for higher degree of connectivities. This technique was purposely designed to find hot spots from a number of predetermined sig-

nificant channels. In this study, MANOVA was applied to MEA recording from inferotemporal cortex of a sheep to study the pairwise relationship between channels in left and right visual cortex. Correlated channels identified when pairwise correlation value during the stimulation is different compared to pairwise correlation values before stimulation.

Another technique for inferring functional connectivities between brain areas showed in Kheiri et al. (2013) by analysing the temporal relationship of gamma waves. Perievent histogram used to visualise a significant peak for correlated rate and timing of signals. Functional connection between motor cortex, hippocampus, entorhinal cortex and piriform cortex of 7 Wistar rats was measured by Shannon entropy values of the perievent histograms as the connectivity factors for each channel pairs. Connectivity network mapped using graphical model based on the connectivity factors. Pattern of the network was compare for several different factors including behaviour, time periods, days and across subjects.

Phase locked oscillations is another analysis method used to detect synchrony in time series signals. The approach was applied by Lee (2002) to a raw signals recorded from supplementary motor area of a rhesus monkey. The wavelet cross spectrum of two parallel signals from two neurons was calculated by the average of wavelet cross spectrum which vary with time and scale of the transform. Synchronized activities addressed by a consistent phase relationship between actively spiking neurons.

Coherence analysis also have been widely used to quantify functional relationship between brain signals. For instance, study by Bokil et al. (2007) show coherence estimates can be used to find a relationship for LFP datasets with unequal sample sizes. The signals were used to distinguish coherence event in an experiment of eyes closed and eyes open conditions recorded from frontal and parietal lobe. The analyses were based on predetermined distributional properties using jackknifed estimates to capture non stationary behaviour of the signals.

An example of software packages for analyses of neural signals recorded from extracellular activities have been developed by Kwon et al. (2012). The package constructed using three preprocessing modules; pre-conditioning, spike detection and spike sorting as well as three analysis module; Single unit analysis, multi unit analysis and ensemble analysis. Functional analysis within this package use scale space signals generated by Haar wavelet transform of the spikes signals. Pairwise relationship between neurons was then inferred by the population spiking patterns followed by multiscale clustering method as an algorithm for identification of neuronal functional connectivities. Similar pattern between the signals will be presented in similarity matrix and quantified by Pearson correlation coefficient (Kwon et al., 2012).

The above discussion on MEA recording and analyses show various recording techniques and computational methods implemented to infer functional connections from the large volume of MEA data set. Advancement in MEA recording techniques increase the possibilities to simultaneously monitor and record electrical activities from many neurons located in different regions of the brain. Available signal processing techniques for preprocessing of MEA dataset helps in producing clean spike train signals for further analyses of neuronal connectivity. The aim of this thesis is to develop efficient techniques for analysing large dataset of neuronal signals to observe the structure of functional interactions between neurons within the same brain sub-region and also across different sub-regions.

The linear interactions from large scale recording of spike trains can be estimated and the connectivity can be analysed according to the framework presented in Figure 2.22. The simulated and MEA spike train signals will be analysed using Neurospec 2.0 (Halliday, 2005) to define pairwise connectivities between neurons using coherence values. This is follow by multivariate analysis to compute the partial coherence values. Coherence and partial coherence values will determine the binary and weighted connectivity matrix. These matrices will be used to construct the neuronal network for network measure (Rubinov & Sporns, 2010)

and structure analysis, and also for network visualisation.

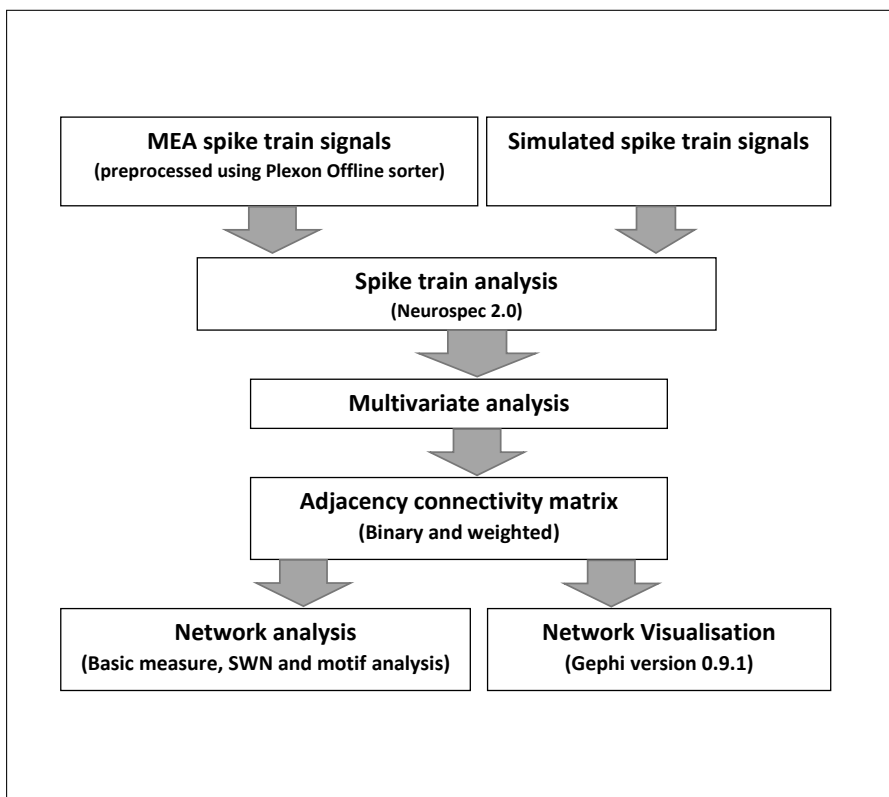


Figure 2.22: Framework for estimation of pairwise neuronal interactions and connectivity analysis on MEA and simulated spike train signals.

2.7 Chapter summary

Brain is divided into several functional regions and works as a global and dynamic complex systems through neuronal communication. Integration of information from different brain regions yield different pattern of functional neuronal network. Neurons as the basic building block of the brain play a major role in transmitting and receiving information. Electrical signalling and synaptic transmission is the basic interaction mechanisms between neurons. Comprehensive representation of electrical and chemical interaction using appropriate mathematical equations and equivalent electrical circuit increase the possibilities to predict the functional interaction of the neurons using sophisticated neuron model. Neuronal network mapping contributes in inferring the functional interaction between brain region.

Observation of the electrical properties of the brain especially action potential signals on specific mental processes enable the construction of functional interaction network. Availability of good quality action potential signals is crucial to study the functional interaction of the neuron. Various methods for recording single-unit and multi-unit of neuronal signals are available. MEA record extra-cellular activity in a large neuronal population that produce high dimensional datasets. Stable statistical and computational methods in analysing such data set is crucial to predict the functional interaction among neurons. Mathematical description of spectral estimation, coherence and partial coherence analysis will be discussed in the following chapter.

Chapter 3

Spectral Analysis

Large scale recording of spikes train signals requires statistical and computational tools to efficiently characterize interaction structure among the observed neurons. This chapter describes linear interactions among neuronal signals using estimated spectrum undertaken in frequency domain (Rosenberg et al., 1989). Neuronal interaction between neurons can be classified into two; unconditional and conditional relationship. Unconditional relationship is the condition of interaction between two neurons without consideration of common effects from other neurons normally known as predictors. This type of relationship can be estimated using coherence analysis (Rosenberg et al., 1989). On the other hand, the strength of conditional relationship between two neurons will consider the predictor effect, and this can be estimated using multivariate partial coherence analysis (Rosenberg et al., 1998). Both types of analysis can be used to observe interaction of neurons from different brain areas using spikes, LFPs or a combination of spike and LFP (hybrid analysis) signals (Halliday et al., 1995).

Multivariate partial coherence analysis discussed in this chapter is an approach to analyse conditional interaction between spike trains with consideration of multiple predictors. Consider ordinary coherence without considering any predictor is of order zero. So when a partial coherence contains p number of predictors, it is said to be of order p . The factor of computational complexity increases for higher order multivariate partial coherence analysis. Different approach of

computing higher order partial coherence using ordinary second order spectra will be discussed (Dahlhaus, 2000). Multivariate partial coherence analysis is computationally economical compared to the previous method of using partial auto- and cross-spectra (Dahlhaus et al., 1997).

3.1 Spectral estimation

To address the spiking pattern for each neuron, the spike signal need to be simplified by the time of occurrence for each spike. Dynamic neuronal response can be treated probabilistically considering the sequence of spike firing times as a series of point events denoted by $N_i(t)$ for $i = 1, 2, 3, \dots$, so that $N_1(t)$ indicates the total number of spikes from neuron 1 in time interval from 0 to time t . Point process of spikes firing times is assumed to be orderly considering the spikes do not occur simultaneously in sufficiently small sampling interval, dt . Electrical activity from assembly of neurons recorded as LFP signals can be treated as a time series denoted by $X_i(t)$ for $i = 1, 2, 3, \dots$, so that $X_1(t)$ indicates the real valued time series of LFP from channel 1. LFP time series assumed to be zero mean and sampled by dt , equal to sampling interval for spikes point process.

The discrete events known as random point process of spike trains with non-negative integer-valued therefore can be considered as a stochastic signals (Brillinger, 1975). Assuming that both spikes point process and LFP time series data are independent from any time argument, both type of data considered as stationary. Subsequently, both type of data are also assumed to satisfy a mixing conditions, whereby the sample values of each event well separated in time are statistically independent (Halliday et al., 1995).

Spectral estimation of spikes and LFP signals are constructed based on parameters in frequency domain formed after finite Fourier transform of the whole recorded data. The record, R consists of L separated disjoint segments of T , so $R = LT$. Process N_1 transformed by finite Fourier transform of l^{th} segment

($l = 1, 2, \dots, L$) of R with segment length T at frequency λ is defined as (Halliday et al., 1995)

$$d_{N_1}^T(\lambda, l) = \int_{(l-1)T}^{lT} e^{-i\lambda t} dN_1(t) \approx \sum_{(l-1)T \leq \tau_j < lT} e^{-i\lambda \tau_j}. \quad (3.1)$$

τ_j are equal to times when events of N_1 occur. Transformation of time series $X_1(t)$ is defined as (Halliday et al., 1995; Brillinger, 1972)

$$d_{X_1}^T(\lambda, l) = \int_{(l-1)T}^{lT} X_1(t) e^{-i\lambda t} dt \approx \sum_{t=(l-1)T}^{lT-1} e^{-i\lambda t} X_{1t}. \quad (3.2)$$

3.2 Cross spectral estimation

Individual spikes and LFPs processes defined above can be characterized by second order spectral analysis. The second order spectrum or pairwise cross spectrum between processes N_1 and N_2 , time series X_1 and X_2 , and process N_1 and time series X_1 (hybrid) can be defined respectively by the mathematical expression of (Halliday et al., 1995)

$$f_{N_1 N_2}(\lambda) = \lim_{T \rightarrow \infty} \frac{1}{2\pi T} E\{d_{N_1}^T(\lambda) \overline{d_{N_2}^T(\lambda)}\} \quad (3.3)$$

$$f_{X_1 X_2}(\lambda) = \lim_{T \rightarrow \infty} \frac{1}{2\pi T} E\{d_{X_1}^T(\lambda) \overline{d_{X_2}^T(\lambda)}\} \quad (3.4)$$

$$f_{N_1 X_1}(\lambda) = \lim_{T \rightarrow \infty} \frac{1}{2\pi T} E\{d_{N_1}^T(\lambda) \overline{d_{X_1}^T(\lambda)}\} \quad (3.5)$$

which can be estimated by averaging disjoint sections of the data

$$\hat{f}_{N_1 N_2}(\lambda) = \frac{1}{2\pi LT} \sum_{l=1}^L d_{N_1}^T(\lambda, l) \overline{d_{N_2}^T(\lambda, l)} \quad (3.6)$$

$$\hat{f}_{X_1 X_2}(\lambda) = \frac{1}{2\pi LT} \sum_{l=1}^L d_{X_1}^T(\lambda, l) \overline{d_{X_2}^T(\lambda, l)} \quad (3.7)$$

$$\hat{f}_{N_1 X_1}(\lambda) = \frac{1}{2\pi LT} \sum_{l=1}^L d_{N_1}^T(\lambda, l) \overline{d_{X_1}^T(\lambda, l)}. \quad (3.8)$$

The auto spectrum is a useful information indicating the distribution of data, whether it is a Poisson or non-Poisson process as well as providing information of rhythmic components presented by that particular data (Halliday, 2005). Definition and estimation for auto-spectrum of one point process or one time series can be expressed by replacing the different index subscript with the same index, for example by replacing N_2 by N_1 in equations 3.3 and 3.6 for auto-spectrum of process N_1 , $f_{N_1N_1}(\lambda)$.

The variance of estimated parameters defined above can be approximated in order to construct the confidence limits. For example, data distribution for auto-spectrum $\hat{f}_{N_1N_1}(\lambda)$ can be estimated by $\text{var}\{\hat{f}_{N_1N_1}(\lambda)\} \approx L^{-1}(f_{N_1N_1}(\lambda))^2$ (Bloomfield, 2000), where L is the number of section previously used in spectral estimation procedure. The expression of variance is then can be simplified as $\text{var}\{\ln \hat{f}_{N_1N_1}(\lambda)\} \approx L^{-1}$ after applying the natural log as the variance stabilising transform (Halliday, 2005). By plotting the estimated second order spectrum on a \log_{10} scale,

$$\text{var}\{\log_{10}(\hat{f}_{N_1N_1}(\lambda))\} = (\log_{10}(e))^2 L^{-1} \quad (3.9)$$

the resulting spectral at frequency λ with 95% confidence limits can be expressed as

$$\log_{10}(\hat{f}_{N_1N_1}(\lambda)) \pm 0.851L^{-1/2} \quad (3.10)$$

3.3 Coherence analysis

Linear dependency of unconditional relationship between selected pair of hybrid or non-hybrid processes in frequency domain can be predicted by coherence function, defined by the magnitude-squared of the correlation between particular processes (Rosenberg et al., 1989). For instance coherences of processes N_1 and N_2 at frequency λ can be written as

$$\left| R_{N_1N_2}(\lambda) \right|^2 = \lim_{T \rightarrow \infty} \left| \text{corr}\{d_{N_1}^T(\lambda), d_{N_2}^T(\lambda)\} \right|^2. \quad (3.11)$$

Following the expression of correlation:

$$\text{corr}\{d_{N_1}^T(\lambda), d_{N_2}^T(\lambda)\} = \frac{\text{cov}\{d_{N_1}^T(\lambda), d_{N_2}^T(\lambda)\}}{\sqrt{\text{var}\{d_{N_1}^T(\lambda)\}\text{var}\{d_{N_2}^T(\lambda)\}}}, \quad (3.12)$$

coherence interpretation in equation 3.11 can be expressed as

$$\left|R_{N_1N_2}(\lambda)\right|^2 = \frac{\left|f_{N_1N_2}(\lambda)\right|^2}{f_{N_1N_1}(\lambda)f_{N_2N_2}(\lambda)} \quad (3.13)$$

which can be estimated using estimation of auto- and cross-spectra defined in section 3.2 as

$$\left|\hat{R}_{N_1N_2}(\lambda)\right|^2 = \frac{\left|\hat{f}_{N_1N_2}(\lambda)\right|^2}{\hat{f}_{N_1N_1}(\lambda)\hat{f}_{N_2N_2}(\lambda)}. \quad (3.14)$$

Coherence functions is bounded by magnitude value from 0 to 1 which represent the strength of correlation between selected processes. Coherence value of 0 shows uncorrelated processes and 1 shows completely correlated processes (Brillinger, 2001; Rosenberg et al., 1989). A similar coherence function can be used in hybrid processes by replacement of the appropriate second order spectra (Halliday et al., 1995).

For the coherence functions defined above, estimation of the upper line of 95% confidence limit on coherence plot with hypotheses of linearly independent processes can be expressed (Halliday et al., 1995) as

$$1 - (0.05)^{1/(L-1)} \quad (3.15)$$

where L is the number of disjoint sections. Processes with coherence values below the 95% confidence limits line consider as not linearly associated. Estimation of coherence values in this section however is limited to linear pairwise interaction between spikes, LFPs or hybrid signals. Multivariate association between processes measured by partial coherence analysis will be discussed in the following section.

3.4 Partial coherence analysis

Existence of several simultaneously recorded MEA signals increases the possibilities to explore conditional relationship between neurons. Coherence estimation between several hybrid or non-hybrid processes known as partial coherence estimation can be directly developed by extending the procedure for ordinary coherence analysis (Brillinger, 2001; Rosenberg et al., 1989; Halliday et al., 1995). Interaction between multiple number of neurons can be characterized using partial coherence analysis between spikes, LFPs and between spike and LFP (hybrids analysis) (Halliday et al., 1995). The order of the partial coherence depends on the number of predictor used in the analysis. In this section, the definition of first order partial coherence which measure interaction between two processes with respect to one predictor effect will be discussed as a background for higher order partial coherence.

Association between process N_1 and process N_2 with common linear effect of process N_3 can be measured by first order partial coherence of (Halliday, 2005)

$$\left| R_{N_1 N_2 / N_3}(\lambda) \right|^2 = \lim_{T \rightarrow \infty} \left| \text{corr} \left\{ d_{N_1}^T - \left(\frac{f_{N_1 N_3}}{f_{N_3 N_3}} \right) d_{N_3}^T, d_{N_2}^T - \left(\frac{f_{N_2 N_3}}{f_{N_3 N_3}} \right) d_{N_3}^T \right\} \right|^2 \quad (3.16)$$

which suppressing the dependencies on λ and l . This expression leads to the hypotheses of $|R_{N_1 N_2 / N_3}(\lambda)| = 0$ when any observed association between process N_1 and process N_2 are totally due to common linear effect of process N_3 . First order partial coherence from equation 3.16 can be defined using partial spectra following the analogy of equation 3.13 (Brillinger, 2001; Rosenberg et al., 1989; Halliday et al., 1995) as

$$\left| R_{N_1 N_2 / N_3}(\lambda) \right|^2 = \frac{\left| f_{N_1 N_2 / N_3}(\lambda) \right|^2}{f_{N_1 N_1 / N_3}(\lambda) f_{N_2 N_2 / N_3}(\lambda)}. \quad (3.17)$$

Partial cross- and auto-spectrum used in equation 3.17 can be defined as

$$f_{N_1 N_2 / N_3}(\lambda) = f_{N_1 N_2}(\lambda) - \frac{f_{N_1 N_3}(\lambda) f_{N_3 N_2}(\lambda)}{f_{N_3 N_3}(\lambda)}. \quad (3.18)$$

By using the estimated value of second order spectra in section 3.2 the expression in equation 3.18 can be estimated by (Brillinger, 2001; Rosenberg et al., 1989; Halliday et al., 1995)

$$\hat{f}_{N_1N_2/N_3}(\lambda) = \hat{f}_{N_1N_2}(\lambda) - \frac{\hat{f}_{N_1N_3}(\lambda)\hat{f}_{N_3N_2}(\lambda)}{\hat{f}_{N_3N_3}(\lambda)} \quad (3.19)$$

leading to the expression of estimated first order partial coherence of

$$\left| \hat{R}_{N_1N_2/N_3}(\lambda) \right|^2 = \frac{\left| \hat{f}_{N_1N_2/N_3}(\lambda) \right|^2}{\hat{f}_{N_1N_1/N_3}(\lambda)\hat{f}_{N_2N_2/N_3}(\lambda)}. \quad (3.20)$$

Estimation of the upper line of 95% confidence limit for partial coherence plot can be expressed (Halliday et al., 1995) as

$$1 - (0.05)^{1/(L-p-1)} \quad (3.21)$$

where L is the number of disjoint sections used in spectral estimation and p is the number of predictors used in partial coherence analysis. Partial coherence values below the 95% confidence limits line consider as lack of linear association between processes without common linear effect of p . Partial coherence analysis would be a useful technique to discriminate between direct and indirect connection between neurons. Interaction between large number of neurons from different region of the brain can also be analysed using higher order partial coherence analysis.

3.5 Higher order partial coherence analysis

High order partial coherence analysis refer to partial coherence analysis which is introduced in the previous section but using multiple predictors. This section will describe the key idea of the approach used in this project to infer interaction between neurons either within the same region or across different parts of the brain using vector valued and matrix valued processes (Halliday et al., 1995). Processes from multiple neurons in two separate regions of the brain can be represented by

matrix of $\mathbf{X}(t)$ and $\mathbf{Y}(t)$ with the vector component processes of X_1, X_2, \dots, X_r and Y_1, Y_2, \dots, Y_s , respectively showing the real valued stationary increments of either point processes or time series.

Higher order partial coherence between i^{th} and j^{th} component of matrix \mathbf{X} with common linear effect of component \mathbf{Y} can be directly expressed following the equation 3.17 (Halliday et al., 1995) as

$$\left| R_{X_i X_j / \mathbf{Y}}(\lambda) \right|^2 = \frac{\left| f_{X_i X_j / \mathbf{Y}}(\lambda) \right|^2}{f_{X_i X_i / \mathbf{Y}}(\lambda) f_{X_j X_j / \mathbf{Y}}(\lambda)} \quad (3.22)$$

where higher order partial spectra will follow the analogy of equation 3.18 which expressed in a form of spectral density matrix as

$$F_{\mathbf{X}\mathbf{X}/\mathbf{Y}}(\lambda) = F_{\mathbf{X}\mathbf{X}}(\lambda) - F_{\mathbf{X}\mathbf{Y}}(\lambda) F_{\mathbf{Y}\mathbf{Y}}^{-1}(\lambda) F_{\mathbf{Y}\mathbf{X}}(\lambda). \quad (3.23)$$

Equation 3.22 can then be estimated as by estimated spectra computed using equation 3.6, 3.7 or 3.8 as

$$\left| \hat{R}_{X_i X_j / \mathbf{Y}}(\lambda) \right|^2 = \frac{\left| \hat{f}_{X_i X_j / \mathbf{Y}}(\lambda) \right|^2}{\hat{f}_{X_i X_i / \mathbf{Y}}(\lambda) \hat{f}_{X_j X_j / \mathbf{Y}}(\lambda)} \quad (3.24)$$

Consider ordinary coherence without considering any predictor is of order zero. So when a partial coherence contains p number of predictors, it is said to be of order p . The factor of computational complexity increases for higher order partial coherence analysis with high p . Computation for equation 3.22 is time consuming because it requires $((r-2) \times (r-2))$ calculations of higher order partial spectra in equation 3.23 for each of $\frac{r(r-1)}{2}$ pairwise relationship at all frequency, λ .

3.6 Multivariate partial coherence analysis

Different approach of computing higher order partial coherence namely multivariate partial coherence (MVPC) will be discussed here. This analysis using ordinary second order spectra (Dahlhaus, 2000) is suitable to overcome the computational

complexity issue in higher order partial coherence discussed in the previous section. This approach of analysis is computationally economical compared to using partial auto and cross-spectra (Dahlhaus et al., 1997).

As discussed in section 3.5, a group of neurons can be represented by matrix of \mathbf{X} as

$$\mathbf{X}(t) = \begin{bmatrix} X_1(t) \\ X_2(t) \\ \vdots \\ X_r(t) \end{bmatrix}$$

The second order spectral estimates for the group of neurons can be defined using equation 3.3, 3.4 or 3.5 and represented as a spectral density matrix. For example the spectral density matrix for components of $\mathbf{X}(t)$ can be represented as

$$F_{\mathbf{X}\mathbf{X}}(\lambda) = \begin{bmatrix} f_{X_1X_1}(\lambda) & f_{X_1X_2}(\lambda) & \cdots & f_{X_1X_r}(\lambda) \\ f_{X_2X_1}(\lambda) & f_{X_2X_2}(\lambda) & \cdots & f_{X_2X_r}(\lambda) \\ \vdots & \vdots & \ddots & \vdots \\ f_{X_rX_1}(\lambda) & f_{X_rX_2}(\lambda) & \cdots & f_{X_rX_r}(\lambda) \end{bmatrix}.$$

According to inverse variance lemma for partial correlation analysis by Whittaker (1990), it can be assumed that the diagonal elements of the inverse spectral matrix, $F_{\mathbf{X}\mathbf{X}}(\lambda)^{-1}$ are equal to the reciprocal of partial auto-spectra

$$diag[F_{\mathbf{X}\mathbf{X}}(\lambda)^{-1}] = \begin{bmatrix} \frac{1}{f_{X_1X_1/\mathbf{Z}}(\lambda)} & & & 0 \\ & \ddots & & \\ 0 & & & \frac{1}{f_{X_rX_r/\mathbf{Z}}(\lambda)} \end{bmatrix} \quad (3.25)$$

where \mathbf{Z} is the common linear effect of all the remaining variables. Following to the same inverse variance lemma, it can also be assumed that the negative value of rescaled inverse of spectral density matrix are equal to partial cross-spectral

matrix with common linear effect of all the remaining variables, \mathbf{Z}

$$F_{\mathbf{X}\mathbf{X}}(\lambda)^{-1} = \begin{bmatrix} 1 & -f_{X_1X_2/\mathbf{Z}}(\lambda) & \cdots & -f_{X_1X_r/\mathbf{Z}}(\lambda) \\ -f_{X_2X_1/\mathbf{Z}}(\lambda) & 1 & & -f_{X_2X_r/\mathbf{Z}}(\lambda) \\ \vdots & & \ddots & \vdots \\ -f_{X_rX_1/\mathbf{Z}}(\lambda) & -f_{X_rX_2/\mathbf{Z}}(\lambda) & \cdots & 1 \end{bmatrix} \quad (3.26)$$

The definition of partial auto- and cross spectral matrix in equation 3.25 and 3.26 may be used to replace partial auto- and cross-spectral terms in equation 3.22 so that

$$-R_{X\mathbf{X}/\mathbf{Z}}(\lambda) = (\text{diag}[F_{X\mathbf{X}}(\lambda)]^{-1})^{1/2} (F_{X\mathbf{X}}(\lambda)^{-1}) (\text{diag}[F_{X\mathbf{X}}(\lambda)]^{-1})^{1/2} \quad (3.27)$$

and multivariate partial coherence can be expressed as

$$\left| R_{X\mathbf{X}/\mathbf{Z}}(\lambda) \right|^2 = \left| (\text{diag}[F_{X\mathbf{X}}(\lambda)]^{-1})^{1/2} (F_{X\mathbf{X}}(\lambda)^{-1}) (\text{diag}[F_{X\mathbf{X}}(\lambda)]^{-1})^{1/2} \right|^2 \quad (3.28)$$

which is also bounded by coherence value from 0 to 1. Calculating multivariate partial coherence using inversion of spectral matrix is computationally efficient compare to equation 3.22. The equation 3.28 require only $(r \times r)$ matrix inversion of spectral matrix that reduce the computational complexity in computing multivariate partial coherence using higher order partial spectra. This technique is suitable for inferring conditional relationship between neuronal signals from high volume of MEA data.

The spectral density matrix can be estimated by direct substitution of estimates of the appropriate spectra computed using equation 3.6, 3.7 or 3.8. Spectral density matrix for components of $\mathbf{X}(t)$ can then be estimated as

$$\hat{F}_{\mathbf{X}\mathbf{X}}(\lambda) = \begin{bmatrix} \hat{f}_{X_1X_1}(\lambda) & \hat{f}_{X_1X_2}(\lambda) & \cdots & \hat{f}_{X_1X_r}(\lambda) \\ \hat{f}_{X_2X_1}(\lambda) & \hat{f}_{X_2X_2}(\lambda) & \cdots & \hat{f}_{X_2X_r}(\lambda) \\ \vdots & \vdots & \ddots & \vdots \\ \hat{f}_{X_rX_1}(\lambda) & \hat{f}_{X_rX_2}(\lambda) & \cdots & \hat{f}_{X_rX_r}(\lambda) \end{bmatrix},$$

so that auto- and cross- spectral matrix can be estimated as

$$\text{diag}[\hat{F}_{\mathbf{X}\mathbf{X}}(\lambda)^{-1}] = \begin{bmatrix} \frac{1}{\hat{f}_{X_1 X_1/\mathbf{Z}}(\lambda)} & & 0 \\ & \ddots & \\ 0 & & \frac{1}{\hat{f}_{X_r X_r/\mathbf{Z}}(\lambda)} \end{bmatrix} \quad (3.29)$$

and

$$\hat{F}_{\mathbf{X}\mathbf{X}}(\lambda)^{-1} = \begin{bmatrix} 1 & -\hat{f}_{X_1 X_2/\mathbf{Z}}(\lambda) & \cdots & -\hat{f}_{X_1 X_r/\mathbf{Z}}(\lambda) \\ -\hat{f}_{X_2 X_1/\mathbf{Z}}(\lambda) & 1 & & -\hat{f}_{X_2 X_r/\mathbf{Z}}(\lambda) \\ \vdots & & \ddots & \vdots \\ -\hat{f}_{X_r X_1/\mathbf{Z}}(\lambda) & -\hat{f}_{X_r X_2/\mathbf{Z}}(\lambda) & \cdots & 1 \end{bmatrix}. \quad (3.30)$$

Following to equation 3.28 the multivariate partial coherence can then be estimated by

$$\left| \hat{R}_{X X/\mathbf{Z}}(\lambda) \right|^2 = \left| (\text{diag}[\hat{F}_{\mathbf{X}\mathbf{X}}(\lambda)^{-1}]^{1/2}) (\hat{F}_{\mathbf{X}\mathbf{X}}(\lambda)^{-1}) (\text{diag}[\hat{F}_{\mathbf{X}\mathbf{X}}(\lambda)^{-1}]^{1/2}) \right|^2. \quad (3.31)$$

Definition of the above quantities can be extended to find the multivariate partial coherence between variables in two or more groups of neurons. Consider another group of neurons

$$\mathbf{Y}(t) = \begin{bmatrix} Y_1(t) \\ Y_2(t) \\ \vdots \\ Y_s(t) \end{bmatrix},$$

the second order spectral estimation of two groups of neurons can be represented simultaneously using a larger size of matrix combining both components of $\mathbf{X}(t)$

and $\mathbf{Y}(t)$ which also includes a cross-spectra of components $\mathbf{X}(t)$ and $\mathbf{Y}(t)$.

$$\hat{F}_{\mathbf{XY}}(\lambda) = \begin{bmatrix} \hat{f}_{X_1X_1}(\lambda) & \hat{f}_{X_1X_2}(\lambda) & \cdots & \hat{f}_{X_1X_r}(\lambda) & \hat{f}_{X_1Y_1}(\lambda) & \hat{f}_{X_1Y_2}(\lambda) & \cdots & \hat{f}_{X_1Y_s}(\lambda) \\ \hat{f}_{X_2X_1}(\lambda) & \hat{f}_{X_2X_2}(\lambda) & \cdots & \hat{f}_{X_2X_r}(\lambda) & \hat{f}_{X_2Y_1}(\lambda) & \hat{f}_{X_2Y_2}(\lambda) & \cdots & \hat{f}_{X_2Y_s}(\lambda) \\ \vdots & \vdots & \ddots & \vdots & \vdots & \vdots & \ddots & \vdots \\ \hat{f}_{X_rX_1}(\lambda) & \hat{f}_{X_rX_2}(\lambda) & \cdots & \hat{f}_{X_rX_r}(\lambda) & \hat{f}_{X_rY_1}(\lambda) & \hat{f}_{X_rY_2}(\lambda) & \cdots & \hat{f}_{X_rY_s}(\lambda) \\ \hat{f}_{Y_1X_1}(\lambda) & \hat{f}_{Y_1X_2}(\lambda) & \cdots & \hat{f}_{Y_1X_r}(\lambda) & \hat{f}_{Y_1Y_1}(\lambda) & \hat{f}_{Y_1Y_2}(\lambda) & \cdots & \hat{f}_{Y_1Y_s}(\lambda) \\ \hat{f}_{Y_2X_1}(\lambda) & \hat{f}_{Y_2X_2}(\lambda) & \cdots & \hat{f}_{Y_2X_r}(\lambda) & \hat{f}_{Y_2Y_1}(\lambda) & \hat{f}_{Y_2Y_2}(\lambda) & \cdots & \hat{f}_{Y_2Y_s}(\lambda) \\ \vdots & \vdots & \ddots & \vdots & \vdots & \vdots & \ddots & \vdots \\ \hat{f}_{Y_sX_1}(\lambda) & \hat{f}_{Y_sX_2}(\lambda) & \cdots & \hat{f}_{Y_sX_r}(\lambda) & \hat{f}_{Y_sY_1}(\lambda) & \hat{f}_{Y_sY_2}(\lambda) & \cdots & \hat{f}_{Y_sY_s}(\lambda) \end{bmatrix}.$$

Note that the matrix is divided into four subdivision where top left and bottom right of the matrix $\hat{F}_{\mathbf{XY}}(\lambda)$ are the estimated spectral density matrix of components from matrix $\mathbf{X}(t)$ and $\mathbf{Y}(t)$, respectively. Representation of the cross-spectral estimated by combination of the components in matrix $\mathbf{X}(t)$ and $\mathbf{Y}(t)$ shown in another two subdivisions. Spectral estimation with a component of $\mathbf{X}(t)$ as an input and a component of $\mathbf{Y}(t)$ as the output shown in the top right of the matrix, while the bottom left represent the opposite direction of spectral input and output.

Following to the similar definition in equation 3.29, 3.30 and 3.32, the conditional relationship between neurons from different groups can be estimated by

$$\left| \hat{R}_{XY/Z}(\lambda) \right|^2 = \left| (diag[\hat{F}_{\mathbf{XY}}(\lambda)^{-1}]^{1/2}) (\hat{F}_{\mathbf{XY}}(\lambda)^{-1}) (diag[\hat{F}_{\mathbf{XY}}(\lambda)^{-1}]^{1/2}) \right|^2. \quad (3.32)$$

Note that the inversion of spectral density matrix is the main parameter used to discriminate either direct or indirect connection between processes or series of group $\mathbf{X}(t)$ and/or $\mathbf{Y}(t)$. MVPC analysis discussed in this chapter is an approach to compute conditional connectivity weight between neurons considering the common effect from other predictor neurons. This method is suitable for analysing functional interactions within a large group of neuronal population or between two or more groups of neurons. The strength of interactions computed using MVPC analysis will be a useful information to construct the neuronal connec-

tivities as the basic framework for the development of neuronal network mapping.

3.7 Chapter summary

With emergence of MEA technology in recording high volume of neuronal signals, the approach of multivariate analysis becomes crucial to identify the pattern of interaction between neurons. This chapter described point process and time series spectral estimation for the purpose of coherence analysis as an approach for measuring association among neurons. Conditional pairwise interaction between neurons then can be distinguished using partial coherence analysis which measure the linear relationship among the signals with consideration on the common effects from other neurons. First order partial coherence analysis describe interaction between three neurons which shows how one neuron can be considered as a predictor or not for other two associated neurons. The approach can be extended in a form of matrices for the analysis of multiple processes to determine connectivity among multiple associated neurons using partial estimated auto- and cross-spectra to construct higher order partial coherence estimates. Computationally economical approach called multivariate partial coherence analysis introduced to overcome computational complexity issue in the previous approach using higher order partial coherence analysis. MVPC approach is based on the idea of inversion of second order spectral density matrix, suitable for connectivity analysis within and across groups of neurons. These methods will be a foundation to further mapping the neuronal interaction using conditional and unconditional connectivity weight. Network theory for analysis of neuronal connectivity will be discussed in the next chapter.

Chapter 4

Network Theory and Metrics

Network science offers useful insights into complex system that are composed of individual components linked together. Examples of complex network systems include the Internet, World Wide Web, telephone network, human social connections, biochemical networks and neural networks. There are three different aspects of network studies, 1) the individual components, 2) the interactions between these components, and 3) the pattern of connections in a given network. An extensive set of mathematical, computational and statistical tools have been developed for analysing and visualising networks(Newman, 2010).

Visualisation can be a useful tool for interactive exploration of networks components and interactions. Application of visualisation tools can also help in observation of features in underlying structure of the network. Network visualisation tools normally embed various algorithms of network analysis depending on the nature of the network studied.

In order to analyse brain connectivity, we need to comprehend the theory of networks. This subject is widely used in neuroscience to explore various type of network information like network metrics, network structures and network models. Distinction between directed or undirected networks needs to be made before undertaking network analysis (Rubinov & Sporns, 2010). Directed network is a network with directions to show the flow of information between network compo-

nents. Information in undirected network can flow in both directions of the link that connects the network components. Further distinction between weighted and unweighted (binary) network also needs to be specified before conduction of network analysis.

One goal of this research is to use network measures to explore the undirected network of conditional and unconditional interactions between neurons. This chapter covers the theory of networks which includes several network measures that will be used to analyse the neuronal interactions from simulated and experimentally recorded spike train signals. This network measure analysis are implemented in Matlab using the Brain Connectivity Toolbox (Rubinov & Sporns, 2010).

4.1 Network measures applied to neuronal interactions

When working with functional connections between neurons, chapter 3 discussed two types of connections: conditional and unconditional relationships. Conditional relationships are the interaction between neurons after removal of the common effects which is derived by MVPC, eq 3.32. Unconditional relationships are the interactions between neurons without consideration of any predictors, derived from coherence, Eq. 3.14. In both cases, the connections between neurons are represented as a matrix that will be used to represent the networks. Network measures can be used to analyse the connectivity matrix and explore the properties of the interactions through calculation of a range of network metrics described below.

A connectivity matrix is called an adjacency matrix A , that composed of n nodes and l edges. The number of nodes, n will determine the size of the matrix, $n \times n$. The edges can be binary, a_{ij} or weighted, w_{ij} . This can be seen in Eq. 4.1

for an example of binary adjacency matrix, A_b and Eq. 4.2 for an example of weighted adjacency matrix, A_w .

$$A_b = \begin{bmatrix} 0 & 1 & 1 & 0 & 0 \\ 1 & 0 & 0 & 0 & 0 \\ 1 & 0 & 0 & 1 & 1 \\ 0 & 0 & 1 & 0 & 1 \\ 0 & 0 & 1 & 1 & 0 \end{bmatrix} \quad (4.1)$$

$$A_w = \begin{bmatrix} 0 & 0.25 & 0.5 & 0 & 0 \\ 0.25 & 0 & 0 & 0 & 0 \\ 0.5 & 0 & 0 & 0.25 & 1 \\ 0 & 0 & 0.25 & 0 & 1 \\ 0 & 0 & 1 & 1 & 0 \end{bmatrix} \quad (4.2)$$

Here, a_{ij} represent the presence or absence of edge between nodes i and j , w_{ij} represents the weight for the edge to show the strength of interaction between nodes i and j in a range of 0 to 1. The diagonal elements for both binary adjacency matrix, a_{ii} and weighted adjacency matrix, w_{ii} are considered as zero, there are no self-connections. The matrix for association between neurons at the micro-scale level in brain connectivity studies is also known as the association matrix (Bullmore & Sporns, 2009).

This study will focus on undirected networks analysis, where a_{ij} and w_{ij} are considered equal to a_{ji} and w_{ji} , respectively. Thus the matrices A_b and A_w are symmetrical about the main diagonal. Figure 4.1 shows example of weighted and binary networks for A_b and A_w for the same pattern of interactions. These matrices illustrate the symmetrical nature of A_b and A_w . The maximum possible number of edges for A_b or A_w is $\binom{n}{2} = \frac{1}{2}n(n-1)$. For example the maximum number of edges for a 5-node network is $\frac{5(4)}{2} = 10$ edges, see Figure 4.1.

The adjacency matrix A allows an exploration of the network properties from a mathematical perspective using various network metrics. Properties of

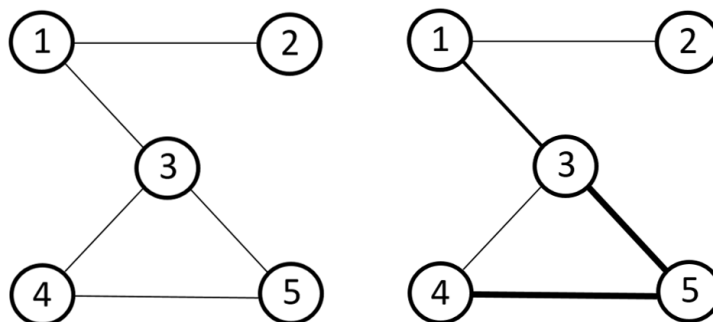


Figure 4.1: Binary and weighted network examples for A_b (left) in Eq. 4.1 and A_w (right) in Eq. 4.2. In the binary case the edge between two nodes is indicated by a line to indicate the presence of a connection from node i to node j . The strength of connection between two nodes can be represented by various thickness of the edge lines as shown in the weighted network (right).

local and global interactions in a network can be viewed from two different perspectives using network measures; segregation and integration. Local interaction is a localized communication within a small group of nodes, and global interaction is a holistic communication across the entire network. In a complex network, combination of local information processing in small groups of nodes and efficient information transfer between these groups represent the coexistence of the two opposing perspectives, network integration and network segregation (Tononi et al., 1994).

Segregation is a characteristic of a network for the relative independence of local groups, normally known as the cliquishness between the nodes in local groups and usually measured using network grouping metrics for detection of clusters and modules (Sporns, 2013). Integration is normally measured by the network path length to explore the pathways for efficient communication and integration of distributed information in a network. Additionally, network motifs and network small worldness will also be applied in this thesis to characterize the structure of sub-graphs and topology of networks. Analysis of network small worldness involves comparison of the network with random or regular networks. See Figure 4.2 for examples of regular and random networks with 20 nodes with

an average of 4 connections per node. Statistical comparison should be done by comparison with a null-hypotheses network with similar size as the tested network (Rubinov & Sporns, 2010).

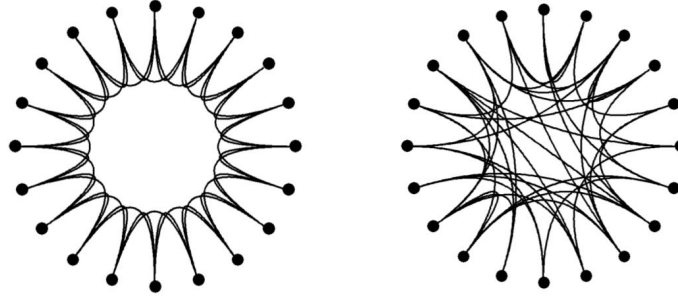


Figure 4.2: A regular network (left) shows similar pattern of synchronized interactions across the entire network and a random network (right) shows random connections across a network with non-existence of specific pattern of interactions. Both regular and random networks consist of 20 nodes with an average of 4 connections per node.

4.1.1 Degree

Node degree is the most important measure in network theory. Node degree is defined as the number of edges that connect a node to the rest of the network. The degree of a node indicates how important a neuron is in the neuronal network by the number of edges connected to it. For an undirected graph of n nodes the binary node degree is defined (Rubinov & Sporns, 2010) by

$$k_i = \sum_{j \in N} a_{ij}, \quad (4.3)$$

where N is the set of all nodes in the network. a_{ij} represents an edge between nodes i and all of its neighbours j , where a_{ij} is equal to 1 if there is a link between neuron i and j , and 0 for unconnected neighbour. For weighted undirected

networks the weighted degree is defined (Rubinov & Sporns, 2010) as

$$k_{wi} = \sum_{j \in N} w_{ij} \quad (4.4)$$

where w_{ij} is the edge weight. The weighted node degree is also known as node strength.

The node degree distribution is a useful measure for a network with a large number of nodes. The distribution indicates the presence of highly connected nodes or network hubs. This can be shown by a histogram or cumulative frequency distribution. The frequency distribution will be used in this thesis to compare between highly connected nodes of unconditional networks and less connected nodes of conditional networks.

4.1.2 Path length and network efficiency

As mentioned earlier in this chapter, a network is composed of nodes and edges. Edges are links that connect two nodes in a network. Nodes can be connected directly or indirectly through intermediate nodes. A path is an ordered sequence of all possible ways for a node to reach another node. The shortest distance between two nodes is of particular interest since it is often the most effective pathway. The shortest path length between node i and node j is defined as

$$d_{ij} = \sum_{a_{uv} \in i \leftrightarrow j} a_{uv} \quad (4.5)$$

where $i \leftrightarrow j$ indicates the number of edges as the shortest pathway between nodes i and j . For weighted undirected networks the path length between node i and node j is defined as

$$d_{ij}^w = \sum_{w_{uv} \in i \leftrightarrow j} f(w_{uv}) \quad (4.6)$$

where f is a function converting from functional connectivity weight to path distance, and $i \leftrightarrow j^w$ indicates the shortest weighted path distance between nodes i and

j . Shorter distance is usually interpreted as a more effective communication between nodes.

An estimation of travelling ability through a network indicates how well integrated the network is. This is given by the average of shortest path lengths between all possible pairs of nodes, known as the characteristic path length (Watts & Strogatz, 1998) and calculated as

$$L = \frac{1}{n} \sum_{i \in N} L_i = \frac{1}{n} \sum_{i \in N} \frac{\sum_{j \in N, j \neq i} d_{ij}}{n-1}. \quad (4.7)$$

Note that L_i is the average distance between the node i and all other network nodes. Lengths between disconnected nodes are set to infinity for both binary and weighted networks. For weighted undirected networks the weighted characteristics path length is calculated as

$$L^w = \frac{1}{n} \sum_{i \in N} \frac{\sum_{j \in N, j \neq i} d_{ij}^w}{n-1}. \quad (4.8)$$

This measure indicates the global integration of nodes in the network. Regular networks usually have longer path lengths compared to random networks because of the regular local connections from each node. Random networks have both local connections and also long range edges that connect distant nodes. These long range edges can decrease the characteristics path length of a network.

An alternative measure of network integration is known as global efficiency. This measure is inversely proportional to the characteristic path length, L and calculated as (Latora & Marchiori, 2001)

$$E_{glob} = \frac{1}{N(N-1)} \sum_{i \neq j \in A} \frac{1}{d_{ij}}. \quad (4.9)$$

E_{glob} measure the effectiveness of information transfer between nodes in a network. It is consider as 0 for disconnected nodes.

The efficiency of information transfer can also be measured as a local measure for each node, i by evaluating the average efficiency of sub-network of the neighbours of i . The local efficiency is given by (Latora & Marchiori, 2001)

$$E_{loc} = \frac{1}{N} \sum_{i \in A} E(A_i). \quad (4.10)$$

Global and local efficiency measure are meaningful measures to quantify a network with disconnected node (Achard & Bullmore, 2007).

4.1.3 Clustering coefficient

The clustering coefficient, C , is another important network metric that measures a local property of a node neighbourhood (Watts & Strogatz, 1998). C is the fraction of three-node triangles around a node computed as

$$C = \frac{1}{n} \sum_{i \in N} C_i = \frac{1}{n} \sum_{i \in N} \frac{2t_i}{k_i(k_i - 1)} \quad (4.11)$$

where C_i is the clustering coefficient for node i ($C_i = 0$ for $k_i < 2$), and t_i is number of triangles around a node i ,

$$t_i = \frac{1}{2} \sum_{j, h \in N} a_{ij} a_{ih} a_{jh}. \quad (4.12)$$

Clustering coefficients range from 0 to 1. $C = 1$ indicates a fully connected network where all nodes are connected to each other. Regular networks usually have higher clustering coefficients compare to random networks because of strong association between adjacent nodes in the regular network. For weighted undirected networks the clustering coefficient is calculated as (Onnela et al., 2005)

$$C^w = \frac{1}{n} \sum_{i \in N} \frac{2t_i^w}{k_i(k_i - 1)}. \quad (4.13)$$

t_i^w is the sum of triangles intensities around node i ,

$$t_i^w = \frac{1}{2} \sum_{j,h \in N} (w_{ij}w_{ih}w_{jh})^{\frac{1}{3}}. \quad (4.14)$$

Clustering coefficients indicate the global segregation of nodes in the network.

4.1.4 Modularity

Modularity, Q is a measure of segregation in a network. It is known as a community detection measure that classifies nodes in a network into non-overlapping groups. Each group consists of a set of nodes with a maximum number of edges within a group, and a minimum number of edges between groups. Modularity of a network (Newman, 2006) is given by

$$Q = \frac{1}{l} \sum_{i,j \in N} \left(a_{ij} - \frac{k_i k_j}{l} \right) \delta_{m_i m_j}, \quad (4.15)$$

where l is the number of edges in the network computed as,

$$l = \sum_{i,j \in N} a_{ij}. \quad (4.16)$$

Note that m_i is the module of group containing node i , and the quantity $\delta_{m_i m_j}$ is 1 if i and j are in the same group, and 0 otherwise. For weighted undirected networks the modularity (Newman, 2004) is calculated as

$$Q^w = \frac{1}{l^w} \sum_{i,j \in N} \left(w_{ij} - \frac{k_i^w k_j^w}{l^w} \right) \delta_{m_i m_j}, \quad (4.17)$$

where l^w is the sum of all weights in the network computed as,

$$l^w = \sum_{i,j \in N} w_{ij}. \quad (4.18)$$

Modularity indicates the presence of natural divisions in a network. This measure is useful to discover and understand the global structure of a network.

4.2 Network motifs

Network motifs are useful network measures for inference of the basic building blocks of a complex network. Network motifs represent several patterns of interconnection between nodes that recur in a network when compared to a similar size of random network (Milo et al., 2002). Network motif measures are commonly used to detect the structure and characteristics of sub-networks in a complex network. Analysis using network motifs depends on a pre-specified number of nodes for the motif size. In this analysis, a network is decomposed into several network motifs counted in frequency of occurrence. The numbers of a specific motif which are found are determined by statistical comparison against a null-hypothesis random network (Milo et al., 2002).

Motif detection starts by determining the motif size by specifying the number of nodes for the sub-network, M . Then enumeration of the sub-networks will produce various patterns of network motif depending on the specified motif size. The number of motifs found increases with increases in motif size, M . For instance, Figure 4.3 shows six different sub-networks from motif size, $M = 4$. Rewired benchmark networks retain the degree distribution of the network, and lost the modular architecture of the network. Some of the spurious connections in the rewired network might be due to that loss in modules.

The number of occurrences of a sub-network motif h_i , J_{h_i} will be summarized in frequency histogram for a comparison with the number of occurrence of a sub-network motif in null-hypothesis random networks, $J_{h_i, \text{rand}}$. Random networks with same numbers of nodes and edges as the original network are constructed, where occurrence of sub-networks in these random networks is by chance. Statistical comparison with random networks using z -scores will highlight over-represented sub-networks in the original network. The z -score of motif

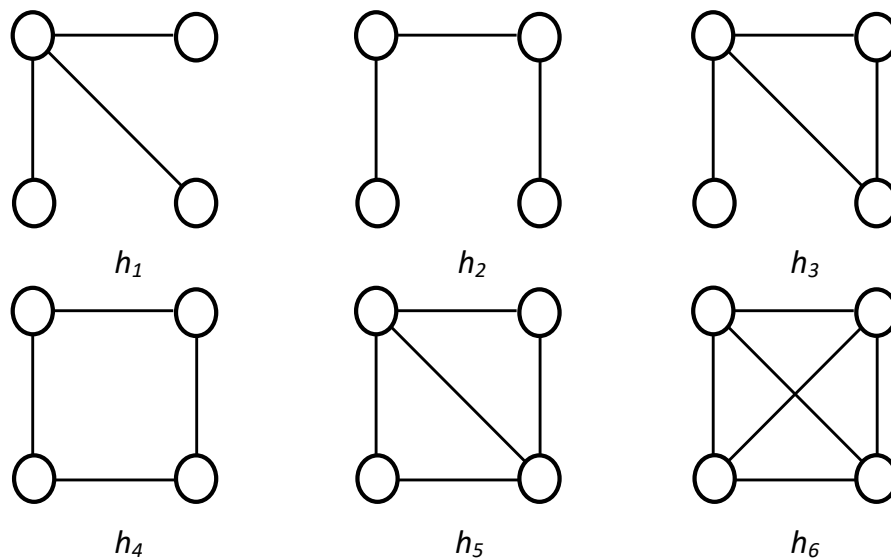


Figure 4.3: Six possible sub-network patterns with undirected motifs ID: h_1 , h_2 , h_3 , h_4 , h_5 and h_6 from motif size, $M = 4$.

h_i (Milo et al., 2002) is calculated as

$$z_{h_i} = \frac{J_{h_i} - \langle J_{h_i, \text{rand}} \rangle}{\sigma^{J_{h_i, \text{rand}}}}. \quad (4.19)$$

$\langle J_{h_i, \text{rand}} \rangle$ is the mean of J_{h_i} in an ensemble of random networks. $\sigma^{J_{h_i, \text{rand}}}$ is the standard deviation of J_{h_i} in random networks. A significant z -score indicates a higher frequency occurrence in the original network compared to random networks. Appearance of specific motifs in a network helps in exploration of functional and structural connectivity in a complex network (Sporns & Kötter, 2004).

Motif detection tools are classified into two groups, using network centric and motif centric algorithms (Wong et al., 2011; Ribeiro et al., 2009). Network centric looks for motifs across the entire network. Motif centric detection is examination of single specific motif across the network. In this project, the network centric motif discovery will be done using a tool for fast network motif detection known as FANMOD (Wernicke & Rasche, 2006). This user-friendly motif detection tool is freely available online at <http://theinf1.informatik.uni-jena.de/motifs/>. FAN-

MOD was selected because of its suitability for motif detection in undirected network, and it can detect larger motifs of up to size 8. FANMOD is a fast and efficient motif detection tool which uses a node-sampling strategy for exhaustive sub-network census (Wong et al., 2011).

4.3 Network small-worldness

Small-worldness is a topological property of a highly clustered network with a small number of long range connections, for example through intermediate acquaintances in social networks. Existence of small-world network (SWN) structure has been extensively proven in social networks. The network of scientific collaborations is a good example of social network that consists of a large number of groups of scientists from worldwide institutions, representing densely connected clusters. Connections between these groups are established through intermediate acquaintances, these are the long range connectors across groups. A combination of these two network properties represents the SWN structure (Newman, 2001), which is a common property in any social network. SWN properties indicates the co-existence of network segregation and integration, which is believed to be important for brain functional networks (Sporns et al., 2000).

Network Small-worldness can be defined using two network metrics, path length, L and clustering coefficient, C described in section 4.1.2 and 4.1.3. The definition of small-world networks by Watts & Strogatz (1998) was done by a comparison of these two metrics derived from the original network compared with regular network and random network. The nodes in regular networks are mostly connected to their nearest neighbours, meaning that this network is highly clustered with large path length. The irregular patterns of connectivity in random networks means that this network is poorly clustered with low path length. A small-world network has characteristics that are in-between of these networks with high C for network segregation and low L for network integration (Watts & Strogatz, 1998) as shown in Figure 4.4. SWN organization is considered as

an optimal structure for a complex network because of the coexistence of both network integration and segregation (Sporns & Honey, 2006).

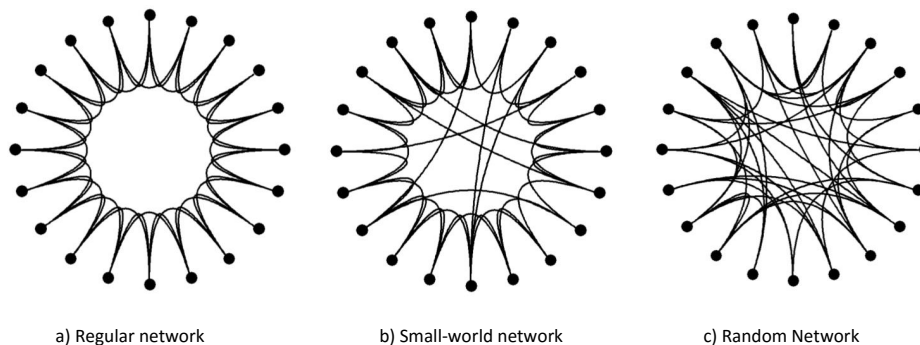


Figure 4.4: This figure show (a) a regular network with high values of C and L , (b) a small world network with optimum connections with coexistence of segregation and integration properties represent high C and low L , and (c) a random network with low values of C and L . All of these networks consist of 20 nodes with an average degree of 4 connections per node.

One measure of network small-worldness, S is defined in a single statistic by Humphries & Gurney (2008) as

$$S = \frac{C/C_{rand}}{L/L_{rand}}, \quad (4.20)$$

where C_{rand} and L_{rand} are the clustering coefficients and characteristic path lengths for a random network with same size, where these original and random networks must have the same number of nodes and average node degree. C and L are the clustering coefficients and characteristic path lengths for the original network under analysis. A network exhibits SWN characteristics when $S \gg 1$. SWN attributes reflects simultaneous organization of global and local network structure. For weighted undirected networks the measure of network small-worldness, S^w is calculated (Rubinov & Sporns, 2010) as

$$S^w = \frac{C^w/C_{rand}^w}{L^w/L_{rand}^w}. \quad (4.21)$$

A network is said to be a small-world network if $S^w \gg 1$. An aggregate measure of small-worldness and weighted small-worldness potentially cause high S index for a non-SWN network when L and L^w is less than L_{rand} and L^w_{rand} , respectively.

In this thesis, an equivalent of Erdős–Rényi (E–R) random network with the same number of nodes and edges is constructed for calculation of SWN attributes in a network (Humphries & Gurney, 2008; Blocher, 2010). These are well established random network models published in 1959 (Erdős & Rényi, 1959; Boccaletti et al., 2006). An E–R random graph is generated by randomly assigning each edge to a node pair with an equal probability. Node degree distributions are equally probable, resulting in a Poisson degree distribution in a large random graph. Random network has low values of C and L which deviate from the real-world networks. The weighted random graphs are constructed by randomly reshuffle the weighted edges of the original network (Bolaños et al., 2013) on E–R random graph to preserve the connectivity strengths but destroying the network structure. E–R random network have been extensively used in calculation of SWN attributes (Fraiman et al., 2014; Mader et al., 2015).

4.4 Chapter summary

This chapter discussed several network measures that will be used in this thesis to explore conditional and unconditional connectivity of undirected neuronal networks. Measures like node degree, characteristics path length and clustering coefficient provide basic descriptors for a network. These basic measures will also be used to explore differences between weighted and binary networks. More complex measure like modularity, motif and small-worldness provide more insight into the detailed structure of a network. The following chapters 5 and 6 discuss the usefulness of these measures for analysis of features, and the structure of neuronal networks for both simulated and real spike train signals.

Chapter 5

Spiking neuronal network model: Network measures analysis

This chapter presents the functional connectivity analysis on simulated signals generated using a cortical network model based on a conductance formulation, in order to verify the stability and scalability of MVPC network analysis. Scalability of the approach is investigated through application of MVPC analysis to simulated spike train data with up to 100 simultaneous spike trains generated from a 2D network of excitatory and inhibitory cortical neurons. Stability of MVPC estimates is investigated using simulated spike train data with up to 198 predictors, using a combination of simulated cortical neuron data and additional Poisson spike train predictors.

This chapter also explains the application of the proposed MVPC analysis for quantification of neuronal interactions using network measures as described in chapter 4. Network analysis is applied to binary and weighted connectivity strength derived from coherence and MVPC to determine the differences in unconditional and conditional networks of known spike train interactions.

5.1 Neuronal networks configuration

Two networks with different patterns of interactions were simulated using the point-cortical neural model as defined in section 2.3.4. The simulations were developed by Halliday (2005) and implemented in C program. A conductance-based synaptic interaction model generated spike trains according to a biophysical representation of the neurons. This network model receives input from populations of excitatory inputs, inhibitory inputs and synaptic inputs from other cells in the same network. Each input is generated from an exponential interspike-interval distribution triggered by a separate random spike train firing at 40 spikes/sec. Excitatory and inhibitory populations provide 4000 EPSPs/sec and 1000 IPSPs/sec of background synaptic activation to each cell. EPSP and IPSP conductances are modeled based on the conductance scaling factor, G_{syn} , and the time constant, τ_{syn} (Rall, 1967; Halliday, 2005) as

$$g_{syn}(t) = G_{syn}\tau_{syn}\exp(-t/\tau_{syn}). \quad (5.1)$$

Values for the parameters of the cortical network model used in this thesis were set according to Halliday (2005) specified in Appendix A.1.

The first network structure which consists of 75 excitatory and 25 inhibitory neurons was previously used for first-order partial coherence analysis in Halliday (2005). This network model with 100 nodes of neurons is known as Network A in this chapter. The second network, Network B consists of 200 nodes of excitatory and inhibitory neurons with a different pattern of interactions. Table 5.1 presents the configurations of neuronal networks simulated for testing the scalability and stability of the proposed MVPC analysis, followed by verification of MVPC-based functional connectivity on the known network structure and finally implementation of network measure analysis.

Figure 5.1 shows the center-surround regular network pattern for each excitatory neuron and inhibitory neuron for Network A. This network consists of 100

Table 5.1: Connectivity configurations for Network A and Network B.

Configuration	Network A	Network B
Number of nodes	100*	200
Excitatory neurons	75%	79%
Inhibitory neurons	25%	21%
Data length	300 sec**	600 sec
Connectivity pattern	Center-surround regular network	Small-world network
Network Analysis	Node degree, path length and motifs	Node degree and small-worldness

* Notice that another 100 spike train predictors were added to Network A for scalability testing of MVPC.

** Notice that range of data length for stability testing of MVPC is between 100 sec to 300 sec.

nodes arranged in 10 x 10 2D sheet that adopts different connectivity pattern of local excitation and inhibition. Positions of excitatory and inhibitory neuron models for Network A are presented in figure 5.2. Network B is presented in figure 5.3. This is a model of small-world network generated with rewiring probability of 0.05 (Watts & Strogatz, 1998; Brugger & Schwirzer, 2011). Network B consists of 200 nodes that adopts similar connectivity pattern of excitation and inhibition. The simulation for Network A and Network B were used to generate 300 sec and 600 sec of data, respectively. The output spike times from all neurons in both networks were logged with a 1 msec sampling interval.

Output firing rates for Network A range between 18.96 spikes/sec to 133.92 spikes/sec with mean rate of 58.76 spikes/sec. Output firing rates for Network B range between 5.21 spikes/sec to 456.70 spikes/sec with mean rate of 88.74 spikes/sec. The histogram plots for the output firing rates of Network A and Network B are shown in Figure 5.4a and 5.4b. The histogram plots for the coefficient of variation (COV) of Network A and Network B are shown in Figure 5.4c and 5.4d. Network B shows a higher output spike rate and COV compared to Network A.

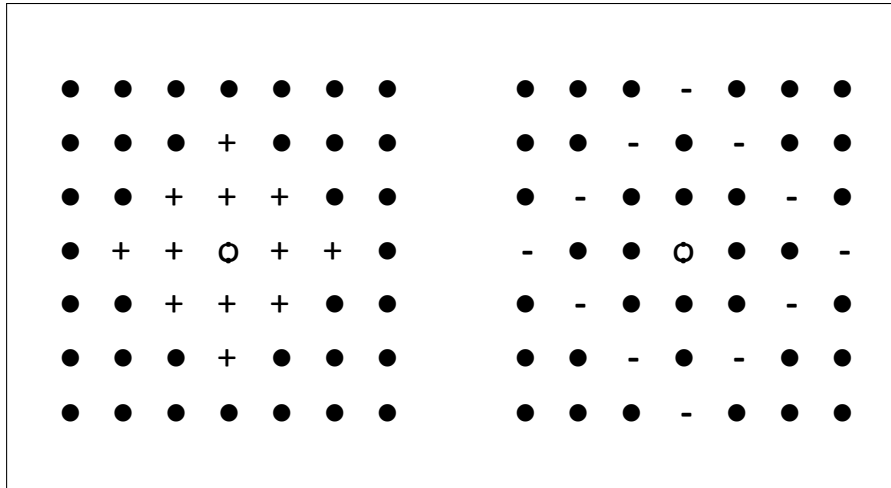


Figure 5.1: 2D planar sheet connectivity for simulation of excitatory (left) and inhibitory (right) neuron. Each character indicates the position of a neuron in Network A. 'O' is the presynaptic neuron, '+' are the postsynaptic neurons receiving excitatory inputs from 'O', '-' are the postsynaptic neurons receiving inhibitory inputs from 'O' and '•' are other neurons not receiving any input from 'O'. Designation of excitatory or inhibitory neuron for 2D connectivity in Network A is presented in figure 5.2.

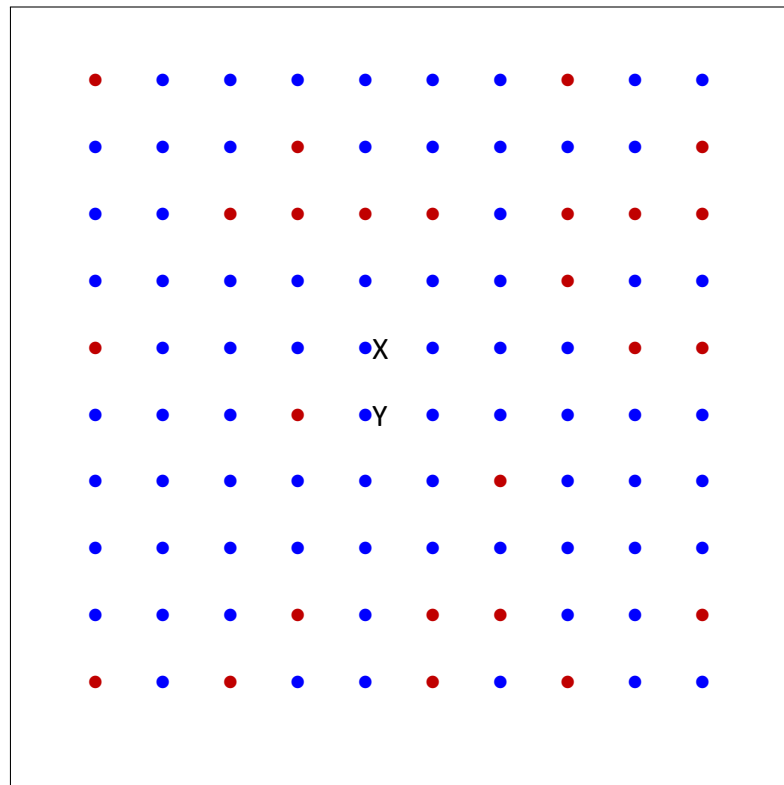


Figure 5.2: Positions of excitatory and inhibitory neurons for simulation of Network A. Blue dots are the excitatory neurons and red dots are the inhibitory neurons. X and Y indicate the positions of neurons for pairwise connectivity analysis using different numbers of predictors in section 5.2.

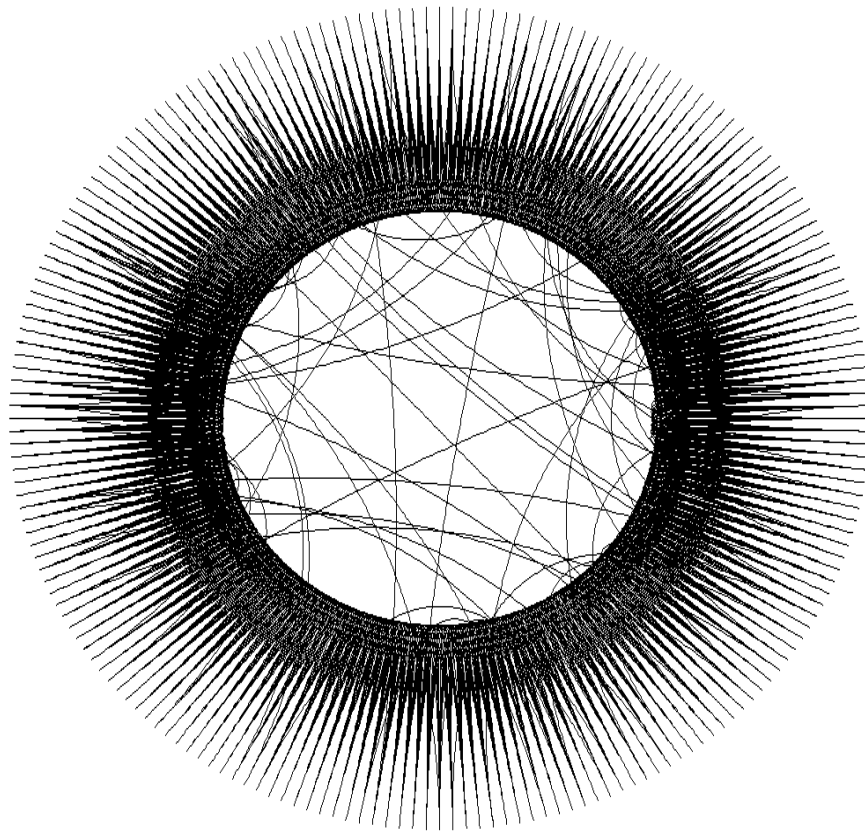


Figure 5.3: Network B is a model of small-world network generated with rewiring probability of 0.05 (Watts & Strogatz, 1998). This network consists of 200 nodes that adopts similar connectivity pattern of excitation and inhibition.

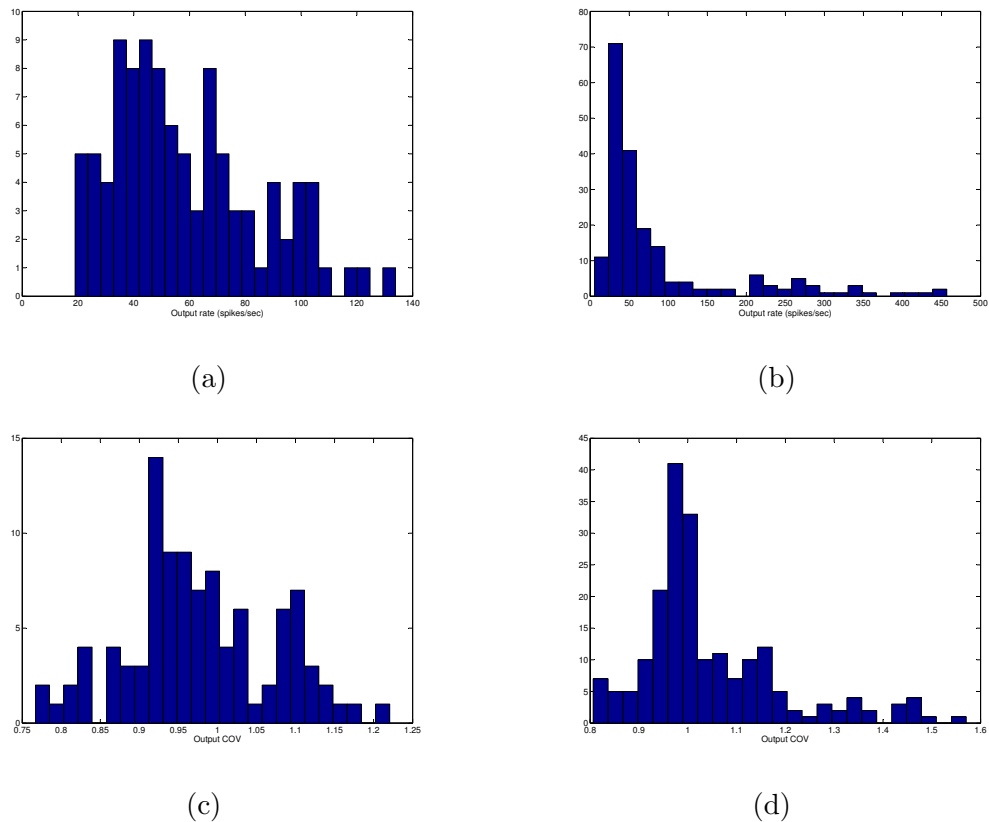


Figure 5.4: Left column: histogram plot for the (a) output firing rates and (c) output COV for model A of 100 neurons. Right column: histogram plot for the (b) output firing rates and (d) output COV for model B of 200 neurons.

5.2 Scalability test for MVPC analysis

This section discusses the scalability of MVPC analysis on Network A using different numbers of predictors. Matrix inversion of estimated cross-spectra is subject to the condition that spike train record length should be greater than the number of spike trains (Walden, 2000). This is tested here to show the stability of MVPC analysis on different data lengths. Figure 5.5 shows the result of MVPC analysis on a set of 100 spike trains using 100 sec, 200 sec and 300 sec length of data. Original coherence is included for comparison. Partial coherence should be less than or equal to ordinary coherence. Different data lengths produce different plots of partial coherence values. MVPC analysis on a set of 200 spike trains with only 100 sec of data is not stable. Longer data lengths generate stable MVPC

analysis. Therefore, the scalability test for MVPC analysis in this section will be implemented on 300 sec data length due to the maximum number of predictors which is equal to 198 spike trains.

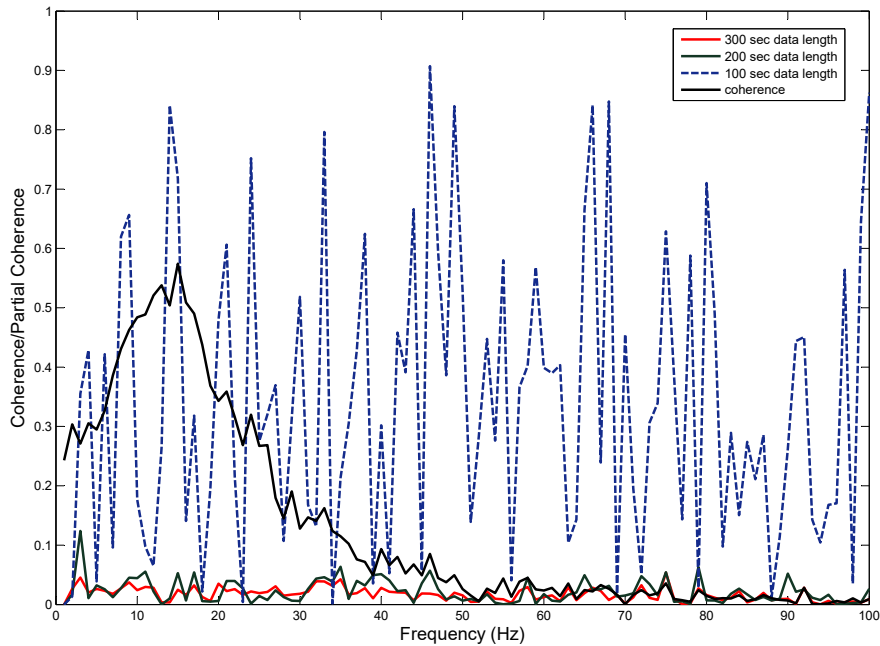


Figure 5.5: Figure shows different partial coherence values from MVPC analysis on 100 spike trains with different data lengths, 100 sec, 200 sec and 300 sec. Original coherence is included for comparison. Partial coherence should be less than or equal to ordinary coherence. Longer data lengths generate stable MVPC analysis.

Scalability test for higher order MVPC analysis were conducted by gradually increasing the number of predictors for conditional interaction between neurons X and Y from Network A. Neurons X and Y are selected because of the location in the middle of the network in Figure 5.2. Output firing rates for X and Y are 92.62 spikes/sec and 80.75 spikes/sec, respectively. The COV of spike trains for these two neurons are 0.95 and 1.10.

The second order spectrum of X and Y were estimated according to Equation 3.6 with $L=292$ using segment length, $T = 1024$. The sampling rate for the 300 sec spike trains data is 1 msec. Unconditional pairwise relationship between these two neurons is estimated by coherence, $|\hat{R}_{XY}(\lambda)|^2$ as in equation 3.14.

Coherence value will be the marker for comparison of conditional interaction between X and Y. Conditional interaction between the neurons are measured by partial coherence estimates, $|\hat{R}_{XY/Z}(\lambda)|^2$ as in Equation 3.32, where the number of predictors in Z is the manipulated parameter for MVPC scalability tests.

The first scalability test is conducted on a group of ten predictors located adjacent to neurons X and Y in Network A, to look at the predictive effect from the closest neurons as shown in Figure 5.6. The plot in Figure 5.7 shows comparison between ordinary coherence and partial coherence plots for pairwise interaction between X and Y using 1 to 10 predictors located around neurons X and Y. The number of predictors were increased by grouping the neurons according to the sequence of numbers in Figure 5.6. For example, MVPC analysis with three predictor neurons will consider neurons 1, 2 and 3 as the predictors. The plot in Figure 5.7 shows that magnitudes of partial coherence estimates decrease with increasing numbers of predictors. Significant reduction in partial coherence values indicates strong common influence from the 10 closest predictor neurons on the unconditional pairwise interaction between X and Y.

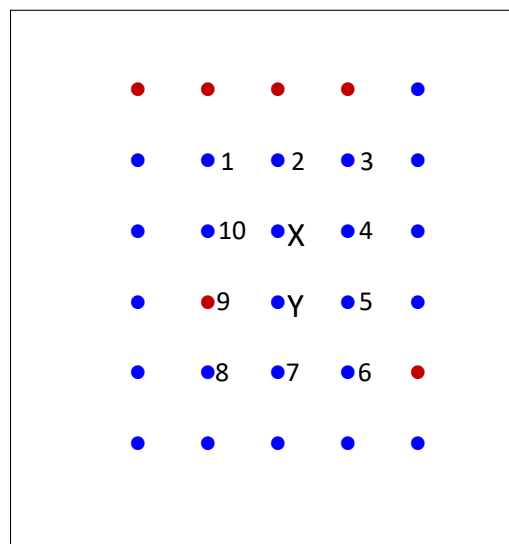


Figure 5.6: Figure shows position of 10 predictor neurons located around neurons X and Y. Blue dots show the excitatory neurons and red dots show the inhibitory neurons.

The next scalability test for higher order MVPC analysis were conducted to quantify conditional relationship between neurons X and Y using several group

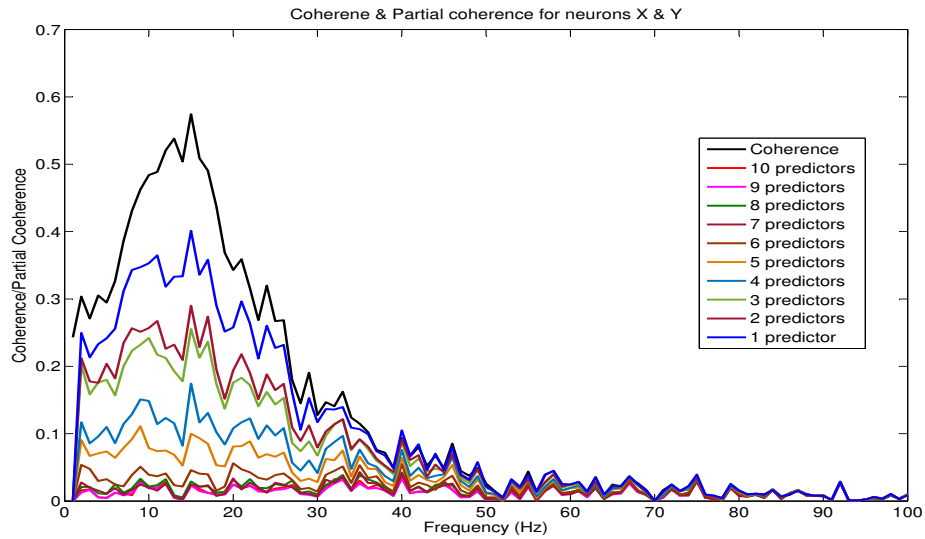


Figure 5.7: Figure shows comparison between coherence and partial coherence values after gradually increasing the number of predictors from 1 to 10 neurons located around neurons X and Y as shown in Figure 5.6.

of predictors. Figure 5.8 (a) to 5.8 (d) shows different groups of predictors for pairwise conditional interaction between neurons X and Y in Network A. The group of predictors were highlighted in the green boxes, which used 20, 40, 60 and 80 predictors.

The result in Figure 5.9 shows a comparison between ordinary coherence and partial coherence plots for pairwise interaction between X and Y using different number of predictors. As might be expected, the magnitudes of the partial coherence estimates drop off with increasing numbers of predictors. This indicates that the strength of connectivity between X and Y reflects the reciprocal connections of the adjacent neurons. Removing the effect from 20 predictors located farthest from X and Y will only slightly reduce the connectivity strength up to 27 Hz.

The partial coherence values continue to reduce with increasing number of predictors. Gradual reductions in partial coherence values show that neurons in each group of predictors are contributing indirectly to pairwise unconditional relationship between X and Y. Inclusion of all 98 other neurons as the predictors shows the lowest partial coherence value with largest reduction for up to 50 Hz

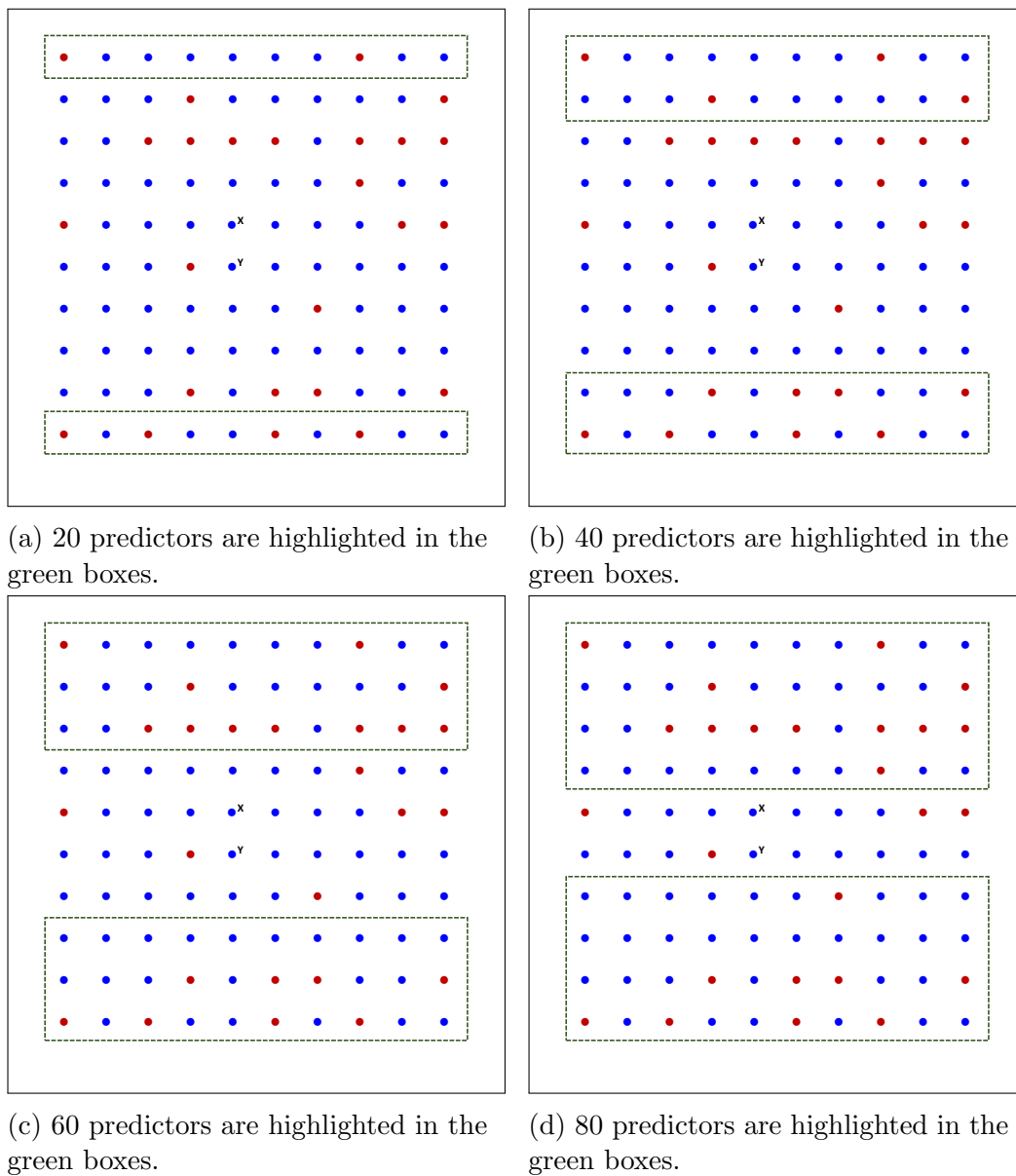


Figure 5.8: Figure (a) to (d) show neurons X and Y positioned in the middle of 2D network with the predictors highlighted in the green boxes. Blue dots show the excitatory neurons and red dots show the inhibitory neurons.

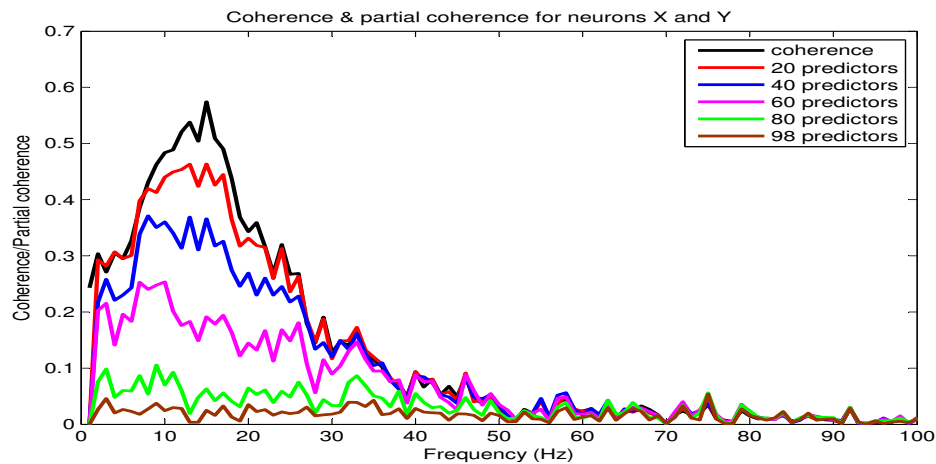


Figure 5.9: Figure shows comparison between coherence and partial coherence values after gradually increasing the number of predictors for pairwise interaction between neurons X and Y.

compared to ordinary coherence. This lowest partial coherence value suggests the conditional relationship that is closer to the real strength of interaction between X and Y.

It is apparent that MVPC analysis using all available predictors in Network A exhibits a similar pattern of conditional connectivity strength as the previous analysis in Figure 5.7 using less predictors located around neurons X and Y. The results in Figure 5.9 and Figure 5.7 show that one nearby predictor leads to a better prediction for connectivity between X and Y than 20 faraway predictors. This indicates that predictors effect for this network are affected by the distance from X and Y. Further investigation on specific predictor could identify the most influential neurons that is interconnected between X and Y.

MVPC analysis using ten closest predictor neurons produces similar partial coherence as seen in the analysis using 98 predictors. This indicates that ten closest neurons surrounding X and Y are the most influential predictors which contribute to the pairwise unconditional relationship between X and Y. MVPC analysis considering all available predictor neurons should provide an accurate

strength of interaction representing the connection between X and Y. Consideration of higher number of predictors could provide connectivity measures that will take into account the intermediate effect of surrounding neurons. Running the analysis with specific predictor neurons can help in searching for the most influential contributor for pairwise unconditional relationship over a particular range of frequencies.

In the third scalability test, 100 poisson spike trains were added to Network A as additional predictors in order to test the scalability of the proposed method on a set of 200 spike trains. This means that the conditional relationship between the two neurons is subject to a combination of additional poisson spike trains and spike trains from the available predictor neurons. These additional predictors are uncorrelated with network activity so they should not effect partial coherence estimates. Figure 5.10 shows comparison between ordinary coherence and partial coherence plots for pairwise interaction between X and Y using similar group of predictors as in the previous test with an additional 100 Poisson spike trains. The result produce similar plots as in the previous test in Figure 5.9 using the same group of predictors without additional spike train predictors. As might be expected, the additional Poisson spike trains are not contributing to the pairwise interaction between X and Y. These experiments prove that MVPC analysis is scalable for a large number of predictor neurons, currently tested up to 198 predictors.

5.3 Conditional and unconditional network analysis

This section provides comparison between unconditional and conditional network analysis using two basic measures, node degree and path length. Both measures were described in chapter 4. Unconditional and conditional edges of Network A are constructed using coherence and MVPC analysis, respectively. Weighted

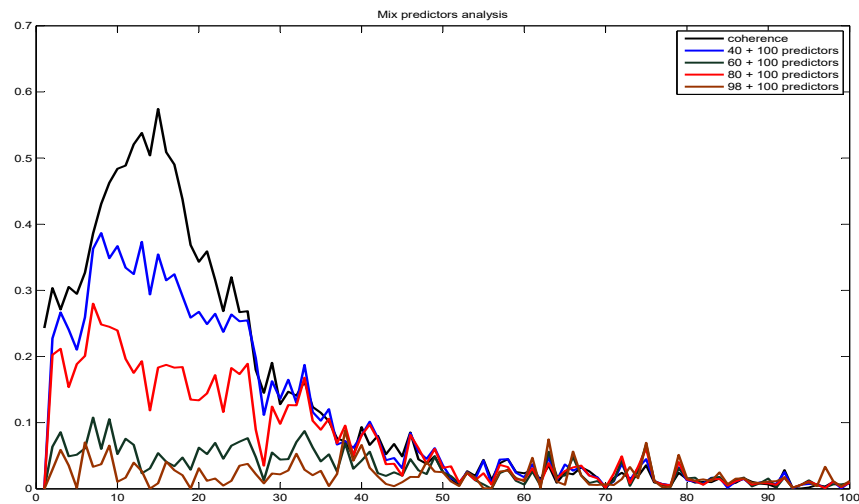


Figure 5.10: Figure shows comparison between coherence and partial coherence values after gradually increasing the number of predictors around neurons X and Y, with combination of additional 100 poisson spike trains.

unconditional and conditional edges were determined by the mean coherence and partial coherence values over a 0 to 30 Hz frequency range using Equations 3.14 and 3.32 respectively. A significance threshold value was applied for unconditional and conditional edge weight using the corresponding 95% confidence limits for coherence (0.0102) and partial coherence (0.0154).

All network graphs in this chapter are plotted using an open-source network visualization software, Gephi version 0.9.1 (Bastian & Heymann, 2009). Figure 5.11 and 5.12 show the unconditional and conditional networks for Network A with node number referring to the position of nodes according to Figure 5.13(top). Weighted edges between nodes show the strength of connectivity constructed from coherence and MVPC analysis. Thicker edges show stronger functional connections between neurons. These graphs are plotted using the ForceAtlas 2 layout in Gephi 0.9.1 due to its ability to organize node positions by transformation of the edge weights into the strength of attraction and repulsion forces (Jacomy et al., 2014).

The unconditional network of Figure 5.11 shows dense connections between

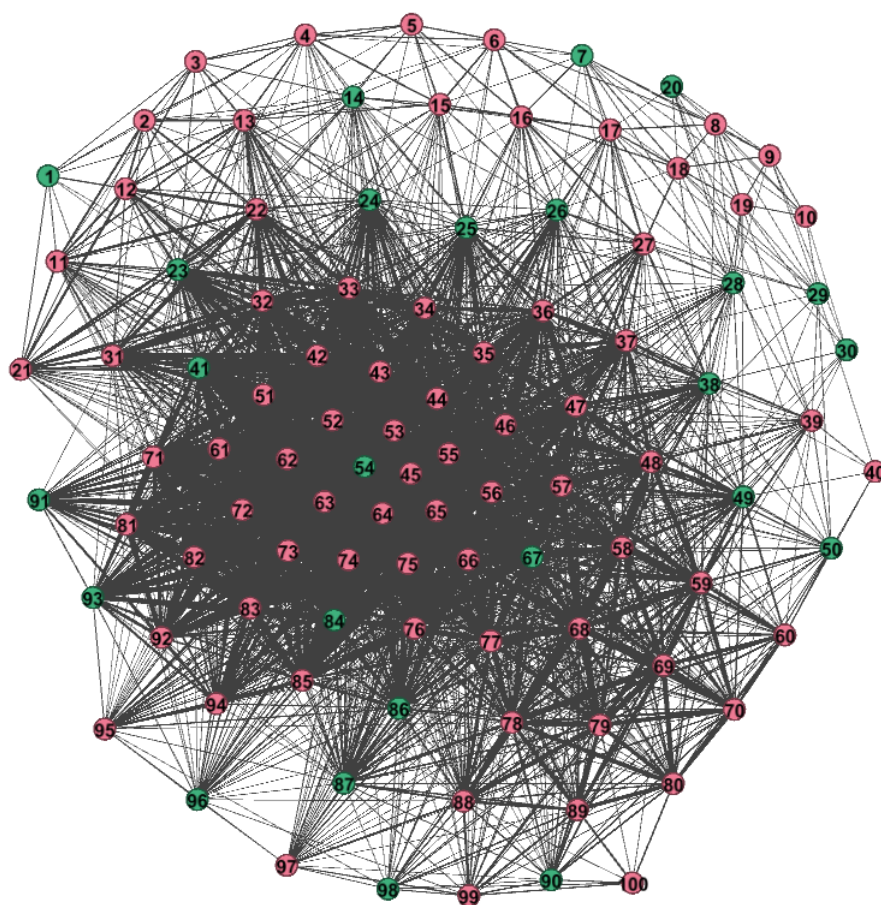


Figure 5.11: Unconditional weighted network for simulated Network A with excitatory neurons (red) and inhibitory neurons (green). Links between nodes show weighted edges constructed from coherence analysis. Thicker edges show stronger connections.

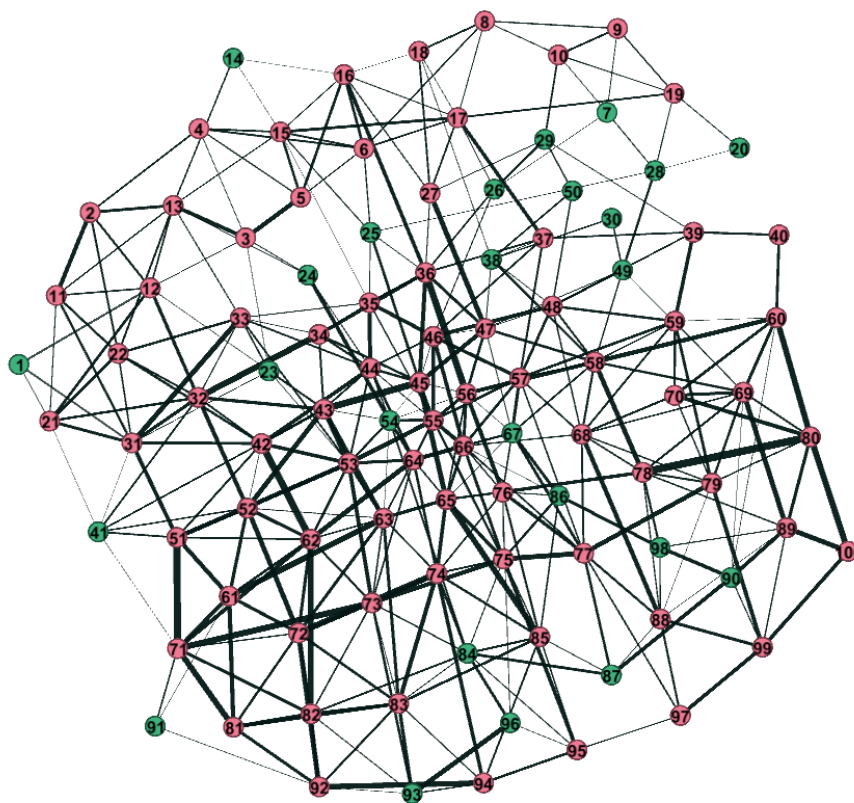


Figure 5.12: Conditional weighted network for simulated Network A with excitatory neurons (red) and inhibitory neurons (green). Links between nodes show weighted edges constructed from multivariate partial coherence analysis. Thicker edges show stronger connections.

nodes with a range of interaction strengths. Estimation of connectivity strength using MVPC analysis on the same dataset produces conditional network with only 383 conditional edges that is 84.33% reduction from 2444 edges in unconditional network. The conditional network is presented in Figure 5.12. Conditional network shows varying strength edges of local connections from a node to its neighbours which shows the reorganization of node positions due to excitatory and inhibitory neuron activities. Comparison between both networks suggests that conditional network indicates more accurate edges according to organization of neurons in the simulated network. Application of network metrics are useful to assist the visual observation of the graph providing a quantitative description of network structure and organization.

5.3.1 Node degree analysis on simulated network.

Node degree is the most fundamental network measure for analysis of connectivity patterns. Degree is defined in Section 4.1.1 as the number of neighbours connected to a node. This measure shows the importance of individual nodes where a network node with a high node degree has many edges connected to it. Figure 5.13 shows color-coded graphs of the degree for 100 nodes in Network A. The degree for each node is depicted using color scale as shown on the right of the graph.

Comparison between the graph for conditional and unconditional node degree shows a different range of degree for Network A. Node degree for unconditional network shows high number of connections for most of the nodes compared to the conditional network. The maximum value of node degree for the conditional and unconditional network is 13 and 80, respectively. Elimination of common effects in the conditional network reduces node degree substantially. Lower conditional node degree are captured in Figure 5.13(middle). Conditional node degrees are range between 2 to 13 as expected according to the simulated model of Network A. This is in contrast to the unconditional network where most of the nodes are highly connected. Figure 5.13(bottom) shows high variation in

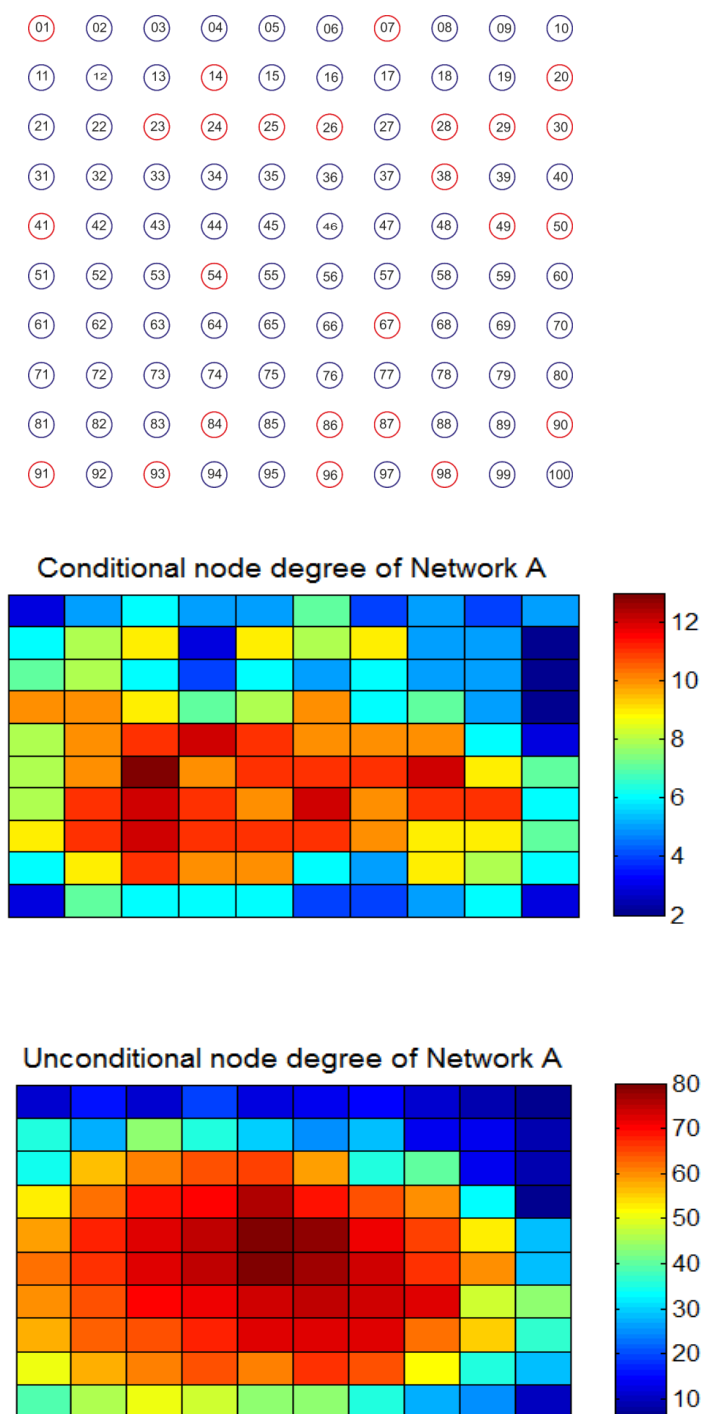


Figure 5.13: Top figure shows position of nodes using number 1 to 100 for simulated Network A. Blue and red circle distinguish between excitatory and inhibitory neurons, respectively. Middle figure shows color-coded graph of conditional node degree for Network A, and bottom figure shows the unconditional node degree for Network A. The values of degree for each nodes middle and bottom plots are arranged according to neurons positions as shown in top figure. Unconditional network shows high number of connections compared to the conditional network. Unconditional node degree range are higher between 6 to 80, compare to the conditional degree. Top figure clearly shows reduction in conditional node degree. Elimination of common effects reduces node degree in the range of 2 to 13 in conditional network as expected according to the simulated model of Network A.

node degree of the unconditional network. This indicates dense interaction before removal of the common effects using partial coherence analysis.

This network was simulated in a single planar sheet of neurons without wrapping of connections at the edge of the network. Both conditional and unconditional network shows high degree of connections at the centre of the network due to decreasing of neuronal interactions at the edge of the network. A torus organization of simulated network could provide better presentation of neuronal interactions by elimination of the lower node degree due to the location of neurons at the edge of the network. Unconditional node degree for Network A shows that neurons located in the middle of the network are having higher degree. The degree gradually decreased from the middle of Network A toward the outer position of the network. For example, Nodes 45 and 55 located in the middle of Network A show highest unconditional node degrees. However most of the neurons with higher conditional node degree for Network A are excitatory neurons, and most of the lower conditional degree are inhibitory neurons. This results seems to show that the conditional node degree for neurons in Network A are influenced by the excitatory and inhibitory activities of Network A.

5.3.2 Path length analysis on simulated network.

Path length is the basic network metric for measuring the shortest pathway between network nodes. Path length is described in Section 4.1.2 as a number of steps in the shortest pathway from a node to each of its neighbours as defined in Equation 4.5. Weighted path length is a weighted measure of path length that takes into account the strength of connections between the nodes as defined in Equation 4.6. The distance between two neurons for the weighted path length is the inverse of coherence and partial coherence for unconditional and conditional network, respectively.

Figure 5.14 and 5.15 shows color-coded graphs of binary path length for con-

ditional and unconditional connectivity in Network A. These graphs show path length from each node to all other nodes, arranged in numbered positions according to Figure 5.13(top). Maximum path length for binary unconditional network is lower than the maximum value for binary conditional path length. Shorter binary unconditional path lengths possibly show the interaction pathway through non-existence edges resulting from common influence effect. For example shortest distance between node 1 and 100 is 3 in unconditional network, which is too short is inconsistent with the simulated model of Network A. The same path length in conditional network is 9 and can be considered as a reliable distance according to the position of neurons and pattern of interaction between neurons in Network A.

Comparison between unconditional and conditional weighted path length in Figure 5.16 and 5.17 is consistent with binary path length comparison. The maximum weighted path length for conditional network (372.2) are higher than those for the unconditional network (114.4). The characteristic path length (weighted = 154.3, binary = 3.5) of conditional network is higher than the characteristic path length of unconditional network (weighted = 26.9, binary = 1.6). Consistent results in binary and weighted path length analysis on conditional network suggests that MVPC analysis is useful tool for inferring neuronal connections for path length analysis.

Figure 5.18 displays binary and weighted path length distributions for unconditional and conditional networks. It is apparent from the distribution of binary path length in unconditional network that the distance between two nodes are between 1 to 3 steps which indicates short pathway between all nodes in Network A. This is inconsistent with the binary path length for conditional network that shows better distribution, which indicates various distance between nodes in Network A consistently within the range of distance specified in simulated model of Network A. Weighted path length data for conditional network appears to be symmetrically distributed in agreement with binary path length distribution. Unconditional network again shows higher distribution of shorter distance for weighted neuronal connections. Comparison between conditional and uncon-

ditional network indicates different distributions of path length. Different ranges appear in path length distributions between conditional and unconditional networks. The binary unconditional networks have shorter range of path length than the binary conditional networks. This is consistent with the weighted unconditional path length analysis.

There is a more consistent path length in the conditional network as expected for neuronal connections in Network A. This can be seen by looking at the range of path length from one neuron to all other neurons in the Network A. Figure 5.19 and 5.20 show binary and weighted path length for neuron 1 in Network A. The position of the neurons is according to the neuronal position of Network A in Figure 5.13(top). Neuron 1 located at the top left of all of the graphs in dark blue color. Realistic distance can be seen in conditional binary path length, for example the highest path length is the distance to neuron 100 at the bottom right of the graph. Weighted conditional path length is consistent with binary conditional path length. Both of the graphs show gradual increment in the distance from Neuron 1 to all other neurons according to the location of the neuron. Weighted path length is also affected by the strength of interactions between neurons contributed by the neuronal excitatory and inhibitory activities. Realistic path length in conditional network demonstrate good consequence of using conditional edges. These results seem to indicate the advantage of MVPC analysis as opposed to coherence analysis in quantification of binary and weighted edges for a more accurate results in further network analysis.

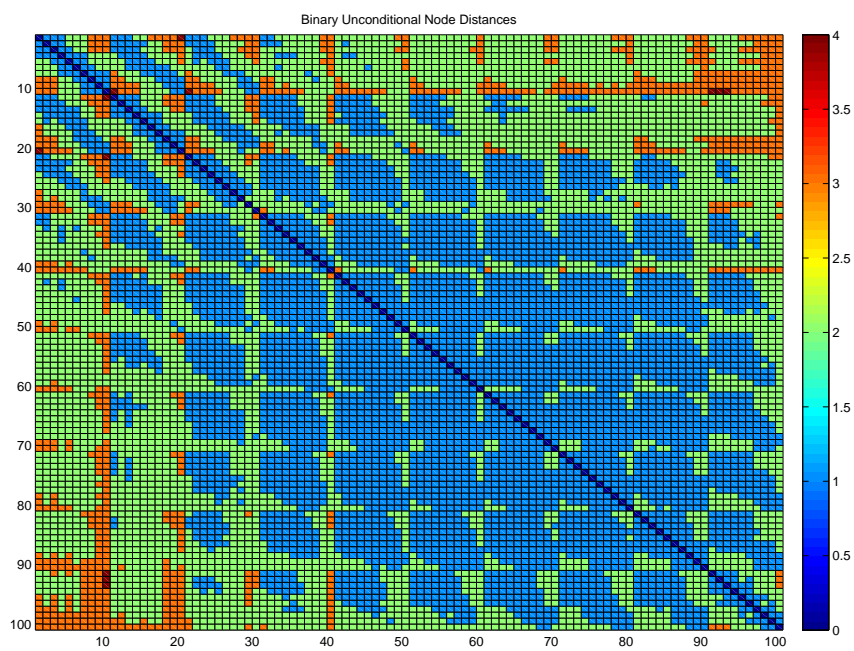


Figure 5.14: Color-coded graphs of binary path length for unconditional network. Position of nodes is according to Figure 5.13(top).

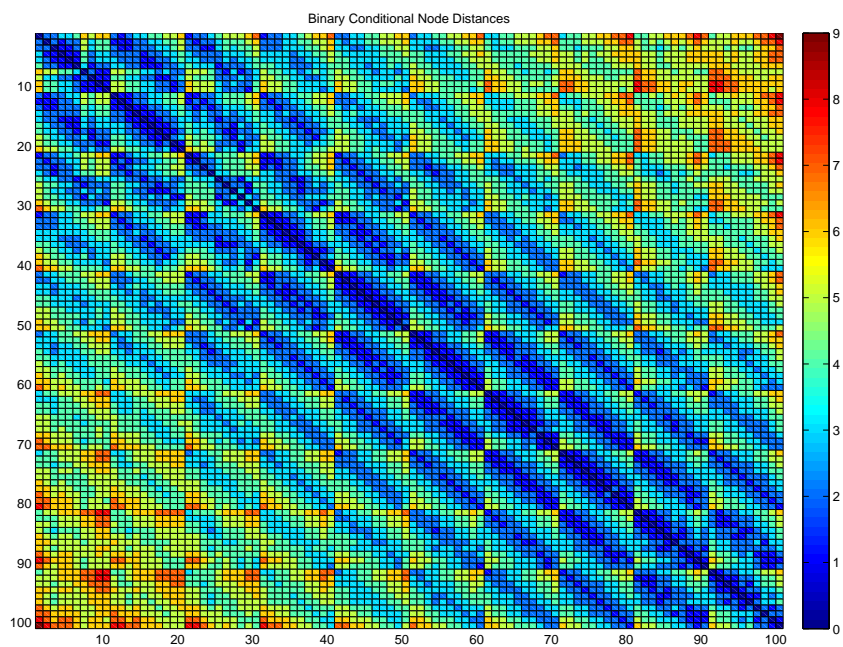


Figure 5.15: Color-coded graphs of binary path length for conditional network. Position of nodes is according to Figure 5.13(top).

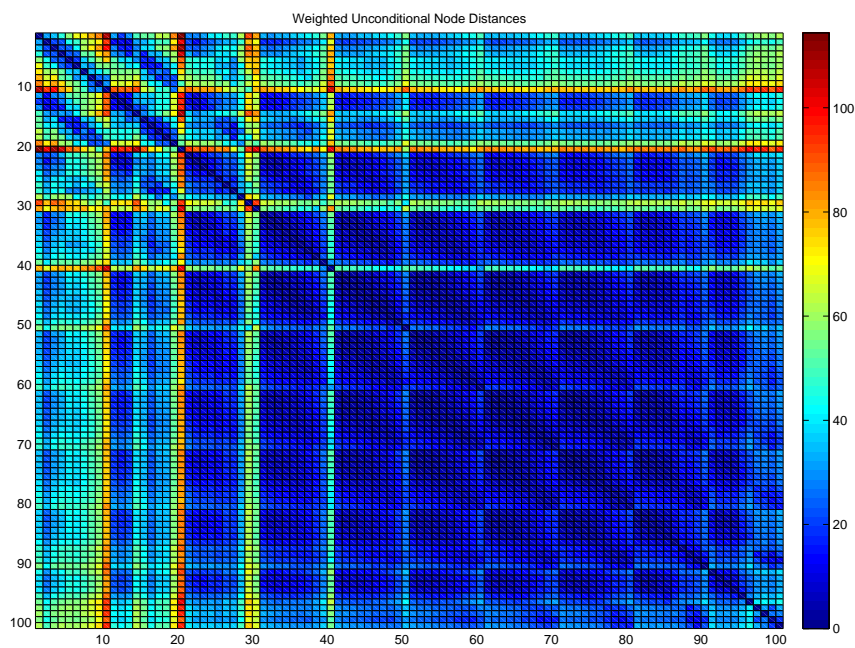


Figure 5.16: Color-coded graphs of weighted path length for unconditional network. Position of nodes is according to Figure 5.13(top).

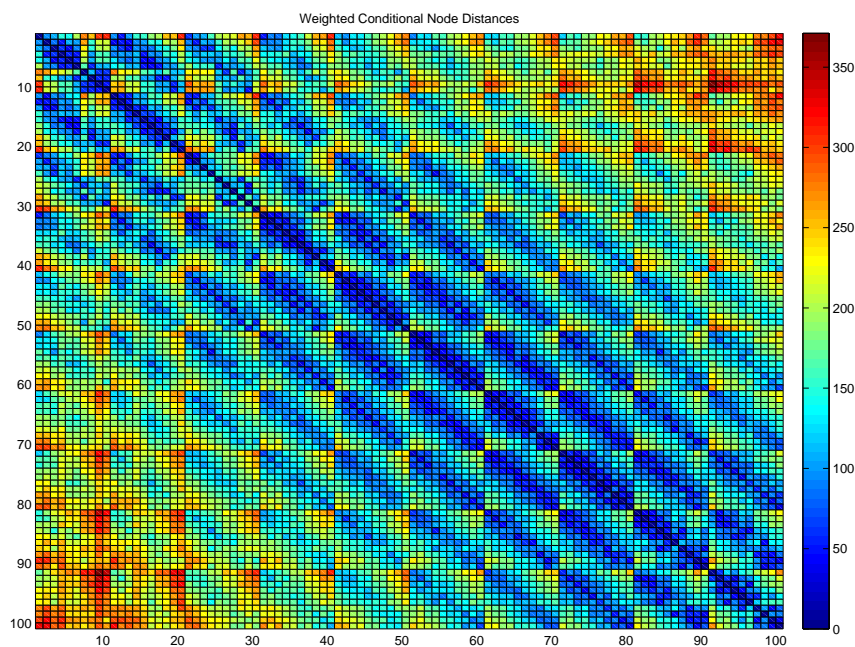


Figure 5.17: Color-coded graphs of binary path length for conditional network. Position of nodes is according to Figure 5.13(top).

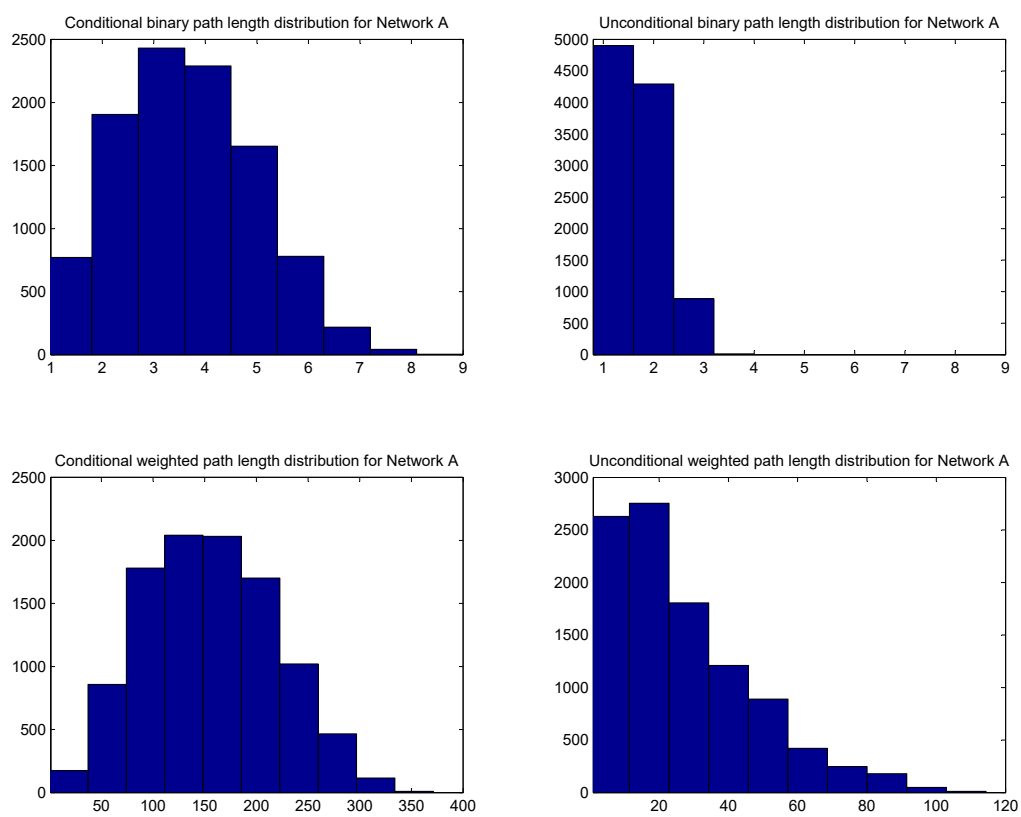


Figure 5.18: Binary and weighted path length distributions for unconditional and conditional connectivity of Network A.

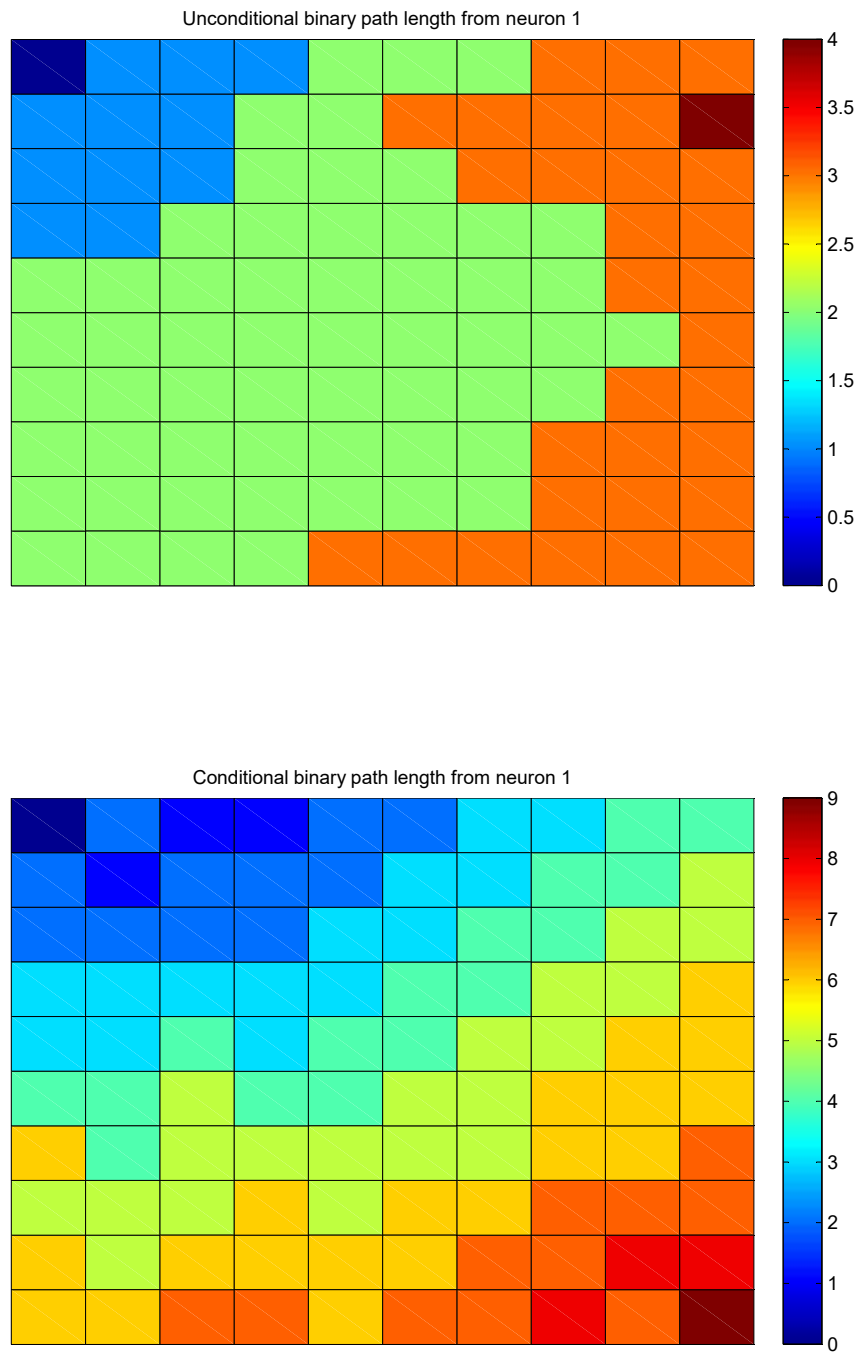


Figure 5.19: Color-coded graphs of binary unconditional path length(top) and conditional path length(bottom) to show the shortest distance from neuron 1 to all other neurons in Network A according to the neurons position in Figure 5.13(top). Neuron 1 located at the top left of both graphs in dark blue color. Realistic distance can be seen in conditional path length, for example the highest path length is the distance to neuron 100 at the bottom right of the graph.

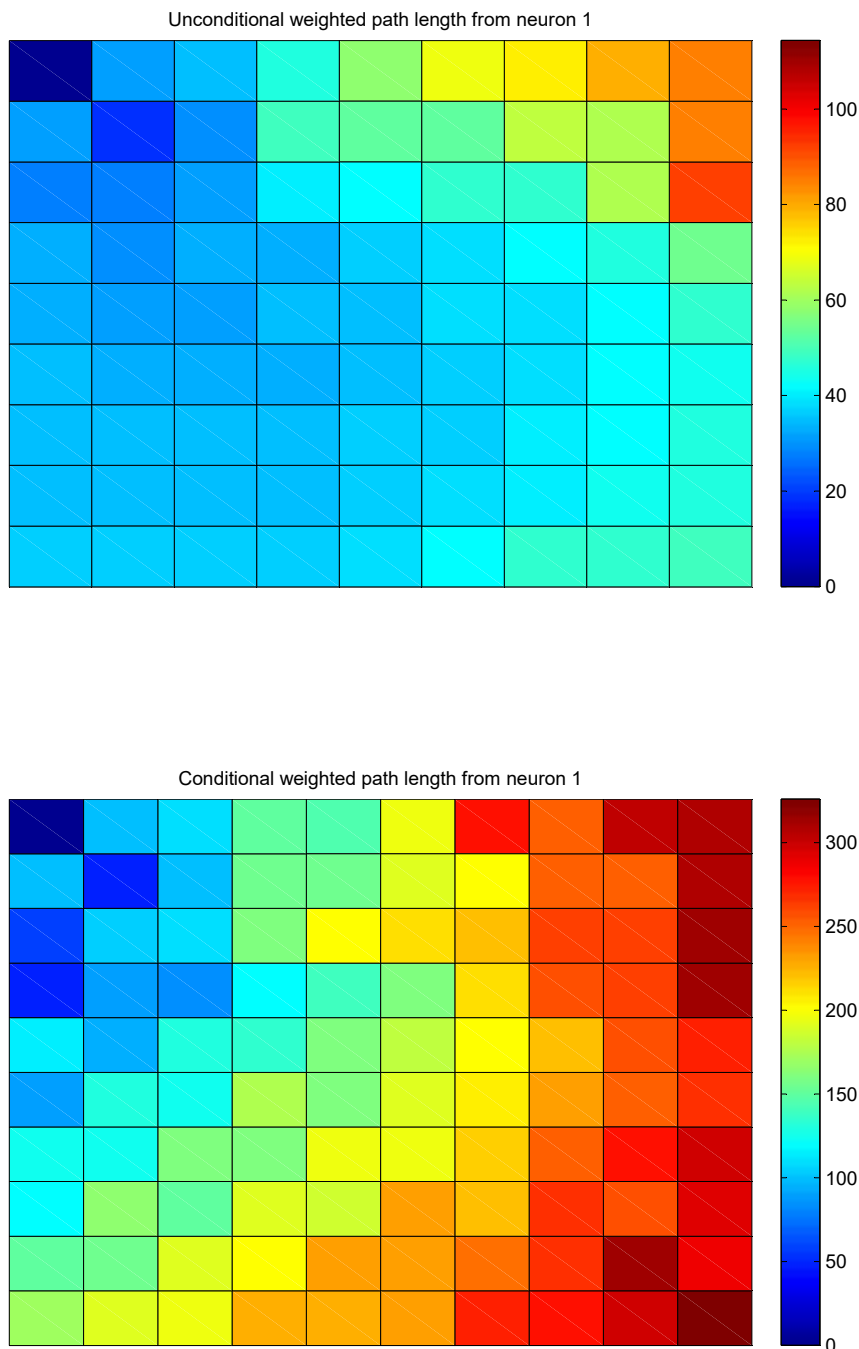


Figure 5.20: Color-coded graphs of weighted unconditional path length(top) and conditional path length(bottom) to show the weighted shortest distance from neuron 1 to all other neurons in Network A according to the neurons position in Figure 5.13(top). Weighted conditional path length in this graph is consistent with binary conditional path length in Figure 5.19 with gradual increment in the distance from Neuron 1 to all other neurons according to the location of the neuron. Weighted path length is also affected by the strength of interactions between neurons contributed by the neuronal excitatory and inhibitory activities.

5.4 Reproducibility of network motifs

This section discusses the ability to reproduce the subgraph connectivity patterns in simulated Network A after implementation of MVPC analysis. Motif detection from network theory as discussed in section 4.2 will be implemented using FANMOD for searching all possible subgraphs as suggested in Ribeiro et al. (2009). FANMOD discover percentage of subgraphs occurrence for motif size between 3 to 8 in the original network. Conditional network constructed of binary edges from MVPC analysis is expected to represent the neuronal interactions with a similar pattern of neuronal connectivity as in Network A. However, conditional interaction from each neuron may also produce a subgraph with some missing edges due to the inhibitory activities from inhibitory neurons.

Table 5.2 and 5.3 present three most frequent subgraphs patterns for motif size 3 to 6 inferred from FANMOD analysis on conditional and unconditional binary network. The subgraph is represented on a network of 6 nodes for a standardized view of subgraph size 3, 4, 5 and 6. The total number of edges in the conditional network is 383, that is 15.67% of the 2444 edges in the unconditional network. FANMOD analysis on conditional network produce 3.26%, 0.92%, 0.33% and 0.002% total subgraphs of size 3, 4, 5 and 6, respectively as compared to the total number of subgraphs of the same size in unconditional network. Increasing the motif size will exponentially increase the numbers of subgraphs. Thus discovery for larger size of subgraphs will reduce the percentage of occurrence for conditional networks as compared to unconditional network.

FANMOD produces different percentage of occurrence for two similar patterns of subgraphs of size 3. The most frequent subgraphs of size 4 to 6 that occur in unconditional network are constructed with higher number of edges than the same size of subgraph in the conditional network. Increasing the motif size to 6 enable for discrimination between expected and unexpected subgraph pattern due to the design of excitatory neuronal interaction in Network A as shown in Figure 5.1(left). The expected pattern for subgraph connecting 6 excitatory neu-

Table 5.2: High frequency occurrence subgraph for conditional network.

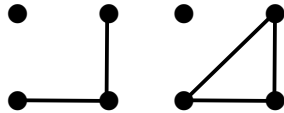
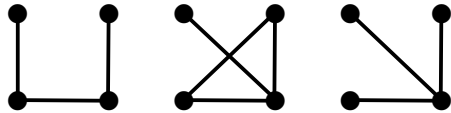
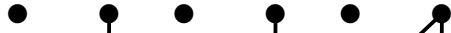
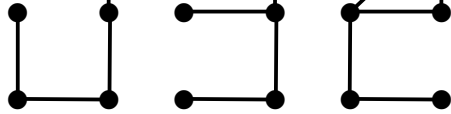
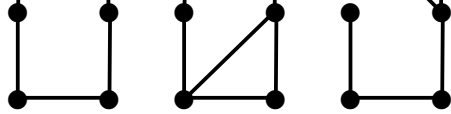
Conditional network, Number of edges = 383	
Motif size	3
Total subgraphs	2190
	
	
Frequency of occurrence	82.83% 17.17%
Motif size	4
Total subgraphs	14182
	
	
Frequency of occurrence	55.35% 24.46% 11.54%
Motif size	5
Total subgraphs	97362
	
	
Frequency of occurrence	33.37% 19.77% 15.00%
Motif size	6
Total subgraphs	687820
	
	
Frequency of occurrence	18.68% 11.39% 11.10%

Table 5.3: High frequency occurrence subgraph for unconditional network.

Unconditional network, Number of edges = 2444	
Motif size	3
Total subgraphs	67267
Frequency of occurrence	55.19% 44.81%
Motif size	4
Total subgraphs	1542098
Frequency of occurrence	33.03% 26.67% 22.13%
Motif size	5
Total subgraphs	29078743
Frequency of occurrence	15.27% 13.75% 12.12%
Motif size	6
Total subgraphs	461109376
Frequency of occurrence	6.98% 6.00% 5.96%

rons with maximum number of edges is illustrated in Figure 5.21. Subgraphs of size 6 from unconditional network show unexpected connections, presented by the dashed line.

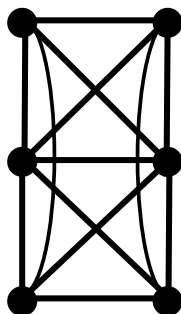


Figure 5.21: The expected pattern for subgraph connecting 6 excitatory neurons with maximum number of edges according to Figure 5.1(left).

Table 5.4 present three most frequent subgraphs patterns for motif size 3 to 6 inferred from FANMOD analysis on unconditional sparse binary network. The sparse binary network is the unconditional network with similar number of edges as the conditional network. The number of unconditional edges are randomly removed to test for motifs reconstruction between both network with similar number of edges. The total subgraphs in the sparse unconditional network is higher than the conditional network for all sizes. FANMOD analysis on sparse unconditional network produce the high frequency occurrence subgraphs for all sizes according to the expected motifs as can be seen in motifs for unconditional network. The frequency for most frequent subgraphs of all sizes in sparse unconditional network are higher than the same size of subgraph in the conditional network. This results show that no significant differences in motifs analysis between the sparse unconditional network and conditional network as 84% of unconditional edges have been removed from the network.

Table 5.4: High frequency occurrence subgraph for sparse unconditional network with similar number of edges to conditional network.

Conditional network, Number of edges = 383	
Motif size	3
Total subgraphs	2641
Frequency of occurrence	96.52% 3.48%
Motif size	4
Total subgraphs	24443
Frequency of occurrence	66.59% 23.46% 7.66%
Motif size	5
Total subgraphs	242640
Frequency of occurrence	39.79% 38.30% 4.69%
Motif size	6
Total subgraphs	2427278
Frequency of occurrence	20.38% 19.94% 19.20%

Higher percentage of the most common subgraph in conditional network with fewer edges than the unconditional network seems to indicate that the occurrence of such subgraph in conditional network is related to a specific topology of the network. There are more reliable motifs with higher percentage found in conditional network which demonstrates good consequences of using conditional edges. These results seem to indicate the advantage of MVPC analysis as opposed to coherence analysis in quantification of the network edges. Removal of common influence from other neurons produce more accurate pairwise connections in the network, hence reveals more accurate result in motif discovery analysis.

5.5 Small world analysis: Binary and weighted network analysis

This section discusses the ability to reproduce the overall connectivity pattern with predetermined SWN network topology in simulated Network B after implementation of MVPC analysis. SWN analysis from network theory as discussed in section 4.3 will be implemented thus several network measures related to SWN are computed for the conditional network. Network B is simulated according to network configuration in Table 5.1 with excitatory and inhibitory activity arrangement as in Figure 5.3.

Conditional network constructed after MVPC analysis is presented in Figure 5.22. This figure suggests the existence of SWN properties in the conditional network by the occurrence of consistent regular connections between nodes and relatively fewer long distance connections. The connectivity of this network matches the design of simulated Network B which used SWN topology. Analysis of SWN metrics complements the visual observation of the graph and assists the description of this network.

The node degree range for the conditional network is between 1 to 13. The

Table 5.5: Network analysis for binary and weighted conditional network with 600 seconds length of spike trains data for simulated Network B.

Network measure	N	C	C_{rand}	L	L_{rand}	S
Binary network	200	0.55	0.06	3.50	2.13	6.89
Weighted network		0.0058	0.00055	279.12	212.83	7.68

average node degree of 10.5 which is close to 12, the average node degree used in the design of Network B. The difference may be due to missing links resulting from effects of inhibitory neuron activities. Summary of SWN analysis for the network constructed from conditional edges inferred by MVPC analysis on 600 seconds length of spike trains data is presented in Table 5.5. This table present the number of node, N , clustering coefficient, C , clustering coefficient for random network, C_{rand} , characteristic path length, L , characteristic path length for random network, L_{rand} and the SWN index, S . The small worldness index is computed according to equation 4.20 and 4.21. A network is said to be a small-world network if $C^w \gg C_{rand}^w$, $L^w \lesssim L_{rand}^w$ and $S^w \gg 1$ (Humphries & Gurney, 2008). The table shows that both binary and weighted conditional network exhibit SWN properties, which confirms visual observation of the network in Figure 5.22.

Unconditional network presented in Figure 5.23 does not exhibit SWN properties with L less than L_{rand} . The network measures analysis on conditional network are able to infer the presence of SWN properties from data generated with known SWN topology. Combination of MVPC analysis with network measure analysis present the possibilities to discover SWN topology from spike trains data set.

5.6 Chapter summary

This chapter begins with three stability tests for MVPC analysis to show that potentially large numbers of predictors can be incorporated. The examples here used

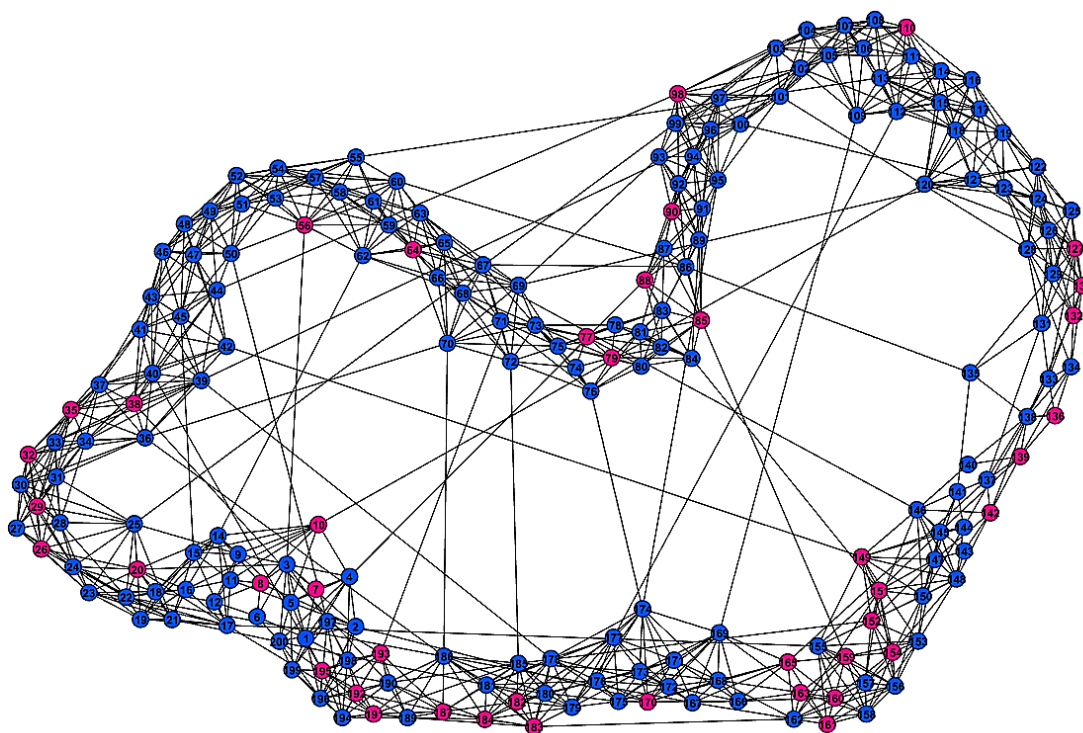


Figure 5.22: Conditional weighted network for simulated Network B. Links between nodes show weighted edges constructed from MVPC analysis. Thicker edges show stronger connections between nodes.

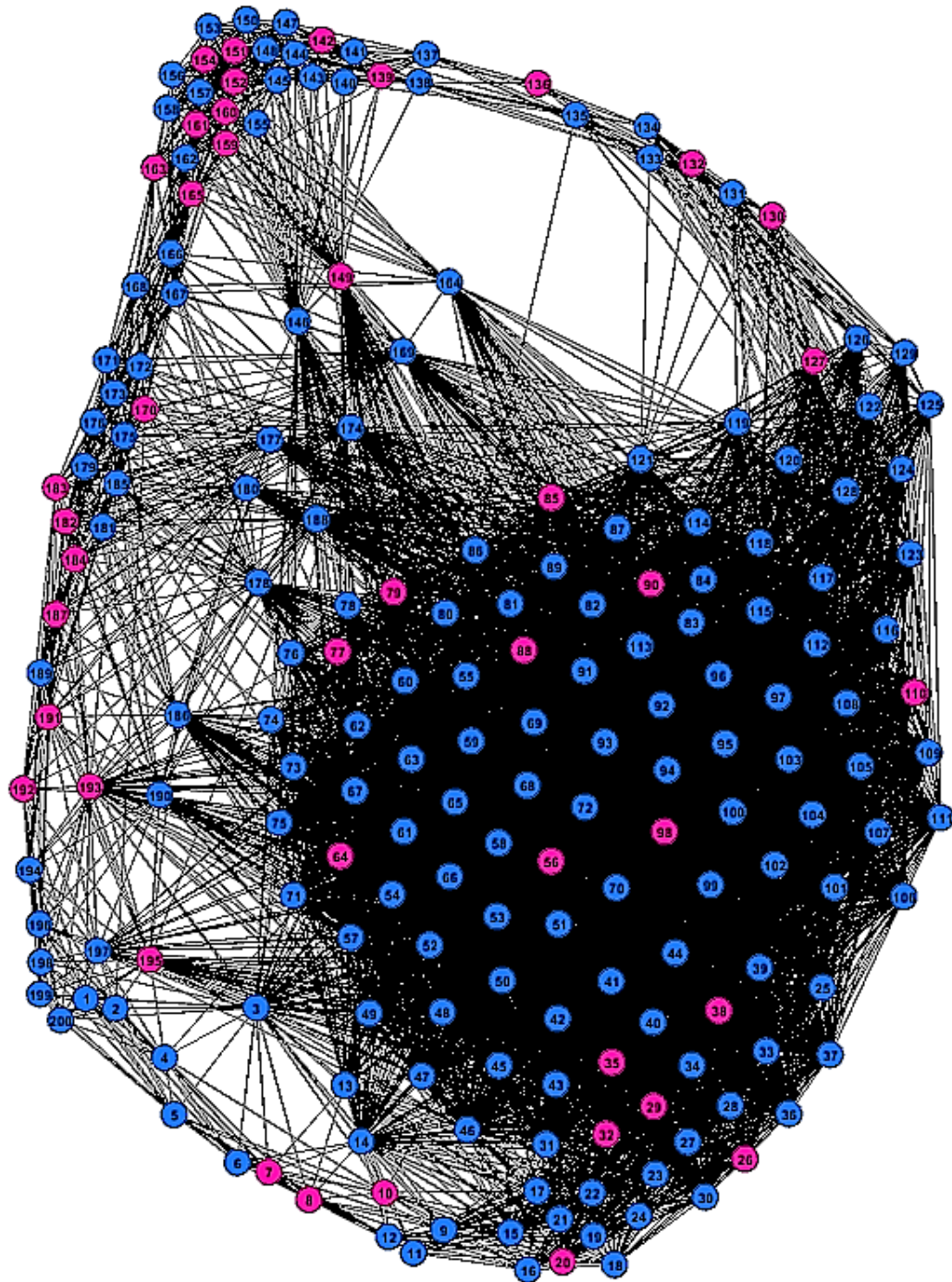


Figure 5.23: Unconditional network for simulated Network B. This network does not exhibit SWN properties as expected for Network B.

up to 200 spike trains, with MVPC calculated using up to 198 predictors. The analysis can select a single predictor or a group of predictors in order to search for the most influential contributors to pairwise relationships over a particular range of frequencies. Application of the proposed MVPC analysis for quantification of neuronal interactions using network measures was demonstrated on simulated networks. Network analysis applied to binary and weighted networks verified the differences in unconditional and conditional networks of known spike train interactions. Comparisons between conditional and unconditional networks using basic network measure, node degree and path length reveals clear differences and consistently highlights the advantages of using MVPC analysis in identification of network edges. Elimination of common effects using partial coherence analysis promises more accurate results in further network analysis. Application of motif detection as a more complex measure reinforces the usefulness of MVPC analysis in the discovery of network subgraphs. Finally, SWN analysis on binary and weighted conditional network supports the application of the proposed MVPC analysis in determination of network edges with or without the connectivity strengths to detect SWN topologies providing valuable details on overall network organization.

Chapter 6

Application of network theory metrics to MEA epileptic seizure data

The process for network analysis has several stages from data acquisition, signal processing and analysis (see Chapter 3) and finally network measures and analysis. This chapter explains about the final stages of network analysis and focuses on application of network theory metrics as described in Chapter 4 to estimate functional connections between MEA neuronal signals. The objective is to represent the network patterns within the same and across different region of the brain using conditional and unconditional connectivity matrices of individual neurons. The functional network descriptions will serve as a fundamental research tool for quantification of neuronal interactions established through multivariate partial coherence analysis. The advent of MEA recording techniques with increasing numbers of electrodes has made the combination of multivariate spike train analysis along with network analysis an important tool to study functional neuronal network properties. These analysis and network quantification will provide valuable opportunities for systematic statistical computation of MEA spike train signals in order to depict the features of conditional and unconditional neuronal network.

The network measures that will be discussed in this chapter includes node degree, path length, clustering coefficient, modularity and small-worldness. Basic measures like node degree, path length and clustering coefficient will be used on both conditional and unconditional networks to compare the differences in binary and weighted network characteristics before and after removal of the common influence edges. The comparisons are expected to highlight the importance of multivariate partial coherence analysis in determination of conditional connections for functional network analysis. Complex measures like small-worldness and modularity will be applied to conditional networks to highlight the integration and segregation properties.

6.1 MEA data set-single unit spike train data from hippocampus

There are several network measures that are suitable for complex network analysis (Rubinov & Sporns, 2010) as discussed in Chapter 4. In this chapter, some of the metrics will be applied to the adjacency matrix to quantify the functional connections formed within the hippocampus. These quantitative measures are used as features to explore the differences between unconditional and conditional network patterns. The approach is applied to MEA signals recorded from a study of connectivity in a model of kainic acid (KA) induced epileptiform activity for mesial temporal lobe epilepsy (mTLE) in rat (Senik et al., 2013).

The MEA signals were recorded using 50 μm diameter stainless-steel electrodes insulated with Teflon (NB Labs, Texas USA). Analogue signals recorded via PBX pre-amplifier were fed to Multichannel Acquisition Processor (MAP) system. This is an integrated system for programmable signals amplification, filtering and real-time spike sorting of multi-channel signals. It has the ability to simultaneously record multiple channels of neuronal spike trains and local field potentials (LFPs). This 64 channels MAP system provide computer-controlled

amplification between x1000 to x32000, and the gain for spikes was set at x1000 for this experiment. The band-pass filtering was set for 500 Hz to 5 Hz.

Spikes sorting and removal of noise artefacts based on the similar neuronal spiking patterns was conducted off-line using Off Line Sorter v3.23; Plexon Inc. The unit spike raster plots for the sorted data were then visualised using NeuroExplorer (v4). A representative unit spike raster showing basal activity and 1 hour post-KA activity within the left (ipsilateral) and right (contralateral) hippocampus are depicted in Figure 6.1. Each vertical tick in the raster display represents the time-stamp of a single neuronal action potential. Spike train signals from neurons in seizure condition reflects changes in individual neuron firing rate and alterations in the neuronal connectivity.

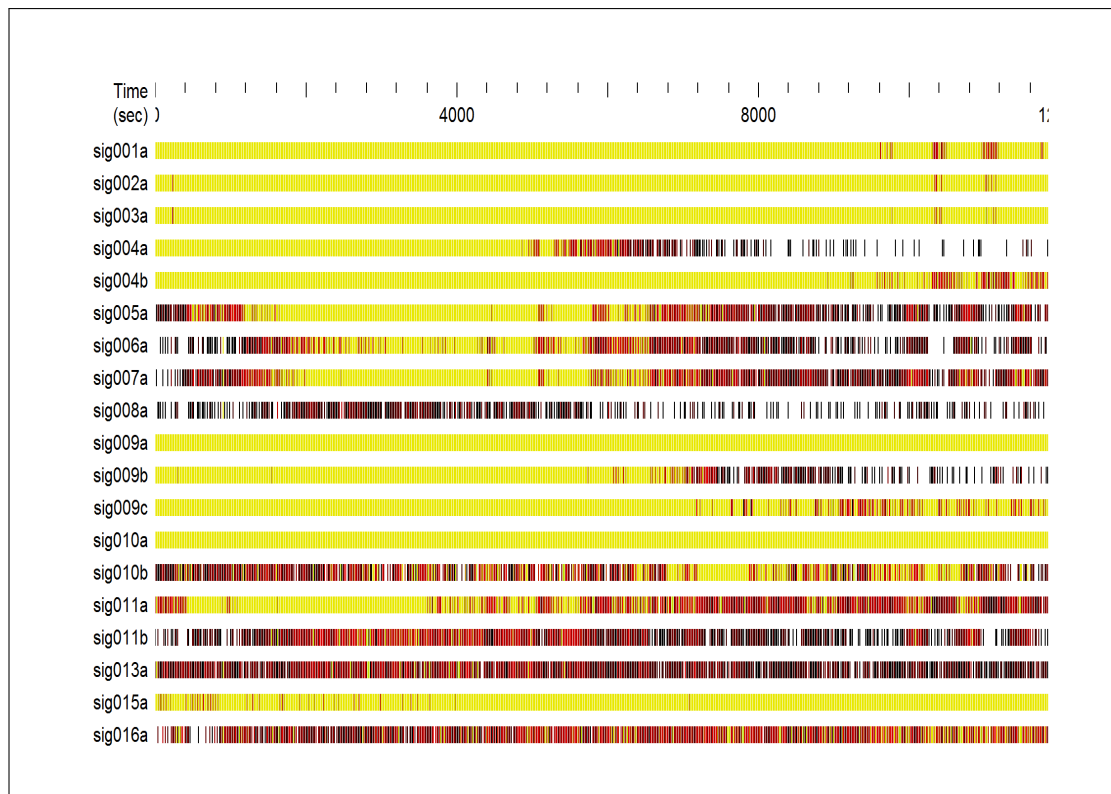


Figure 6.1: Simultaneous recordings of multiple hippocampal neuronal activity. This trace illustrates a sample representation of spontaneous hippocampal unit firing observed over a 600 sec. The colours of the raster represent the firing rate of the neurons ranging from black (slow), red (medium) and yellow (high).

The structure of neuronal connectivity within the hippocampus follows the

synaptic organization between several part that make up the hippocampal formation that consists of Dentate Gyrus, Subiculum and Entorhinal Cortex (Shepherd, 1990). Pyramidal neurons are the principal neurons in hippocampus. The pyramidal cell layer is further divided into the CA1 and CA3 regions as shown in Figure 6.2.

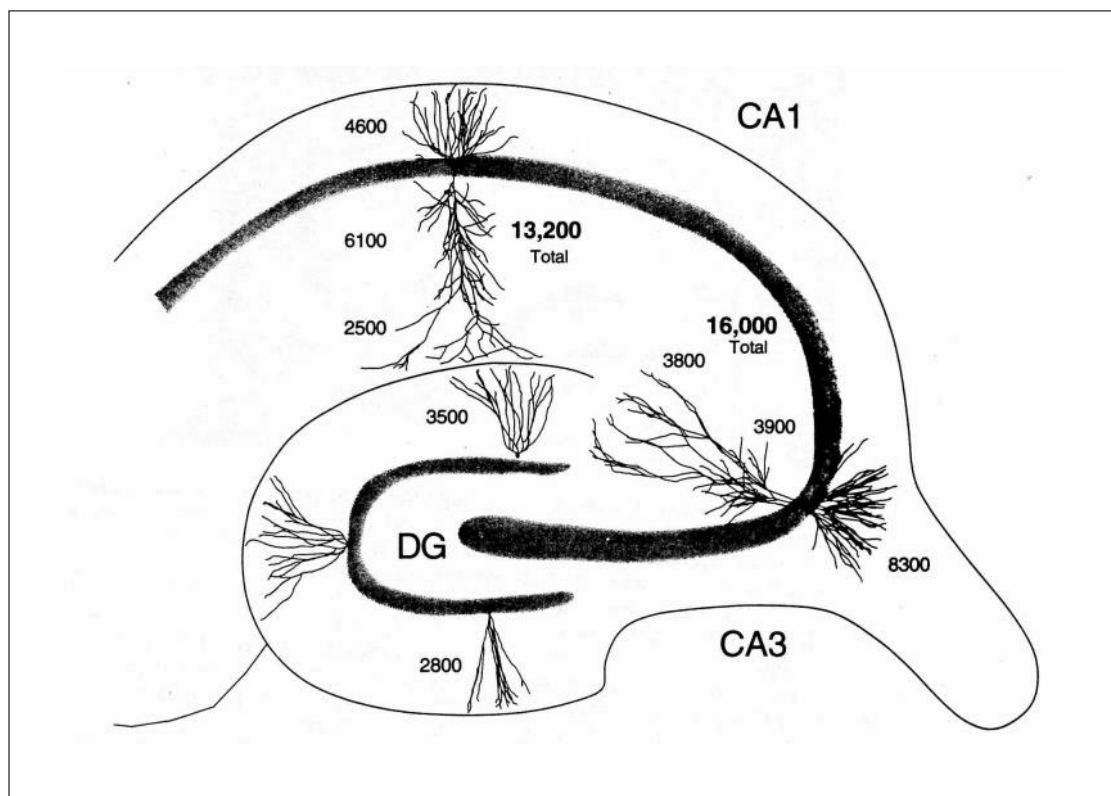


Figure 6.2: Shape and size of the principle neurons in the Dentate Gyrus, CA1 and CA3. Number indicate the dendritic length of the cells. Figure from Shepherd (1990)

Histological verification on the hippocampus confirmed the electrodes position at the targeted coordinate as shown in Figure 6.3. In the experiment, isoflurane anaesthetised Lister-hooded rats (300 - 400 g) had MEA electrodes positioned in the left and right hippocampus for simultaneous recording of spike train activity. A cannula was attached to the electrode array in the left hippocampus to locally deliver saline or kainic acid (1 mM, 1 μ L). Figure 6.4 present the time-line experimental protocols for KA administration and data recording.

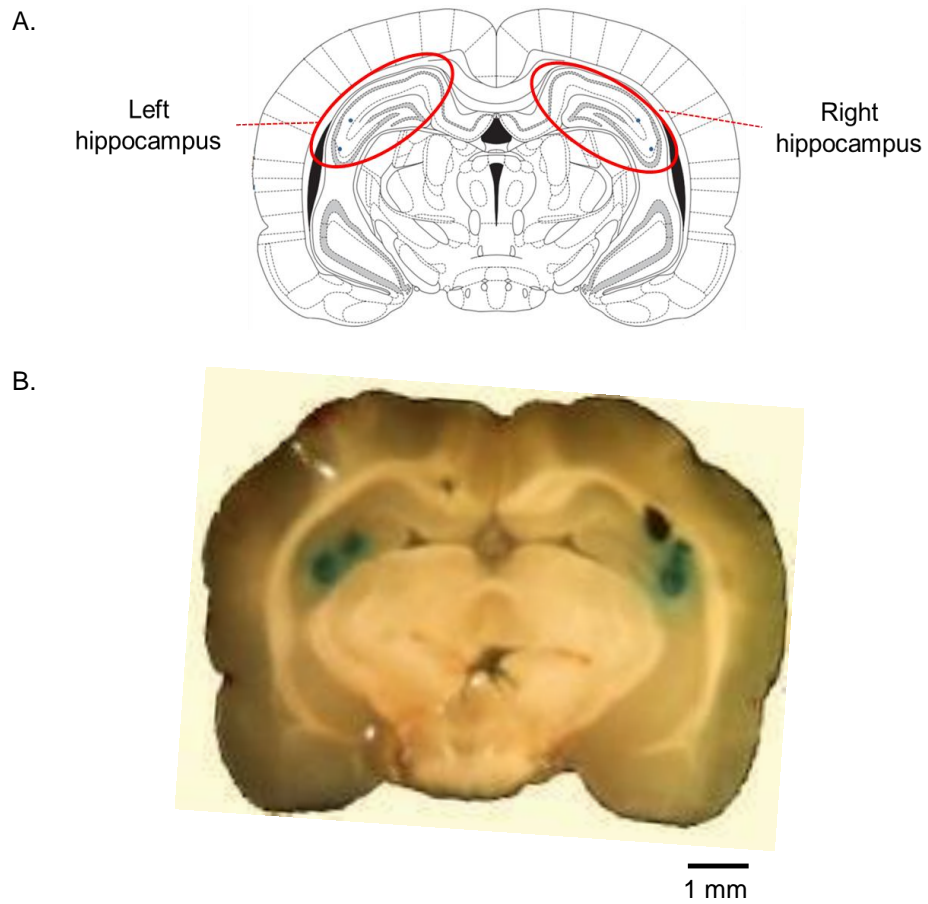


Figure 6.3: A: Schematic representation of the hippocampal recording sites. B: Histological verification of hippocampal recording sites with electrode placement was confirmed by the visible blue dye mark.

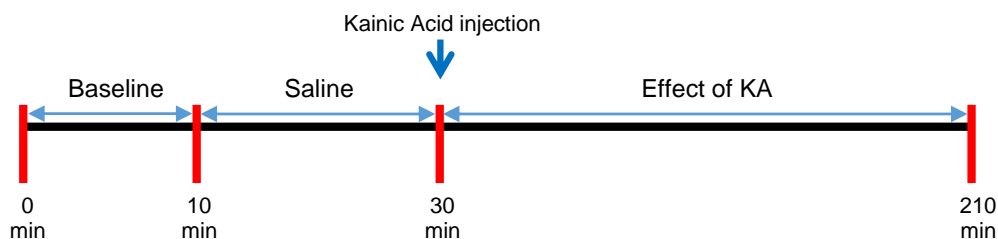


Figure 6.4: Time-line experimental protocols for kainic acid administration. Saline was injected intravenously after 10 min baseline recording followed by local injection of KA after 20 min saline injection. Effect of KA was recorded until 210 minute.

Saline was injected intravenously at 20 min after 10 min basal recording. This is followed by local administration of 1mMol of KA at 30 min and data was recorded in a single recording with overall duration of 210 min. Multiple single units activity filtered at 150 Hz – 9 kHz were recorded using a *Plexon* Multichannel Acquisition Processor (MAP) system. All procedures had ethical approval and were carried out in accordance with the Animals (Scientific Procedures) Act 1986, UK.

Connections between MEA single unit channels will be represented in the form of pairwise coupling, with the strength estimated through multivariate partial coherence analysis. This functional connectivity reflects the strength of conditional interactions among multiple neuronal channels that take into account higher order multivariate linear relationships. The strength of unconditional interactions were obtained through coherence analysis. Both conditional and unconditional connectivity strength are used to define the graphical network that consists of a set of nodes and edges. Each MEA signal corresponds to a single network node and connections among the signals correspond to the functional pathways yielding the undirected network edges.

This work lays the foundation for further exploration of network theories

on both conditional and unconditional networks using MEA data. Comparison between unconditional and conditional network will be done using different network metrics to highlight the changes in network characteristics after removal of common predictor neurons. The network analysis is also applied longitudinally to compare the connectivity changes across time. This is to differentiate the network pattern across four experimental stages as shown in Table 6.1.

Table 6.1: Experimental stages for connectivity analysis across time.

Stage	Experimental protocol	Time, t (min)
1	baseline	$0 < t < 10$
2	saline injection	$10 < t < 30$
3	Kainic acid injection	$t = 30$
4	effect of Kainic acid	$t > 30$

Network measures are applied to the connectivity matrix of spike train signals recorded from CA1 and CA3 hippocampal regions of both hemispheres to characterize the connectivity structure within and across 4 different regions as shown in Table 6.2.

Table 6.2: Four different regions of hippocampus with the corresponding nodes identification number and color of nodes in Figure 6.5 and 6.6.

Region	Node	Color of node
Left CA3	1, 2, 3, 4, 5	orange
Left CA1	6, 7, 8, 9, 10	blue
Right CA3	11, 12, 13, 14	green
Right CA1	15, 16, 17, 18, 19	pink

This dataset contains 19 channels of spike train signals that are split into 43 blocks of approximately 5 min duration. Adjacent blocks were non-overlapping. Coherence and MVPC analysis are conducted for each 5 min block to determine the existence of edges among the nodes, before the analysis of network metrics.

These blocks consisted of 292 segments of length 1024 points. Each block is approximately 300 s, with sampling rate 1 ms. Connectivity strength for each block was analysed separately as described in Section 4.1 for unconditional edges and conditional edges. Weighted unconditional and conditional edges were determined by the mean coherence and partial coherence values over a 0 to 70 Hz frequency range using Equations 3.14 and 3.32 respectively. A significance threshold value was applied for unconditional and conditional edge weight using the corresponding 95% confidence limits for coherence (0.0102) and partial coherence (0.0109).

All network graphs in this chapter are plotted using an open-source network visualization software, Gephi version 0.9.1 (Bastian & Heymann, 2009). Figure 6.5 and 6.6 show the unconditional and conditional networks for the four different stages of the experiment. Each graph shows the network for a segment of five minutes time interval randomly chosen from each stage. Four stages of conditional and unconditional network are visualized on similar time segments for comparison purposes across this chapter. Appearance of nodes in these graphs are classified into four colors to distinguished the four subregions of the left and right hippocampus as shown in Table 6.2. Links between nodes show weighted edges constructed from coherence and MVPC analysis. Thicker edges show stronger functional connections between neurons. These graphs are plotted using the ForceAtlas 2 layout in Gephi 0.9.1 due to its ability to organize node positions by transformation of the edge weights into the strength of attraction and repulsion forces (Jacomy et al., 2014).

Unconditional network of Figure 6.5 show dense connection between nodes with various strength of interaction. Estimation for connectivity strength using MVPC analysis on the same dataset produce conditional network with fewer edges as presented in Figure 6.6. Unconditional network shows strong edges within regions Left CA3 and Left CA1 across all stages of the experiment. This information is masked in unconditional network where strong edges exist both within and across regions. The conditional network may indicate a more reasonable relationship for neuronal interactions since any common effects have been

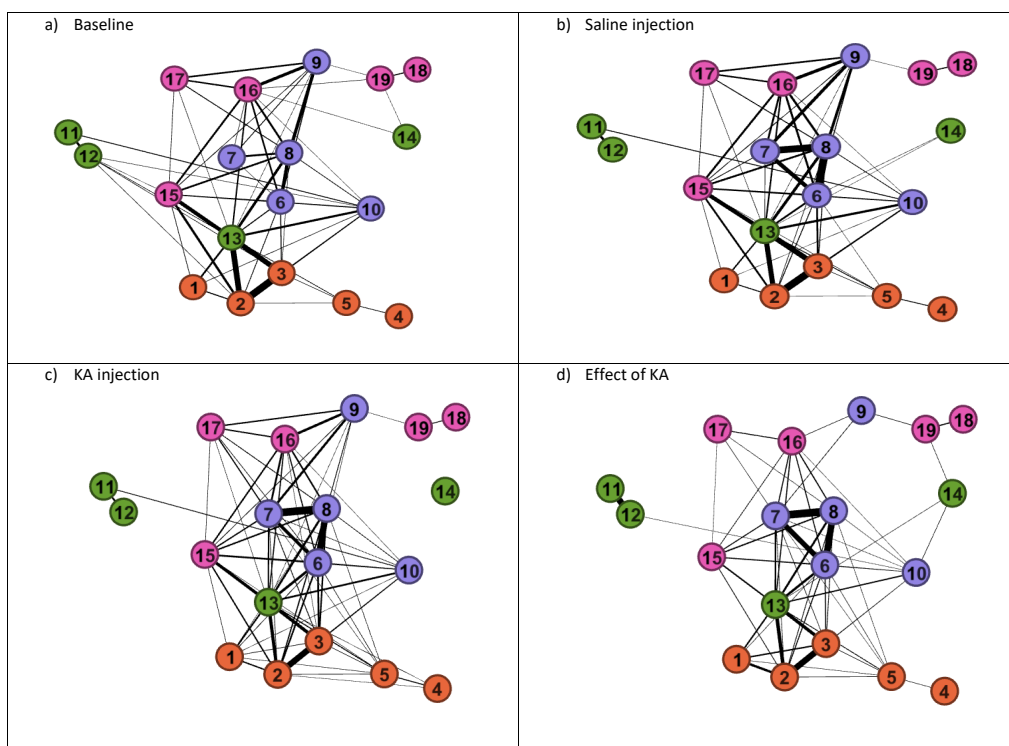


Figure 6.5: Unconditional weighted network for bilateral hippocampal single unit dataset at four different stages: a) baseline, b) saline injection, c) KA injection and d) effect of KA. Different nodes color show different subregions of the hippocampus; orange - CA3 Left, blue - CA1 Left, green - CA3 Right, pink - CA1 Right. Links between nodes show weighted edges constructed from coherence analysis. Thicker edges show stronger connections.

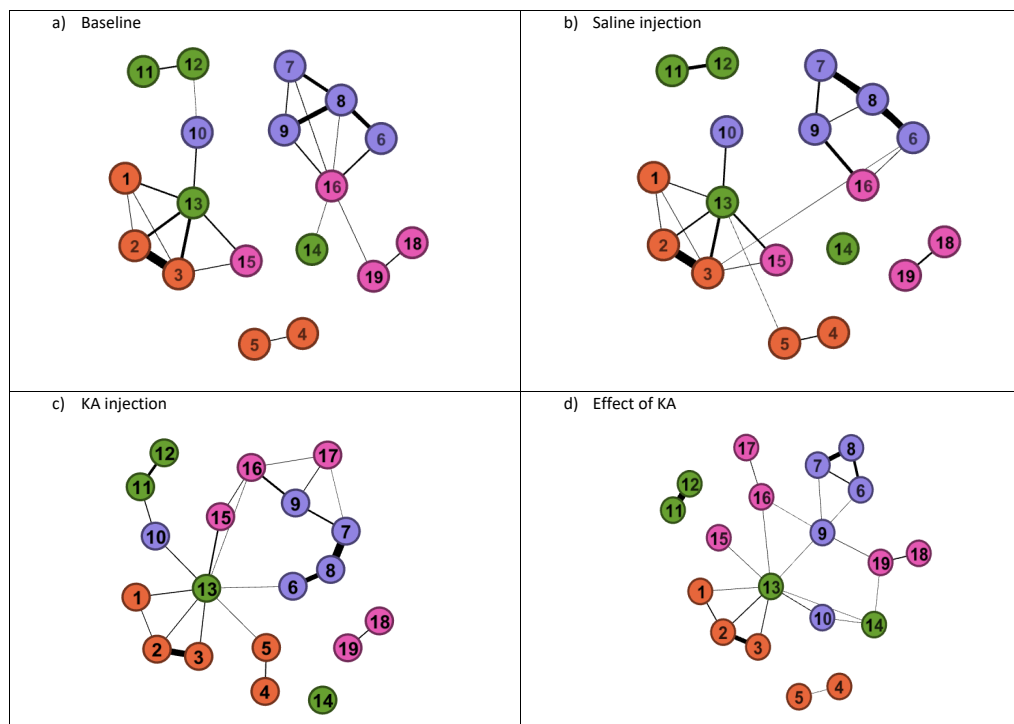


Figure 6.6: Conditional weighted network for bilateral hippocampal single unit dataset at four different stages: a) baseline, b) saline injection, c) KA injection and d) effect of KA. Different nodes color show different subregions of the hippocampus; orange - CA3 Left, blue - CA1 Left, green - CA3 Right, pink - CA1 Right. Links between nodes show weighted edges constructed from multivariate partial coherence analysis. Thicker edges show stronger connections.

removed. Visual observation of the graphs are not clear and it is difficult to describe the structure and organization of the network. Therefore application of network metrics considered in the following sections are useful to interpret the neuronal interactions.

6.2 Node degree

Node degree is the most fundamental network measure for analysis of connectivity patterns. Degree is defined in Section 4.1.1 as the number of neighbours connected to a node. This measure shows the importance of individual nodes where a network node with a high node degree has many edges connected to it. Figure 6.7 shows color-coded graphs of the degree for each channel at a specific time interval. Each channel is presented as an individual node on Y-axis using numbered from 1 to 19. X-axis presents the blocks of time for each five minutes time interval. The degree for each node at a specific time interval is depicted using color scale as shown on the right of the graph.

Figure 6.7(top) shows conditional node degree and figure 6.7(bottom) shows unconditional node degree.

Comparison between the graph for conditional and unconditional node degree shows a different pattern across time. Node degree for unconditional network shows high number of connections for most of the channels compared to the conditional network. The maximum value of node degree for the conditional and unconditional network is 10 and 13, respectively. Elimination of common effects in the conditional network reduces node degree. Lower node degree are captured in conditional network and most of the node degree are less than 5 across all time blocks. This is in contrast to the unconditional network where most of the nodes are highly connected. High variation in node degree of the unconditional network indicates dense interaction before removal of the common effects using partial coherence analysis. Node degree of conditional network shows low number of neighbours connected to a node across the experiment except for node 13.

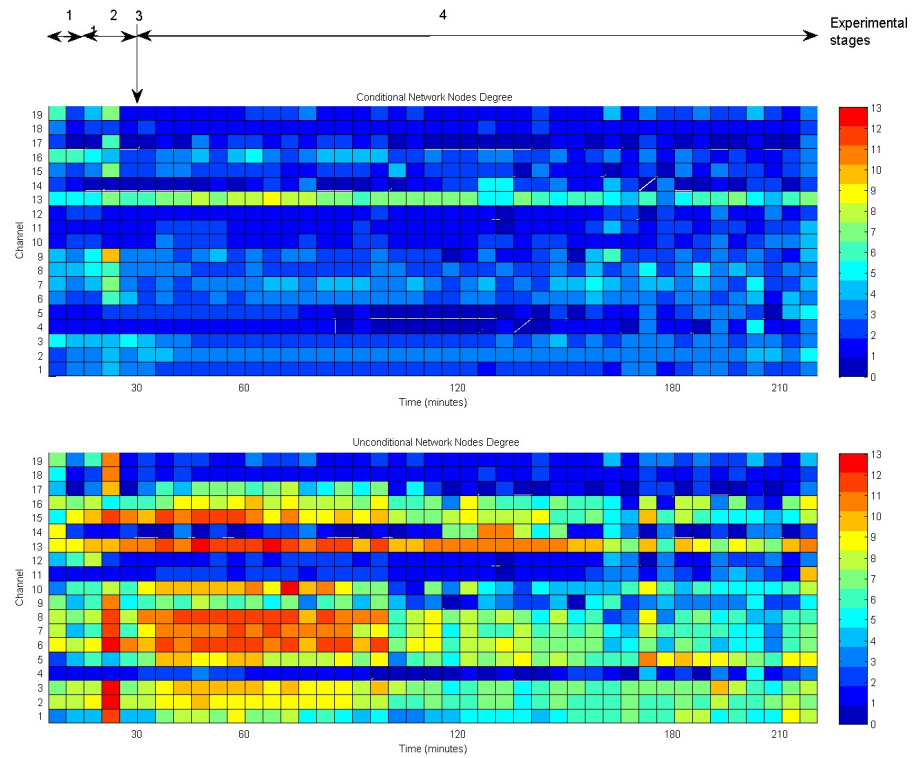


Figure 6.7: Top figure shows color-coded graph of node degree for conditional network, and bottom figure shows the node degree for unconditional network for 19 channels of spike train signals that are split into approximately 5 min time-blocks. The degree is depicted using similar color scale for both conditional and unconditional network. Node degree for unconditional network shows high number of connections compared to the conditional network. Elimination of common effects reduces node degree and most of the node degree in conditional network are less than 5 across all time-blocks except for node 13 with a maximum degree of 9. This node is considered as the possible network hub as seen in figure 6.6 where node 13 from left CA3 is a possible connector node for all subregions. This functional role for node 13 is hidden in unconditional network.

Investigation of a functional role for the nodes may be easier after removal of the common effect. Neuron captured on channel 13 of conditional network shows a higher degree with a maximum degree of 9, thus is considered as the possible network hub. This can also be seen in the network graph in figure 6.6 where node 13 from left CA3 plays an important role as a possible connector node for all subregions at all stages. This functional role for node 13 is hidden in unconditional network where most of the nodes are connected to all subregions. Connections within and across subregions are clearer after removal of common effects, so we get a more accurate picture of neuronal interactions with the conditional network.

Node degree distribution is a network measure for comparison of the properties of a network (Bullmore & Bassett, 2011). Further analysis is conducted by observation of the node degree distribution as presented in histograms in Figure 6.8. Degree distribution for conditional networks shows a similar pattern across the four stages where the majority of the nodes are connected to less than 5 nodes with maximum frequency of 8 at stage 3. A highly connected node that appears at stages 3 and 4 may show the effect of KA which increases the neuronal activity of the node 13 as the possible network hub. Conditional node degree distribution shows a small percentage of high degree nodes and a majority of low degree nodes, which is believed to be a more realistic node degree distribution for a neuronal network.

Distribution of unconditional node degree shows a bimodal distribution pattern with two groups of nodes, lower degree nodes (degree ≤ 5) and higher degree nodes (degree > 5). Groups of higher degree nodes exist because of the dense edges of the unconditional network before removal of the common effects. As can be seen in Figure 6.8, big differences appear in node degree distributions between conditional and unconditional network. This suggests that removal of the common effects using MVPC leaves a more accurate node degree distribution in the conditional network.

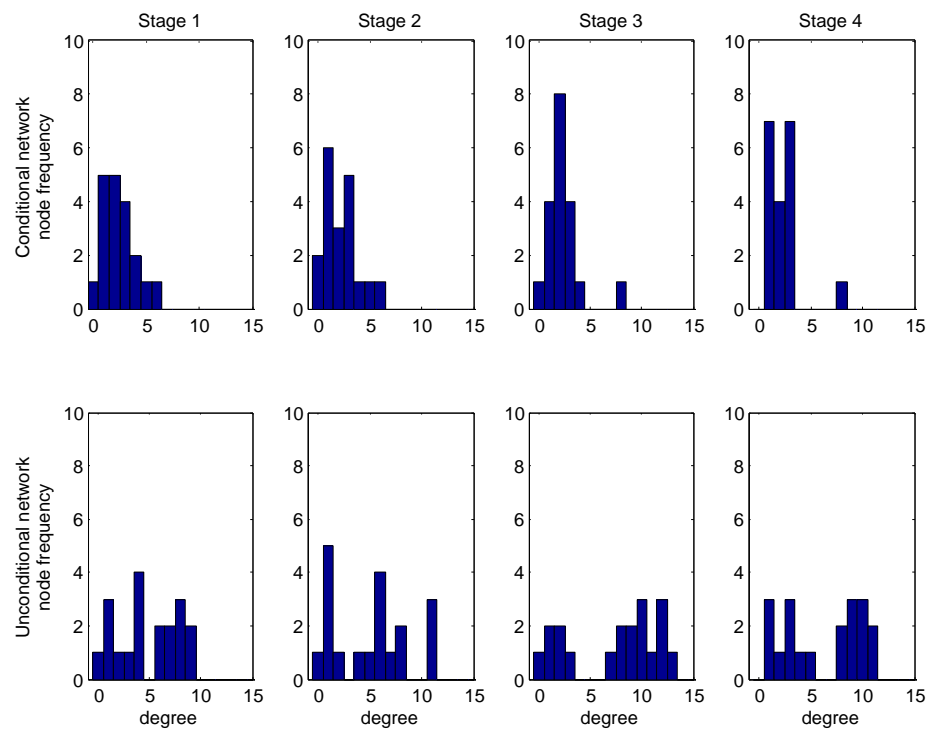


Figure 6.8: Node degree distribution in four stages; baseline, saline injection, KA injection and effect of KA, as described in Table 6.1. Top figure shows histogram for conditional network, and bottom figure shows histogram for unconditional network

6.3 Path length

Path length is the second fundamental network measure after node degree. This metric is used to measure the shortest pathway between network nodes. Path length is defined in Section 4.1.2 as a calculation of the number of steps in the shortest pathway from a node to each of its neighbours as defined in equation 4.5.

Figure 6.9 shows color-coded graphs of the shortest path lengths of conditional network for each pairwise connections at four different stages of the experiment, similar to the experimental stages shown in Figure 6.5 and 6.6. Each channel is presented as an individual node on X- and Y-axis using numbered from 1 to 19. The shortest path length for each connection at a specific stage is depicted using color scale as shown on the right of the graph. Comparison between different experimental stages indicates changes in the number of path lengths for inter- and intra-region interactions. All regions shows decrease number of path lengths from stage 3 to stage 4 for intra-region interactions except region Right-CA1. Increase number of path lengths from stage 3 to stage 4 can be seen for inter-region interactions between region Left-CA1 and Right-CA1.

Weighted path length is a weighted measure of path length that takes into account the strength of connections between the nodes as defined in equation 4.6. Figure 6.10 shows boxplot graphs of weighted and unweighted (binary) path length distributions for both conditional and unconditional networks. Boxplot graphs display the median, 25th and 75th percentiles of the path length distribution for each time-block. X-axis of the graph presents the time-blocks up to 120 minutes. Path length was calculated for each five minute time interval. Y-axis presents weighted/binary path length.

The black dotted line in each graph of Figure 6.10 represents the characteristic path length as defined in equation 4.7. Characteristic path lengths for weighted and binary conditional network fluctuate over the 120 mins with no obvious trends. Comparison between weighted and binary conditional network

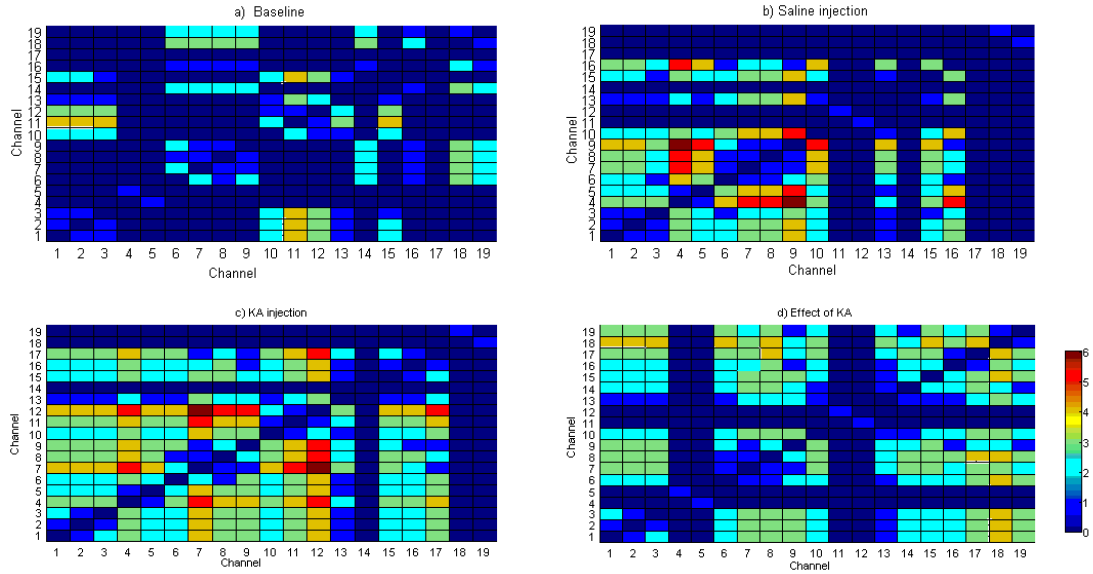


Figure 6.9: Color-coded graphs of the shortest path length of conditional network for each pairwise connections at four different stages of the experiment. Each channel is presented as an individual node on X- and Y-axis. This depicted using color scale as shown on the right of the graph.

indicates slightly different trend where the peak value of binary path length is decreasing after KA injection. The values of weighted and binary characteristic path length for the conditional network are higher than those for the unconditional network. It is apparent that they are significantly different for overall 120 mins data as shown in Figure 6.11. The mean value for characteristic path length (weighted = 111.6, binary = 2.3) of conditional network is larger than the mean value for characteristic path length of unconditional network (weighted = 69.9, binary = 1.8).

Figure 6.10 (b) and (d) displays binary path length distributions for unconditional and conditional networks, respectively. It is apparent from the distribution of binary path length in unconditional network that the distance between two nodes are mostly between 1 to 3 steps across the time-blocks which indicates short communication pathway between the nodes. This is different from the distributions of binary path length in conditional network with various distributions of path length across the time-blocks ranging between 1 to 5 steps.

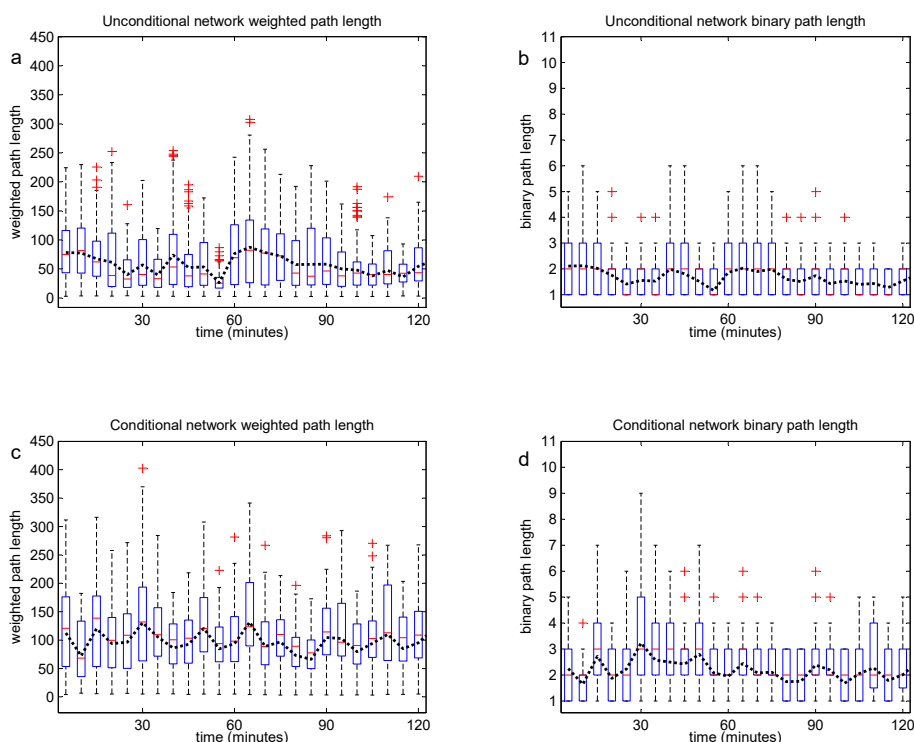


Figure 6.10: Boxplot graphs of (a) weighted path length distributions for unconditional network, (b) binary path length distributions for unconditional network, (c) weighted path length distributions for conditional network and (d) binary path length distributions for conditional network, for each 5 min time-block. X-axis of the graph presents the time-blocks up to 120 minutes. Black dotted line in each graph represents the characteristic path length.

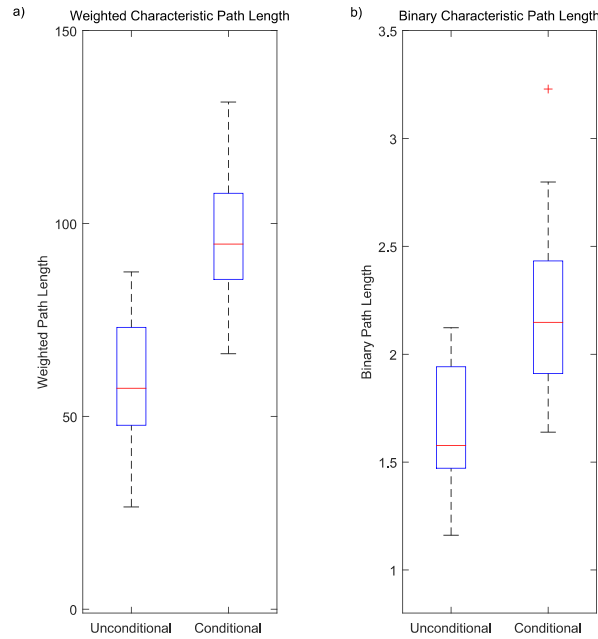


Figure 6.11: Boxplot graphs of (a) characteristic path length distributions and (b) characteristic weighted path length distributions for overall 120 mins. X-axis of the graph presents the type of network.

Shorter path length can be seen in stage 4 of conditional network with most path lengths between 1 to 3, 25 min after KA injection. The maximum path length for unconditional network is 6 at five different time-blocks. The maximum path length for conditional network is 9 at the fifth time-block. This result seems to indicate that KA injection at stage 3 of the experiment may have been related to sudden increment of the path length, and 50% of the conditional path lengths at this time-blocks are between 3 to 9 steps. This transient increase in path length is not seen in the unconditional network.

Figure 6.10 (a) and (c) illustrate weighted path length distributions for unconditional and conditional networks. Weighted path length illustrates the shortest pathway between nodes that take into account the strength of interactions from coherence and MVPC analysis for unconditional and conditional network, respectively. Box plots for weighted unconditional network show many outliers for longer path length compare to conditional network. However, most of the outlier values in distributions of unconditional weighted path length are within the dis-

tributions of conditional weighted path length. Most of the weighted path length data for conditional network appears to be symmetrically distributed, contrary to most of the weighted path length data for unconditional network that seems to be skewed with more values is above the median value (red line inside the box).

Comparison between conditional and unconditional network indicates different distributions of path length. The unconditional networks have shorter path length than the conditional networks. It is apparent that they are significantly different for the overall 120 mins of data as shown in Figure 6.12. The mean value for conditional weighted path length (110.2) is larger than the mean value for unconditional weighted path length (65.7). Consistent with weighted network, the mean value for conditional binary path length (2.5) is also larger than the mean value for unconditional binary path length (1.9).

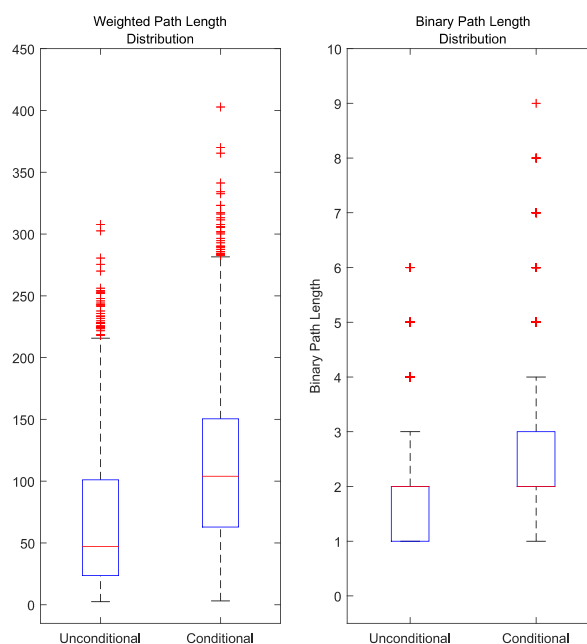


Figure 6.12: Boxplot graphs of weighted and binary path length distributions for overall 120 mins. X-axis of the graph presents the type of network. The mean for both unconditional and conditional binary path length is 2.

Different range appears in path length distributions between conditional and unconditional network for overall 120 mins data. There appears to be a more con-

sistent path length with symmetrical distributions in the weighted conditional network which results as a consequence of using the conditional weighted edges to measure the path length. These results demonstrate that one consequence of using MVPC as opposed to coherence is significantly different network path lengths. This suggests that conditional edges from MPVC analysis should be used to estimate the strength of neuronal interactions because removal of common influence edges alters the path length distributions.

6.4 MEA: Clustering coefficient

Clustering coefficient is used to measure the level of local connectedness between nodes which provides information about network segregation. Clustering coefficient is described in Section 4.1.3 as the fraction of three-node triangles around a node as defined in equation 4.11. Weighted clustering coefficient is a weighted measure of clustering coefficient that takes into account the strength of connections between the nodes as defined in equation 4.13. Figure 6.13 shows boxplot graphs of binary and weighted clustering coefficient distributions for both conditional and unconditional networks. X-axis of the graph presents the time-blocks up to 120 minutes. Clustering coefficient was calculated for each five minute time interval. Y-axis presents binary/weighted clustering coefficient.

Figure 6.13 (a) and (b) displays binary clustering coefficient distributions for conditional and unconditional networks, respectively. Figure 6.13 (c) and (d) illustrates weighted clustering coefficient distributions for conditional and unconditional networks, respectively. Comparison between weighted and binary conditional network indicates different distributions of clustering coefficient. The distribution of binary and weighted clustering coefficient for unconditional networks show higher clustering coefficient compared to conditional networks. 50% of nodes in unconditional network across all time-blocks are highly clustered in both binary and weighted analysis.

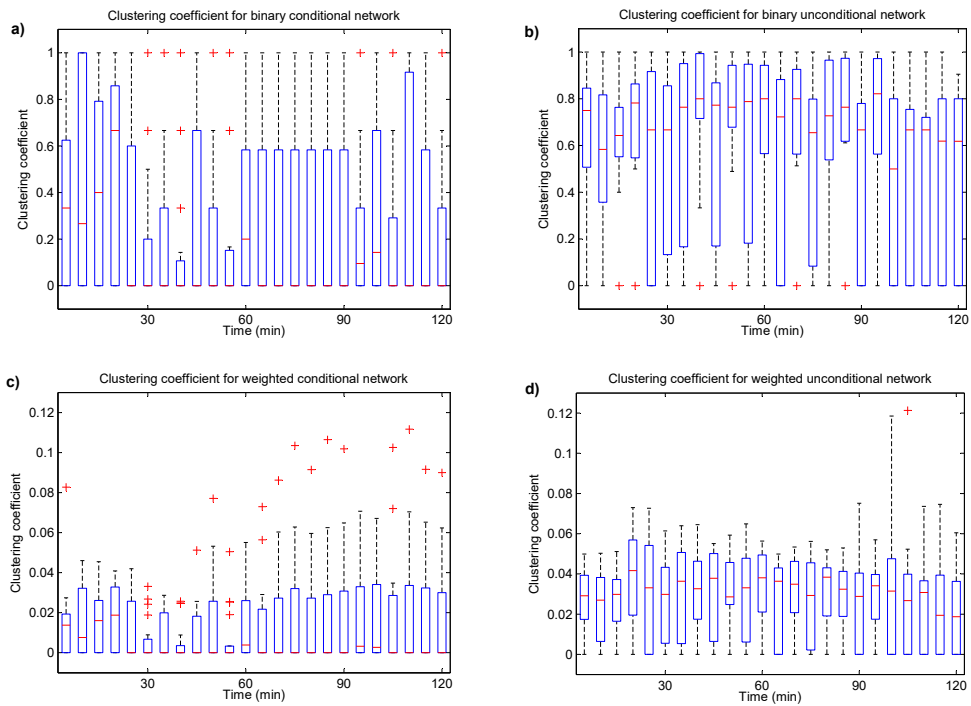


Figure 6.13: Boxplot graphs of (a) binary clustering coefficient distributions for conditional network, (b) binary clustering coefficient distributions for unconditional network (c) weighted clustering coefficient distributions for conditional network, and (d) weighted clustering coefficient distributions for unconditional network, for each 5 min time-block. X-axis of the graph presents the time-blocks up to 120 minutes.

The boxplots for conditional networks present a similar distribution for both binary and weighted clustering coefficients. The fluctuation of higher clustering coefficient values can be seen in stages 1 and 2 before KA injection at 30 min. It appears that the clustering coefficient is decreased at stage 3 at 30 min, which suggests that the connection between neurons may have been affected by the KA injection. The clustering coefficient continues to fluctuate for another 30 minutes. The results seems to indicate that the KA injection may cause a disruption of the information segregation ability within the neuronal network that lasts for around 30 minutes after injection.

These results demonstrate that binary and weighted clustering coefficient is a useful network measure in conditional network analysis. This analysis could identify the changes in network segregation across different stages of the experiment by using clustering coefficient. This suggests that binary and weighted clustering coefficient should be used to estimate the level of network segregation on conditional neuronal network from MPVC analysis.

6.5 MEA: Small-world network

Small worldness is an index that can be defined using two network metrics, path length, L and clustering coefficient, C described in section 4.1.2 and 4.1.3. This measure is described in section 4.3 by a comparison of C and L from the original network with C and L from a random network. A small-world network has characteristics of high C for network segregation and low L for network integration. Weighted small worldness is a generalization of SWN index with a comparison of C^w and L^w from the original network with a weighted random network (Rubinov & Sporns, 2010). A network is said to be a small-world network if $C^w \gg C^w_{rand}$, $L^w \gtrsim L^w_{rand}$ and $S^w \gg 1$ (Humphries & Gurney, 2008).

Figure 6.14 shows simultaneous plot of normalized measure for clustering coefficient, C^w/C^w_{rand} , normalized measure of shortest path length, L^w/L^w_{rand}

and weighted SWN index for conditional network. Each measure was calculated for each 5 minutes time-block. X-axis of the graph presents the time-blocks up to 120 minutes. It is apparent that this network exhibit a small world network topology with high C^w , low L^w and $S^w \gg 1$ across all stages with temporary loss of SWN properties 10 minutes after the KA injection. Values of C^w/C^w_{rand} show higher clustering coefficient of the network compared to the random network. Values of L^w/L^w_{rand} are close to 1 which shows low characteristic path length of the network similar to the characteristic of a random network. High C^w and low L^w yield an optimum connections with coexistence of segregation and integration properties among the MEA channels before, during and 15 minutes after KA injection. This result seems to indicate that the network topology is disrupted shortly after KA injection but gain it optimal communication 15 minutes after KA injection.

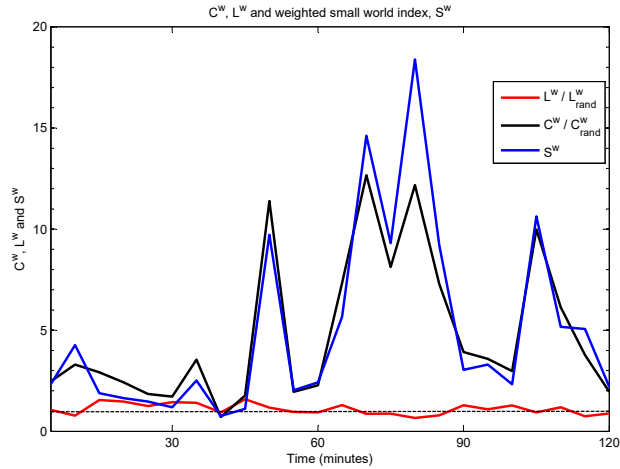


Figure 6.14: Graphs of normalized measure for clustering coefficient, C^w/C^w_{rand} (black line), normalized measure of shortest path length, L^w/L^w_{rand} (red line) and SWN index (blue line) for weighted conditional network. Each measure was calculated for each 5 min time-block up to 120 minutes. Black dotted line was plotted to show the limit of 1, where a network is said to be a small-world network if $S^w \gg 1$. This graph seems to indicate that the network topology is disrupted after KA injection but gain it optimal communication 15 minutes after KA injection.

Characterization of small-worldness properties on conditional MEA network in this section demonstrate that weighted network measures derived from MPVC analysis like weighted characteristic path length and weighted clustering coeffi-

cient are also suitable for higher level of network analysis which manipulate more than one network measure. This suggests that weighted SWN index should be used to simultaneously estimate the level of network segregation and integration on conditional neuronal network from MPVC analysis after removal of the common influence edges.

6.6 MEA: Modularity

Modularity is an alternative measure of segregation after clustering coefficient. Modularity is described in Section 4.1.4 as the community detection measure defined in equation 4.15. Figure 6.15 shows the color-coded modularity measure for 19 MEA nodes on y-axis separated into 4 subregions as described in table 6.2. The color-coded graph displays community detections on conditional network using 6 different colors to show the existence of different modules ranging between 4 to 6 modules for each 5 min time-block across the experiment. X-axis of the graph presents the time-blocks up to 120 minutes.

Figure 6.15(Top) shows discovery of community structure for conditional networks derived from MVPC analysis. It is apparent that this network exhibits a modular structure with both inter- and intra-modular activities. All subregions have specific nodes for both within region and across-region connectivities. For example in subregion right CA3, nodes 11 and 12 are strong contributors for intra-modular activities, node 13 has inter-modular activities with subregion left CA3 and node 14 has inter-modular activities with different subregions across time-blocks. Some nodes are associated with similar modules across all stages. For example, node 1, 2 and 3 are associated with a module in subregion left CA3, node 6 and 8 associated with a module in subregion left CA1, and node 11 and 12 that associated with a module in subregion right CA3. This results seems to indicate that modularity analysis on conditional network can be used to classify the intra-modular nodes that belong to a specific subregion. The effect of KA injection can be seen by appearance of extra modules at stage 4, 15 min after

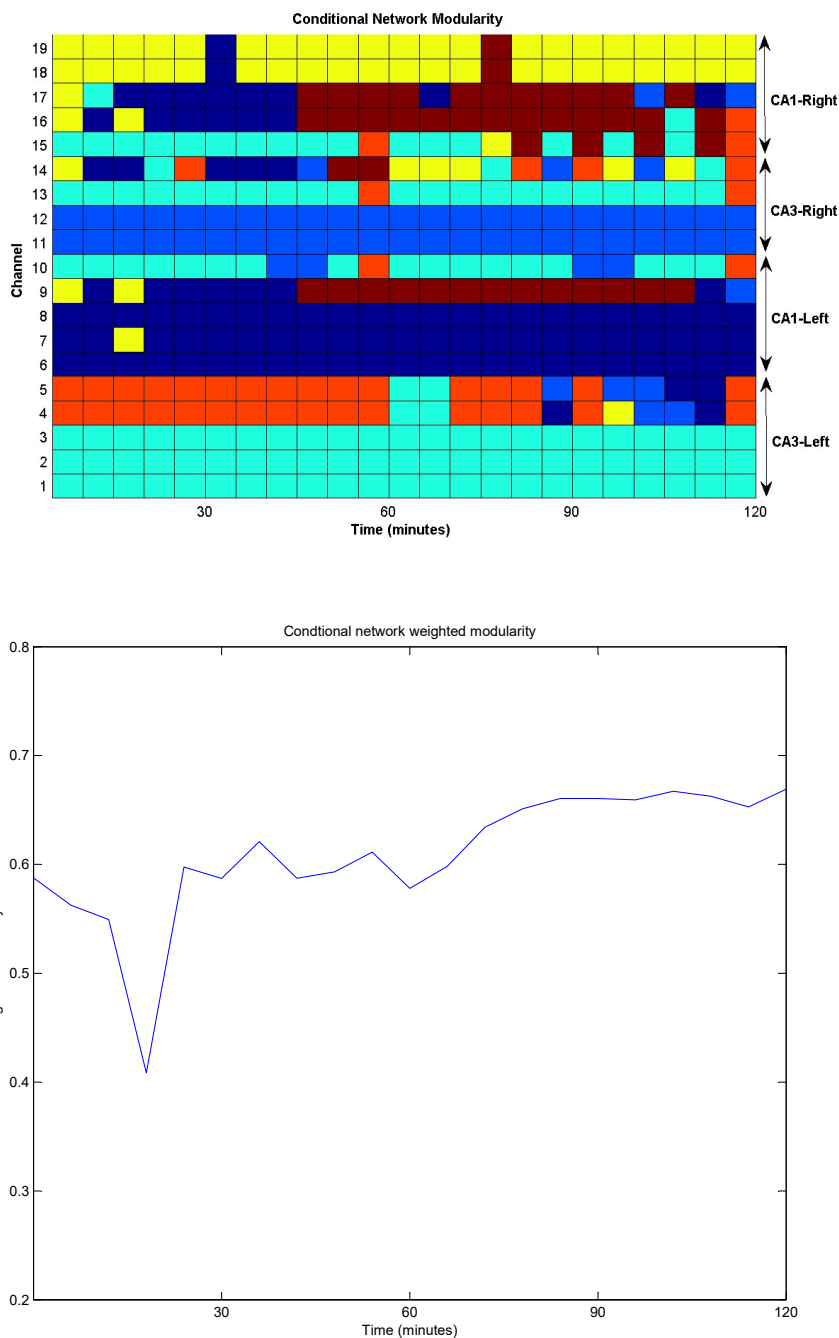


Figure 6.15: Top: Color-coded modularity measure for 19 MEA nodes separated into 4 sub-regions as described in Table 6.2. The color-coded graph displays community detections on conditional network using 6 different colors to show the existence of different modules ranging between 4 to 6 modules for each 5 min time-block across the experiment. Each module is assigned a different color. X-axis of the graph presents the time-blocks up to 120 minutes. Bottom: Average of weighted modularity measure across experimental stages shows increasing number of weighted modularity after the injection.

the injection. Similar trend can be seen in Figure 6.15(Bottom) where average of weighted modularity measure across experimental stages shows increasing number of weighted modularity after the injection.

These results demonstrate that modularity is a useful network measure in conditional network analysis. This network measure should be used to classify nodes into functional modules. This suggests that modularity is a suitable measure to estimate segregation properties on a more accurate conditional neuronal network derived from MPVC analysis.

6.7 Chapter summary

In this chapter network measures were applied to undirected connectivity matrices derived from real MEA data using MVPC analysis. Combination of MVPC analysis along with network analysis provide valuable opportunities for systematic statistical computation of network metrics for MEA spike train signals with large numbers of electrodes. These analyses were applied to both conditional and unconditional neuronal networks consisting of 19 nodes from multi-channels MEA signals recorded from 4 different subregions. Network metrics computed from MVPC analysis give different values compared to those calculated from coherence. In this case we suggest the MVPC metrics are more reliable. Comparison between conditional and unconditional network analysis using basic measures like node degree, path length and clustering coefficient shows differences in network organization at microscopic scales for both binary and weighted network. Removals of the common influence edges using MVPC analysis contributes to the construction of more accurate functional connectivities in undirected conditional network. Network analysis continues with characterization and investigation of segregation and integration properties on conditional network using complex measures like small-worldness and modularity. Classification of different hippocampal subregions presents further information about within and across subregions connectivities. Network analysis across time provide further information on alter-

ation of communication among the nodes at different stages of experiment. Both complex network measures using SWN-index and modularity provide similar conclusion of increased functional coupling between nodes during epileptic seizure. This agree with studies by Martinet et al. (2017) that shows increased functional connections across spatial scales during human epileptic seizure. These results using a model of KA induced epileptiform activity in rat definitely compel future research.

Chapter 7

Conclusions and Further Work

7.1 General Summary

This thesis presents a combination of Multivariate Partial Coherence (MVPC) analysis and network theory measures to quantify neuronal network features using spike trains signals. MVPC analysis provides estimates of conditional network edges that take into account common linear effects in pairwise neuronal connectivity. This approach is based on the inverse variance lemma for higher order partial coherence analysis of multi-channel spike trains signals(Whittaker, 1990; Dahlhaus, 2000). The scalability of MVPC analysis was investigated with up to 198 predictors using a combination of 100 channels of simulated spike train data and an additional 100 Poisson spike train predictors. The simulated neuronal network data was generated using excitatory and inhibitory neurons to compare the differences between network properties in unconditional and conditional networks for spike train interactions.

A combination of MVPC analysis along with network theory analysis provides a systematic approach for multi-channel spike train signals. Application of network measures to both conditional and unconditional networks highlighted the differences in network structure and characteristics between the two representations. Network analysis on a conditional network is able to describe the topological properties of binary and weighted conditional networks. Implemen-

tation of MVPC analysis along with network analysis on multi-electrode array (MEA) spike train suggests that a combination of these methods is able to facilitate the study of connectivity in functional neuronal networks.

7.2 Chapter Summaries and Conclusions

The implementation of MVPC analysis as a tool to determine binary and weighted edges is an effective approach to frequency domain multivariate analysis for the description of synchronized spike trains. The construction of a conditional neuronal network provides new insights, with more accurate connectivities when compared to the unconditional network based on ordinary coherence. This thesis highlights the ability of MVPC analysis as a computationally efficient approach to provide a better representation of functional connectivities from multiple spike trains (see chapter 5). MVPC analysis yields a conditional network with a reduced number of edges compared to the unconditional network, removing indirect edges by taking into account all possible common effects in the network. Comparisons between conditional and unconditional networks using simulated data provide clear evidence for the existence of the indirect edges between neurons that can lead to the inaccurate network representation.

This thesis has made novel contributions by exploring the use of MVPC analysis to determine network edges from multiple spike trains data combined with network measures analysis. Adoption of straightforward network measures such as node degree and path length offer an understanding on the basic properties of the network. Network analysis using complex measures such as clustering coefficient, modularity and motif detection demonstrate the feasibility of combining MVPC analysis with network measures to reveal valuable information within the network. This approach leads to the identification of topological properties of a network using the SWN index. This combination of MVPC analysis with network theory analysis is capable of providing insight into basic, complex and topological network properties.

Chapter 2 describes the functional role of a neuron as the basic building block of the brain. This chapter also gives a description of electrical properties related to neuron synaptic signalling. Several modelling techniques for spiking neuron models were presented in this chapter. Modelling of spiking neuronal network facilitate the evaluation of the proposed method by comparisons of network properties between conditional or unconditional network with the simulated network with known network properties. Neuronal recording methods and spike detection methods in MEA signals were discussed. Understanding the nature of MEA signals helps in the implementation of spike train coherence and partial coherence analysis.

The framework for the most important element of this thesis, MVPC is presented in chapter 3. The explanation of synchronization analysis of pairwise spike train signals begins with the description of Fourier transformation for point process spike trains signals. It continues with estimation of auto- and cross-spectra for computation of coherence and partial coherence. The factor of computational complexity for partial coherence analysis using partial spectra increases with the increasing number of predictors. MVPC is the computationally efficient method discussed in this chapter for computation of multivariate partial coherence with a high number of predictors using the matrix inversion method.

Network theory including basic, complex and topological network measures was discussed in chapter 4. The basic measures of node degree and path length are included for inference of basic network properties in the simulated neuronal network and real MEA signals. Network subgraph motifs were selected as the complex measure to analyse the simulated network due to the feasibility to compare both conditional and unconditional motifs with the known pattern of interactions in the simulated network. Modularity was selected as the complex measure to analyse the network from real MEA signals due to the feasibility to classify the nodes according to the hippocampus sub-regions specified in the physiological data set. Description of small-world network in this chapter assists the analysis of network topological properties in both simulated and real data.

Results for simulated data are reported in chapter 5 which begins with scalability tests for MVPC analysis, which shows successful application of the method on 200 spike trains signals. Quantification of network edges using MVPC analysis yields a more accurate conditional network as expected for the simulated neuronal network based on the network visual representation and basic network metrics analysis compared to unconditional network metrics. Clear differences between conditional and unconditional network can be seen, this verified the existence of indirect edges before removal of the common effects in the unconditional network. Implementation of MVPC analysis provides a more accurate network with more convincing results in further network analysis which includes the detection of network subgraphs and inference of network topological properties. These findings prove the usefulness of the combination of MVPC and network analysis.

Chapter 6 implemented the approach developed in chapter 6 for analysis of 19 spike trains from multi-channel MEA signals recorded from 4 different subregions of the rat hippocampus. Comparison between conditional and unconditional network analysis using basic network measures shows differences in both binary and weighted network properties across different stages of the experiment. Network analysis across time provided further information on alteration of communication among the nodes at different stages of the experiment. Modularity analysis identified several sets of neurons with functional roles for within and across subregion connectivities. A combination of MVPC analysis along with network analysis provide valuable opportunities for systematic connectivity analysis of MEA spike train signals with large numbers of electrodes.

Application of MVPC analysis provides insights into functional neuronal communications with consideration of linear effect of predictor neurons. Scalability analysis proves that MVPC analysis can analyse spike train signals with 100 to 200 predictors. This suggests that MVPC analysis is a viable method to determine connectivity edges and the strength of interactions between neurons. Validation of the approach using simulated spike train signals highlighted the

importance of using conditional networks in further network analysis as opposed to unconditional networks. A combination of MPVC analysis with network metrics analysis represent a useful framework to study the complexity of neuronal interactions. Implementation of network analysis can facilitate understanding of the underlying neuronal network properties using several network metrics. The use of basic network measures appears to be a very useful characterisation of important network properties like the range of node degree, range of distances between nodes and the discovery of hub nodes. The use of more complex network measures like clustering coefficient and modularity appear to be beneficial in summarising data sets into functional groups of neurons as shown in the analysis of 19 channel MEA signals. However, classification into functional groups of neurons would ideally need larger numbers of spike train signal to clearly differentiate the functional role of the group of neurons. SWN analysis on MEA data highlighted the need for a larger network with more channels for analysis of network topological properties to differentiate the short distance edges within clusters from the long distance edges that connect different clusters of neurons. Larger dataset should also provide better classification of the clusters.

7.3 Future work

Using the network analysis framework created in this thesis for simulated and MEA spike train signals opens up opportunities for several new directions of research to be explored. The goal in the study of functional neuronal connectivity is to explore, extract and reveal hidden functional information within the complex neuronal network. The findings presented in this thesis are encouraging and would provide the basis for further development of sophisticated tools in the study of functional neuronal networks.

According to the results obtained in chapter 6, further work is needed to increase the scalability of MVPC analysis with greater numbers of spike trains with possibly different network configurations. Simulation of neuronal networks with

different configurations related to the complex network measures could be used to validate the combination of MVPC analysis with additional network metrics such as closeness centrality, betweenness centrality and participation coefficient (Rubinov & Sporns, 2010). Wide application of network theory using a combination of more network measures for complex network analysis of real physiological data is worthwhile for the discovery of interesting functional properties of the neurons in the network and also in the understanding of the neuronal signalling mechanisms discussed in chapter 2.

Scaling for greater network size by increasing the number of spike trains in MVPC analysis definitely increases the need for longer spike trains signals as presented in section 5.2 due to the stability of the spectral matrix inversion method. Numerical aspects of matrix inversion could be investigated using a spectral matrix diagonal up-weighting method (Medkour et al., 2009). This is likely to be a computational work, as it requires manipulation of the up-weighting parameter.

In this thesis, MVPC analysis is implemented only for spike train data. As discussed in chapter 3, partial coherence analysis is also suitable for analysis of time series, thus MVPC is potentially useful for LFP signals. Future work should develop the usability of the MVPC analysis on LFP signals to find functional interactions between populations of neurons. It is also recommended to validate the method using multiple hybrid signals which combine both LFP and spike train data. This validation could potentially assist in identification of neurons that contribute to synchronisation of different neuronal populations.

The proposed methods in this thesis are not restricted to MEA data and could also be implemented on other spike train and time series data including EEG and neuroimaging data. For example, application of the proposed analysis techniques to resting-state fMRI functional connectivity could be done using 1 Hz sampling rate of 100 channels with frequency resolution of 0.001 Hz. This analysis could be done to 1000 second of fMRI record.

The proposed techniques for neuronal connectivity analysis using a combination of MVPC analysis and network theory metrics present promising results based on more accurate networks, that reveal the hidden network properties. This combination appears to be a viable approach for large data sets of neuronal signals. Application of the method to different types of signals should reveal many interesting aspects of complex neuronal networks. The approach is also suitable for network analysis on specific time or frequency ranges.

This work is also suitable for reconstruction of structural connectivity based on partial coherence functional connectivity. This can be done by topological mapping of the functional and structural connectivity for a detailed comparison of the neuronal pathways in a network. This potentially provide more accurate mapping according to reliable synchronisation computation.

Appendix A

A.1 Neuronal parameters for cortical network model

Table A.1: Neuronal parameters for cortical neuron model of Network A and Network B (Halliday, 2005).

Parameter		Value & Units
R_m	Cell input resistance	40 M Ω
C_m	Cell capacitance	0.5 pF
V_r	Cell resting potential	74 mV
V_{thresh}	Fixed firing threshold	54 mV
V_{reset}	Fixed reset value	60 mV
Excitatory background inputs parameter		
G_{syn}	Conductance scaling factor	4.14 x 10 ⁻⁹
τ_{syn}	Time constant	1.0 msec
V_{syn}	Equilibrium potential for the ionic current	0 mV
Peak synaptic conductance		1.52 nS at 1 msec
Inhibitory background inputs parameter		
G_{syn}	Conductance scaling factor	2.28 x 10 ⁻⁹
τ_{syn}	Time constant	10.0 msec
V_{syn}	Equilibrium potential for the ionic current	-74 mV
Peak synaptic conductance		0.839 nS at 10 msec
EPSP parameter at V_{thresh}		
EPSP magnitude		366 μ V
		500 μ V when activated from V_r
EPSP rise time		0.575 msec
EPSP half width		5.75 msec
IPSP parameter at V_{thresh} (shunting inhibition)		
IPSP magnitude		-366 μ V (hyperpolarization)
		silent when activated from V_r
IPSP rise time		2.75 msec
IPSP half width		11.75 msec

A.2 Frequency of subgraphs in Network A

Table A.2: Frequency of subgraphs with motif size 3, 4 and 5 for conditional and unconditional Network A.

Motif Size	Motif ID	Frequency	
		Conditional network Number of edges = 383	Unconditional network Number of edges = 2444
3	78	82.83%	44.81%
	238	17.17%	55.19%
4	8598	55.35%	13.23%
	4958	24.46%	33.03%
	4382	11.54%	4.75%
	13278	6.04%	22.14%
	27030	1.64%	0.18%
	31710	0.96%	26.67%
5	2133644	33.38%	2.81%
	1083578	19.76%	3.54%
	8948910	15.00%	7.75%
	2133678	9.92%	5.15%
	1256886	5.47%	8.38%
	1150398	3.36%	5.89%
	1084606	2.7%	3.72%
	1150364	2.58%	0.20%
	5361086	1.84%	5.73%
	11046574	1.20%	0.25%
	9997502	1.14%	3.03%
	1289662	1.13%	13.75%
	3387326	0.82%	15.27%
	1082430	0.63%	0.26%
	13190438	0.32%	0.03%
	13225390	0.17%	0.08%
	7598014	0.15%	10.60%
	3248062	0.13%	1.66%
14273982	0.12%	0.14%	
3248028	0.03%	0.001%	
16510910	0.01%	12.12%	

References

- Achard, S. & Bullmore, E. (2007), ‘Efficiency and Cost of Economical Brain Functional Networks’, *Plos*, **3**(2), p. e17.
- Aidley, D. J. (1989), *The physiology of excitable cells*, Cambridge University Press.
- Bastian, M. & Heymann, S. (2009), ‘Gephi : An Open Source Software for Exploring and Manipulating Networks’, in ‘Proceedings of the Third International ICWSM Conference’, pp. 361–362.
- Blocher, J. (2010), ‘Erdős–rényi (e-r) random network matlab code’, <https://github.com/jblocher/matlab-network-utilities/blob/master/contest/erdrey.m>, Accessed on 2015-08-20.
- Bloomfield, P. (2000), *Fourier Analysis of Time Series: An Introduction*, Wiley.
- Boccaletti, S., Latora, V., Moreno, Y., Chavez, M. & Hwang, D. (2006), ‘Complex networks: Structure and dynamics’, *Physics Reports*, **424**, pp. 175–308.
- Bokil, H., Purpura, K., Schoffelen, J.-M., Thomson, D. & Mitra, P. (2007), ‘Comparing spectra and coherences for groups of unequal size.’, *Journal of Neuroscience Methods*, **159**, pp. 337–345.
- Bolaños, M., Bernat, E. M., He, B. & Aviyente, S. (2013), ‘A weighted small world network measure for assessing functional connectivity’, *Journal of Neuroscience Methods*, **212**(1), pp. 133–142.
- Brillinger, D. (2001), *Time Series: Data Analysis and Theory*, Society for Industrial and Applied Mathematics.
- Brillinger, D. R. (1972), ‘The spectral analysis of stationary interval functions’, *Proceeding of the Sixth Berkeley Symposium on Mathematical Statistics and Probability*, **1**, pp. 483–513.

- Brillinger, D. R. (1975), 'The identification of point process systems', *The Annals of Probability*, **3**(6), pp. 909–924.
- Brugger, S. & Schwirzer, C. (2011), 'Small world matlab code', https://github.com/msssm/lecture_files/blob/master/simulation_networks/small_world.m, Accessed on 2015-08-20.
- Bullmore, E. & Sporns, O. (2009), 'Complex brain networks: graph theoretical analysis of structural and functional systems.', *Nature Reviews. Neuroscience*, **10**, pp. 186–198.
- Bullmore, E. T. & Bassett, D. S. (2011), 'Brain graphs: Graphical models of the human brain connectome', *Annual Review of Clinical Psychology*, **7**, pp. 113–140.
- Buzsáki, G., Anastassiou, C. A. & Koch, C. (2012), 'The origin of extracellular fields and currents—eeg, ecog, lfp and spikes.', *Nature reviews. Neuroscience*, **13**(6), pp. 407–420.
- Buzsáki, G., Geisler, C., Henze, D. A. & Wang, X.-J. (2004), 'Interneuron diversity series: Circuit complexity and axon wiring economy of cortical interneurons', *Trends in neurosciences*, **27**(4), pp. 186–93.
- Cabeza, R. & Nyberg, L. (1997), 'Imaging cognition: An empirical review of pet studies with normal subjects', *Journal of Cognitive Neuroscience*, **9**(1), pp. 1–26.
- Cabeza, R. & Nyberg, L. (2000), 'Imaging cognition ii: An empirical review of 275 pet and fmri studies', *Journal of Cognitive Neuroscience*, **12**(1).
- Cadotte, A. J., DeMarse, T. B., Mareci, T. H., Parekh, M. B., Talathi, S. S., Hwang, D.-U., Ditto, W. L., Ding, M. & Carney, P. R. (2010), 'Granger causality relationships between local field potentials in an animal model of temporal lobe epilepsy.', *Journal of Neuroscience Methods*, **189**, pp. 121–129.
- Connors, B. W. & Gutnick, M. J. (1990), 'Intrinsic firing patterns of diverse neocortical neurons', *Trends in Neurosciences*, **13**(3), pp. 99–104.

- Dahlhaus, R. (2000), ‘Graphical interaction models for multivariate time series’, *Metrika*, **51**, pp. 157–172.
- Dahlhaus, R., Eichler, M. & Sandkühler, J. (1997), ‘Identification of synaptic connections in neural ensembles by graphical models.’, *Journal of Neuroscience Methods*, **77**, pp. 93–107.
- David, S. V., Malaval, N. & Shamma, S. a. (2010), ‘Decoupling action potential bias from cortical local field potentials.’, *Computational Intelligence and Neuroscience*, **2010**, p. 393019.
- Dayan, P. & Abbott, L. F. (2005), *Theoretical neuroscience: Computational and mathematical modeling of neural systems*, Taylor & Francis.
- Devilbiss, D. M. & Waterhouse, B. D. (2002), ‘Determination and quantification of pharmacological , physiological , or behavioral manipulations on ensembles of simultaneously recorded neurons in functionally related neural circuits’, *Journal of Neuroscience Methods*, **121**, pp. 181–198.
- Elmslie, K. S. (2001), ‘Membrane Potential’, *Encyclopedia of Life Sciences*, pp. 1–7.
- Erdős, P. & Rényi, A. (1959), ‘On random graphs’, *Publicationes Mathematicae Debrecen*, **6**, pp. 290–297.
- Euler, T. & Denk, W. (2001), ‘Dendritic processing’, *Current Opinion in Neurobiology*, **11**(4), pp. 415–422.
- Fiecas, M. & Ombao, H. (2011), ‘The generalized shrinkage estimator for the analysis of functional connectivity of brain signals’, *The Annals of Applied Statistics*, **5**(2A), pp. 1102–1125.
- Fiecas, M., Ombao, H., Linkletter, C., Thompson, W. & Sanes, J. (2010), ‘Functional connectivity: shrinkage estimation and randomization test.’, *NeuroImage*, **49**, pp. 3005–3014.

- Fraiman, D., Saunier, G., Martins, E. F. & Vargas, C. D. (2014), 'Biological Motion Coding in the Brain: Analysis of Visually Driven EEG Functional Networks', *PLoS ONE*, **9**(1), p. e84612.
- Freiwald, W. A., Valdes, P., Bosch, J., Biscay, R., Jimenez, J. C. C., Rodriguez, L. M., Rodriguez, V., Kreiter, A. K. & Singer, W. (1999), 'Testing non-linearity and directedness of interactions between neural groups in the macaque inferotemporal cortex.', *Journal of Neuroscience Methods*, **94**, pp. 105–19.
- Gabbiani, F. & Midtgaard, J. (2001), 'Neural information processing', *Encyclopedia of Life Sciences*, pp. 1–12.
- Gandrathi, A., Zheng, T., O'Brien, P., Ali, I., O'Brien, T. J. & French, C. R. (2013), 'An in vivo technique for investigating electrophysiological effects of centrally administered drugs on single neurons and network behaviour.', *Journal of Neuroscience Methods*, **219**(2), pp. 197–204.
- Gazzaniga, M. S., Ivry, R. B. & Mangun, G. R. (1998), *Cognitive neuroscience: The biology of the mind*, WW Norton.
- Gerstner, W. & Kistler, W. M. (2002), *Spiking neuron models: Single neurons, populations, plasticity*, Cambridge University Press.
- Halliday, D. M. (2005), 'Spike-Train Analysis for Neural Systems', in G. N. Reeke, Lindsay, K. A., Poznanski, R. R., Sporns, O. & Rosenberg, J. R., eds., 'Modeling in the Neurosciences From Biological Systems to Neuromimetic Robotics', pp. 555–578, CRC Press.
- Halliday, D. M., Rosenberg, J. R., Amjad, a. M., Breeze, P., Conway, B. a. & Farmer, S. F. (1995), 'A framework for the analysis of mixed time series/point process data—theory and application to the study of physiological tremor, single motor unit discharges and electromyograms.', *Progress in Biophysics and Molecular Biology*, **64**(2/3), pp. 237–78.
- Hodgkin, A. L. & Huxley, A. F. (1952), 'A quantitative description of membrane current and its application to conduction and excitation in nerve', *The Journal of Physiology*, **117**(4), pp. 500–544.

- Humphries, M. D. & Gurney, K. (2008), ‘Network ’small-world-ness’: a quantitative method for determining canonical network equivalence.’, *PloS ONE*, **3**(4), p. e0002051.
- Izhikevich, E. M. (2003), ‘Simple model of spiking neurons.’, *IEEE transactions on neural networks / a publication of the IEEE Neural Networks Council*, **14**(6), pp. 1569–72.
- Izhikevich, E. M. (2007), *Dynamical systems in neuroscience*, MIT press.
- Jacomy, M., Venturini, T., Heymann, S. & Bastian, M. (2014), ‘Forceatlas2, a continuous graph layout algorithm for handy network visualization designed for the gephi software’, *PLoS ONE*, **9**(6), pp. 1–12.
- Kandel, E. R., Schwartz, J. H., Jessell, T. M. et al. (2000), *Principles of Neural Science*, volume 4, McGraw-Hill New York.
- Kheiri, F., Bragin, A. & Engel, J. (2013), ‘Functional connectivity between brain areas estimated by analysis of gamma waves.’, *Journal of Neuroscience Methods*, **214**, pp. 184–191.
- Kostelecki, W., Dominguez, L. G. & Pérez Velázquez, J. L. (2011), ‘Single trial classification of magnetoencephalographic recordings using granger causality.’, *Journal of neuroscience methods*, **199**.
- Kwon, K. Y., Eldawlatly, S. & Oweiss, K. (2012), ‘Neuroquest: A comprehensive analysis tool for extracellular neural ensemble recordings.’, *Journal of Neuroscience Methods*, **204**, pp. 189–201.
- Latora, V. & Marchiori, M. (2001), ‘Efficient Behavior of Small-World Networks’, *Physical Review Letters*, **87**(19), p. 198701.
- Laubach, M., Shuler, M. & Nicolelis, M. A. (1999), ‘Independent component analyses for quantifying neuronal ensemble interactions.’, *Journal of Neuroscience Methods*, **94**, pp. 141–154.
- Le Van Quyen, M. & Bragin, A. (2007), ‘Analysis of dynamic brain oscillations: methodological advances.’, *Trends in neurosciences*, **30**(7), pp. 365–73.

- Lee, D. (2002), ‘Analysis of phase-locked oscillations in multi-channel single-unit spike activity with wavelet cross-spectrum.’, *Journal of Neuroscience Methods*, **115**, pp. 67–75.
- London, M. & Häusser, M. (2005), ‘Dendritic Computation’, *Annual Review of Neuroscience*, **28**, pp. 503–32.
- Mader, W., Mader, M., Timmer, J., Thiel, M. & Schelter, B. (2015), ‘Networks: On the relation of bi- and multivariate measures’, *Scientific Reports*, **5**(10805), pp. 1–7.
- Makhtar, S. N., Halliday, D. M., Senik, M. H. & Mason, R. (2014), ‘Multivariate partial coherence analysis for identification of neuronal connectivity from multiple electrode array recordings’, *IEEE Conference on Biomedical Engineering and Sciences*, pp. 77–82.
- Martinet, L.-E., Fiddymont, G., Madsen, J. R., Eskandar, E. N., Truccolo, W., Eden, U. T., Cash, S. S. & Kramer, M. A. (2017), ‘Human seizures couple across spatial scales through travelling wave dynamics’, *Nature Communications*, **8**, p. 14896.
- Medkour, T., Walden, a. T. & Burgess, a. (2009), ‘Graphical modelling for brain connectivity via partial coherence.’, *Journal of Neuroscience Methods*, **180**(2), pp. 374–83.
- Milo, R., Shen-Orr, S., Itzkovitz, S., Kashtan, N., Chklovskii, D. & Alon, U. (2002), ‘Network motifs: simple building blocks of complex networks’, *Science*, **298**(5594), pp. 824–827.
- Newman, M. (2010), *Networks: An Introduction*, OUP Oxford.
- Newman, M. E. (2001), ‘The structure of scientific collaboration networks.’, *Proceedings of the National Academy of Sciences of the United States of America*, **98**(2), pp. 404–409.
- Newman, M. E. J. (2004), ‘Analysis of weighted networks’, *Phys. Rev., E Stat. Nonlinear Soft Matter Phys*, **70**, p. 056131.

- Newman, M. E. J. (2006), ‘Modularity and community structure in networks’, *Proceedings of the National Academy of Sciences of the United States of America*, **103**(23), pp. 8577–8582.
- Nicholls, J., Martin, A. R. & Wallace, B. G. (1992), *From neuron to brain: A cellular and molecular approach to the function of the nervous system*, Sinauer Associates.
- Onnela, J.-P., Saramäki, J., Kertész, J. & Kaski, K. (2005), ‘Intensity and coherence of motifs in weighted complex networks’, *Phys. Rev. E*, **71**, p. 065103.
- Purves, D., Augustine, G., Fitzpatrick, D., Hall, W., LaMantia, A.-S., McNamara, J. & White, L. (2008), *Neuroscience*, Sinauer.
- Quiroga, R. Q. (2007), ‘Spike sorting’, *Scholarpedia*, **2**(12), p. 3583.
- Quiroga, R. Q., Nadasdy, Z. & Ben-Shaul, Y. (2004), ‘Unsupervised spike detection and sorting with wavelets and superparamagnetic clustering’, *Neural Computation*, **16**(8), pp. 1661–1687.
- Rall, W. (1967), ‘Distinguishing theoretical synaptic potentials computed for different Soma-Dendritic distributions of synaptic’, *Journal of Neurophysiology*, **30**(5), pp. 1138–1168.
- Ribeiro, P., Silva, F. & Kaiser, M. (2009), ‘Strategies for network motifs discovery’, *e-Science 2009 - 5th IEEE International Conference on e-Science*, (ii), pp. 80–87.
- Rosenberg, J. R., Amjad, A. M., Breeze, P., Brillinger, D. R. & Halliday, D. M. (1989), ‘The fourier approach to the identification of functional coupling between neuronal spike trains’, *Progress in biophysics and molecular biology.*, **53**, pp. 1–31.
- Rosenberg, J. R., Halliday, D. M., Breeze, P. & Conway, B. a. (1998), ‘Identification of patterns of neuronal connectivity—partial spectra, partial coherence, and neuronal interactions.’, *Journal of Neuroscience Methods*, **83**, pp. 57–72.

- Ruben, P. C. (2001), ‘Action Potentials : Generation and Propagation’, *Encyclopedia of Life Sciences*, pp. 1–7.
- Rubinov, M. & Sporns, O. (2010), ‘Complex network measures of brain connectivity: uses and interpretations.’, *NeuroImage*, **52**(3), pp. 1059–69.
- Salvador, R., Suckling, J., Schwarzbauer, C. & Bullmore, E. (2005), ‘Undirected graphs of frequency-dependent functional connectivity in whole brain networks.’, *Philosophical transactions of the Royal Society B*, **360**, pp. 937–946.
- Senik, M. H., O’Donoghue, M. F. & Mason, R. (2013), ‘Intra- and inter-hippocampal connectivity in a KA-induced mTLE rat model’, in ‘Program No. 143.05. 2013 Neuroscience Meeting Planner’, Society for Neuroscience, New Orleans, LA.
- Shepherd, G. M. (1990), *The synaptic organization of the brain*, Oxford University Press.
- Sporns, O. (2013), ‘Network attributes for segregation and integration in the human brain’, *Current Opinion in Neurobiology*, **23**, pp. 162–171.
- Sporns, O. & Honey, C. J. (2006), ‘Small worlds inside big brains.’, *Proceedings of the National Academy of Sciences of the United States of America*, **103**(51), pp. 19219–19220.
- Sporns, O. & Kötter, R. (2004), ‘Motifs in Brain Networks’, *PLoS Biology*, **2**(11), p. e369.
- Sporns, O., Tononi, G. & Edelman, G. M. (2000), ‘Theoretical neuroanatomy: relating anatomical and functional connectivity in graphs and cortical connection matrices.’, *Cerebral Cortex*, **10**(2), pp. 127–41.
- Tononi, G., Edelman, G. M. & Sporns, O. (1998), ‘Complexity and coherency: integrating information in the brain.’, *Trends in Cognitive Sciences*, **2**(12), pp. 474–84.

- Tononi, G., Sporns, O. & Edelman, G. M. (1994), 'A measure for brain complexity: relating functional segregation and integration in the nervous system.', *Proceedings of the National Academy of Sciences of the United States of America*, **91**, pp. 5033–5037.
- Trappenberg, T. (2010), *Fundamentals of computational neuroscience*, Oxford University Press.
- Troyer, T. W. & Miller, K. D. (1997), 'Physiological gain leads to high ISI variability in a simple model of a cortical regular spiking cell.', *Neural computation*, **9**, pp. 971–983.
- Walden, A. T. (2000), 'A unified view of multitaper multivariate spectral estimation', *Biometrika*, **87**(4), pp. 767–788.
- Watts, D. J. & Strogatz, S. H. (1998), 'Collective dynamics of 'small-world' networks.', *Nature*, **393**, pp. 440–442.
- Wernicke, S. & Rasche, F. (2006), 'FANMOD: A tool for fast network motif detection', *Bioinformatics*, **22**(9), pp. 1152–1153.
- Whittaker, J. (1990), *Graphical models in applied multivariate statistics*, Wiley.
- Williams, S. R. & Stuart, G. J. (2002), 'Synaptic Integration', *Encyclopedia of Life Sciences*, pp. 1–5.
- Wong, E., Baur, B., Quader, S. & Huang, C. H. (2011), 'Biological network motif detection: Principles and practice', *Briefings in Bioinformatics*, **13**(2), pp. 202–215.
- Wu, J., Kendrick, K. & Feng, J. (2007), 'Detecting correlation changes in electrophysiological data.', *Journal of Neuroscience Methods*, **161**, pp. 155–165.